Received May 19, 2022, accepted June 2, 2022, date of publication June 8, 2022, date of current version June 14, 2022.

Digital Object Identifier 10.1109/ACCESS.2022.3180746

An Overview of Four-Leg Converters: Topologies, Modulations, Control and Applications

FÉLIX ROJAS[1], (Member, IEEE), ROBERTO CÁRDENAS[2], (Senior Member, IEEE), CLAUDIO BURGOS-MELLADO[3], (Member, IEEE), ENRIQUE ESPINA[4], (Student Member, IEEE), JAVIER PEREDA[1], (Member, IEEE), CRISTIAN PINEDA[1], (Student Member, IEEE), DAVID ARANCIBIA[4], AND MATÍAS DÍAZ[4], (Member, IEEE)

[1]Department of Electrical Engineering, Pontificia Universidad Católica de Chile, Santiago 7820436, Chile
[2]Department of Electrical Engineering, Universidad de Chile, Santiago 8370448, Chile
[3]Institute of Engineering Sciences, Universidad de O'Higgins, Rancagua 2841959, Chile
[4]Department of Electrical Engineering, Universidad de Santiago de Chile, Santiago 9170124, Chile

Corresponding author: Félix Rojas (felix.rojas@ing.puc.cl)

This work was funded by the chilean Agencia Nacional de Investigación y Desarrollo (ANID) through the Project FONDECYT/11190806 and also supported by Project FONDAP/15110019 Solar Energy Research Center (SERC Chile), Project PCI/BMBF180054, Project PIA/ACT192013, Project FONDEF/ID20i10267; and Project Basal FB0008.

ABSTRACT In three-phase unbalanced systems, where the circulation of zero sequence current is necessary, four-leg converters provide a neutral connection for single-phase or other unbalanced loads typically utilized in three-phase distribution systems. In addition, control of the magnitude and phase of the zero-sequence voltage and/or current are also achieved using four-leg power converters. However, even when four-leg converters have become very important in several fields as for instance, four-leg microgrids and aerospace applications, a comprehensive review of the converter topologies, control methods, modulation methods and output filters have not been hitherto published. In this paper, a comprehensive overview of the state-of-the-art of four-leg converters is presented, based on the selection of over 400 papers published in journals and conferences, identifying mature and incipient topologies, modulation strategies, control schemes and applications. Each topic presented in this work is thoroughly discussed and reviewed, analyzing characteristics, implementation issues, and reported advantages and disadvantages to provide a comprehensive overview of the current research and future challenges in four-leg converters. The most important applications of four-leg converters are also discussed in this work, including stand-alone power supply, uninterruptible power supplies, grid-connected 4-leg inverters, ground power units for aerospace applications, active filtering for power quality enhancement, cooperative control of 4-leg converters for micro-grid applications, among others. Finally, future work and conclusions are highlighted in this paper.

INDEX TERMS Control of unbalanced systems, distribution networks, four-leg converters, unbalanced systems, zero-sequence control.

NOMENCLATURE

3L4W	Three-leg Four-Wire
4L4W	Four-leg Four-Wire
3P3W	Three-phase Three-wire
3P4W	Three-phase Four-Wire
APF	Active Power Filter
AFE	Active Front End
CPS	Current Power Supply
CSC	Current Source Converter
CSR	Current Source Rectifier
CPT	Conservative Power Theory
DSC	Delay Signal Cancellation
DVR	Dynamic Voltage Restorer
EMI	Electromagnetic Interference
FBD	Fryze-Buchholz-Depenbrock
FC	Flying Capacitor
FS-MPC	Finite-Set-Model Predictive Control
GPU	Ground Power Unit
IMC	Indirect Matrix Converter
LV	Low-Voltage
LQR	Linear Quadratic Regulator
MC	Matrix Converter
MG	Microgrid

The associate editor coordinating the review of this manuscript and approving it for publication was Diego Bellan.

MV	Medium-Voltage
NPC	Neutral-point Clamped
PLL	Phase-Lock Loop
PTP	Phase-to-Phase voltage
PTN	Phase-to-Neutral voltage
PCC	Point of Common Coupling
PWM	Pulse Width Modulation
PI	Proportional-Integral
PR	Proportional-Resonant
RRF	Rotating Reference Frame
RC	Repetitive Controller
ROGI	Reduced-Order Generalized Integrator
SAPF	Shunt Active Power Filter
SHE	Selective Harmonics Elimination
SPWM	Sinusoidal PWM
SVM	Space Vector Modulation
SRF	Static Reference Frame
SRPC	Series Reactive Power Compensator
THD	Total Harmonic Distortion
USPSF	Unified Series-Parallel Active Filter
UPQC	Unified Power Quality Conditioner
UPS	Uninterruptible Power Supply
VSC	Voltage Source Converter
VPS	Voltage Power Supply
VSI	Voltage Source Inverter
PV	Photo-Voltaic

I. INTRODUCTION

Power distribution systems are facing a profound transformation, aiming to achieve a re-configurable network, capable to provide DC and AC voltage to efficiently use the energy generated within networks and the energy provided by a transmission system [1], [2]. This shall allow the integration of clean energy generation technologies, such as photovoltaic and wind energy sources [3], [4], modern storage systems based on hydrogen [5], [6], solid-state [7] or lithium-ion batteries technology [8]–[10] and modern electric transportation [11], from small electric bikes [12] to large airplanes [13]–[15], powered by battery-based or hydrogen-based storage systems. A power distribution network or microgrid provides energy to several single-phase loads or unbalanced three-phase loads, i.e., three-phase four-wire (3P4W) systems [16], usually in a radial configuration, managing unbalanced power flows. In these cases, a path for the circulation of zero sequence currents has to be provided, for instance using a bulky Delta/Wye transformer, where the neutral point of the secondary winding is used to ground the winding [17], providing a path for both zero-sequence currents and fault currents respectively. Although this configuration is simple, robust, and requires no extra hardware, the asymmetric magnetic fluxes increase its power losses when the transformer is exposed to moderate unbalanced load levels and produce imbalances at the output voltages supplied to the grid/load [18]. In addition, ground current and neutral current are connected to the same neutral point of the transformer, which can be considered a potential danger to sensitive single-phase loads during a phase-to-ground fault. Furthermore, in the presence of harmonic distortion, transformers suffer from higher iron and winding power losses, especially when unbalanced single-phase loads with a relatively high third-harmonic content are connected to the transformer [19], [20]. This third-harmonic circulates through the delta of the primary winding of the transformer and is also present at the neutral wire of the secondary winding of the transformer. These effects reduce the available nominal power of the transformers, leading to oversized transformers and low-efficiency [21]. Finally, the incapability of power transformers to compensate asymmetrical internal drop voltages, generate unbalanced three-phase output voltages, which may produce extra heating in electrical machines, undesirable ripple in rectifiers, and malfunctioning of protection devices [22]. The transformer in zig-zag configuration has been proposed as an alternative to reduce neutral currents generated by unbalanced loads, however, they suffer from similar problems to those of Delta/Wye configuration [23].

To overcome passive transformer limitations, a dedicated power converter able to compensate negative and zero-sequence currents in four-wire systems is required, especially in 4-leg low-voltage microgrids and electrical energy distribution systems [16], [24], [25]. It must be recalled that three-phase converters can regulate positive and negative voltages but, because of the lack of a fourth wire, can not handle zero-sequence components. Accordingly, the first and simplest approach to provide a path for circulation of zero-sequence current was to split the dc-link capacitors of a two-level three-leg inverter to connect its mid-point to the neutral wire, i.e. a three-leg four-wire (3L4W) converter. Although this configuration achieves control over zero-sequence components, the zero-sequence current flows through the dc-link capacitors, leading to large dc-link capacitance to reduce voltage ripple and reduced utilization of the dc-link voltage [26]; increasing the capacitors footprint, power losses, cost and worsening its performance [27].

Four-leg converters are a promising solution to cope with the above mentioned problems. These converters have a dedicated leg to provide the neutral-wire, i.e. four-leg four-wire (4L4W) converters [24], [28], achieving full dc-link voltage utilization, and providing high performance and controllability over the zero sequence components, allowing to control each of the three Phase-to-Neutral (PTN) voltages independently. Furthermore, four-leg converters enable independent single-phase active and reactive power flow control [29], [30], active compensation of unbalanced droop voltages when acting as voltage power supply [31], smart protections, separation of neutral-wire with earth protection wire and managing of harmonic content [32], [33].

Although the two-level 4L4W VSI is the most reported topology in the literature, the utilization of several other four-leg power converter topologies has been discussed. For instance, multi-level converters as the Neutral Point Clamped [34], Flying Capacitor [35] and T-type [36] have

been presented for four-leg systems. The main advantage of multilevel converters is the higher equivalent switching frequency at the modulated output voltage, enabling the utilization less bulky power filters to produce adequate output-power quality with less power density. This is obtained at the cost of a higher number of semiconductor devices, passive elements, and higher control complexity. Direct AC/AC 4L4W topologies have also been proposed to connect 3P3W to 3P4W systems, as the direct matrix converter [37] and indirect matrix converter [38], which are claimed to have greater power density and reliability compared with back-to-back VSI topologies. However, they require a higher switching frequency, and the output voltage is limited to only 87% of the input voltage, and its input-output dynamic is coupled due to the absence of storage elements. Indeed, because of the instantaneous active power conservation (see [39]), the instantaneous power oscillations at the unbalanced load, are transferred to the input, producing harmonic distortion at the input side current. The interconnection of several inverters, controlled independently, acting as one converter to interface a four-wire network has been also reported as a simpler solution to control zero-sequence current. For instance, parallel connection of three H-bridges [40] or three three-leg inverters [41] has been proposed. This approach allows for a simpler control system and, most importantly, it simplifies the modulation algorithms compared with a single four-leg inverter implementation [42]. This approach also provides the possibility to interconnect several multilevel topologies, greatly improving the number of levels at the output of the converter with an easier modulation and control system [43].

A 4L4W VSI enables the control of positive, negative, and zero-sequence components of the output voltages of the converter. The zero-sequence component represents an additional variable to control when compared with 3L3W converters. To modulate these voltage components, two main groups of modulators have been reported: Space Vector PWM (SVM) methods [44], [45] and carrier-based PWM methods [46], [47]. SVM methods represent converter voltages and reference voltages as vectors in a three-dimensional coordinate frame. This representation can be achieved in an $\alpha\beta 0$ coordinate frame or a natural *abc* coordinate frame. Both methods require: i) identifying the four vectors generated by the converter which are nearest to the reference vector, ii) obtaining the dwell-time for each vector to be applied, and iii) defining a convenient switching pattern. This three-step process can be achieved for both techniques with similar computational burden [48]. The SVM method implemented in *abc* coordinates avoids Clarke transformation and can be implemented together with resonant controllers also in *abc* coordinate frame, this can spare some computational burden [49]. On the other hand, SVM methods in $\alpha\beta 0$ space have the advantage of representing the zero-sequence voltage as one independent variable which can be regulated using zero-sequence controllers implemented in $\alpha\beta 0$ coordinates.

Carrier-based PWM methods are simple to implement and, in this case, each of the four legs modulates a different voltage. A reference voltage signal for each of the four legs of the converter has to be calculated. Typically, a min/max algorithm is used to calculate the fourth-leg reference voltage, which is added to each of the other three phases, namely zero-sequence injection [50]. However, it is difficult to implement different switching patterns for shaping harmonic spectrum and use redundant switching states, especially important in multilevel converters [51]. Hysteresis based regulators have been also presented as a very simple alternative to regulate the output voltages and currents of four-leg power converters [26]. However, this approach can produce steady-state error, variable switching frequency, and large ripple in the neutral current when compared to the ripple produced in the phase currents [52].

In addition, modulator-free non-linear control schemes have been also proposed for controlling zero-sequence voltage and/or current. For instance, in [53], [54] a Finite Set Model Predictive Control (FS-MPC), is proposed, which provides good performance and high dynamic current control, however, FS-MPC does not guarantee a fixed switching frequency for every leg. Instead, the switching frequency depends on the operational point of the converter, leading to uneven power losses distribution [55], [56] and difficulties associated with the design of the output power filters. Some efforts have been lately done to solve this issue, where modulation stages are included in non-linear controllers to guarantee a fixed switching frequency over the whole operating range of the converter [57]–[59].

The capability to control zero-sequence voltages and provide a path for zero-sequence currents make four-leg converters an excellent candidate for applications such as: (i) 3P4W Stand-Alone Power Supplies, which provide a balanced and symmetric three-phase system and single-phase voltages to unbalanced and/or non-linear loads [60], (ii) Ground Power Units (GPUs), which are a particular case of 3P4W Power Supply with a fundamental frequency of 400Hz for aeronautic applications where stringent power quality regulations are enforced [61], [62], (iii) Uninterruptible Power Supplies (UPS) for 3P4W systems where the power output can be synchronized with the grid and its dc-link is connected to battery packages to supply uninterrupted electrical energy to critical loads [63], and (iv) active power filters for 3P4W systems, where harmonic distortion, reactive power and the negative and zero-sequence currents, are eliminated or compensated [64]. In addition, in microgrids applications, four-leg converters can be used in a collaborative mode, where a higher hierarchical controller provides power set-points to the four-leg converters located within the microgrid to compensate imbalances and distortion [65] and also can be used in a non-collaborative mode, where each converter obtain its own reference based on its local measurements [66]. In both cases, active and reactive power flows, as well as harmonic distortion and imbalances produced in the microgrid can be compensated by four-leg converters [16]. Additional applications such as Dynamic Voltage restorer (DVR) [67], Unified Power Quality Conditioner (UPFC) [68] and drive applications,

where the fourth leg is used to reduce the common-mode voltage applied to the machine, limiting or eliminating the bearing current, [69], [70], have been also proposed in the literature.

A. RESEARCH METHODOLOGY

This paper provides a comprehensive literature review for four-leg converters, considering its different topologies, input/output passive filters, grounding configuration, and its modulation strategies. Also, a detailed review of its current applications on electrical systems along with the linear and non-linear control schemes proposed for each of its applications is presented. Finally, a discussion of perspectives and future research challenges is also provided.

The articles included in this review where mainly obtained from the IEEE Xplore database, representing 86% of the total cited papers, also databases as Science Direct, MDPI and IET Digital Library were used, representing 10% of the cited papers. Additionally, 4% of the cited papers were obtained from other sources for citing books, patents and standards (Springer, NREL, ANSI, John Wiley and Sons). To select the papers cited in this review, the following most important keywords were used in all databases, 'Control of Unbalanced Systems', 'Distribution Networks', 'Four-leg Converters', 'Unbalanced System', 'Zero-sequence control', 'Three-Dimensional Modulation', 'Zero-Sequence Injection', 'Ground Power Units', 'Unbalanced Microgrids', 'Four-Wire Systems'. Thereafter, a selection criteria was implemented based on the quality of the paper and suitability with the content of our contribution. This selection process revealed the most important topics on four-leg converters, and was the base for creating the structure of this paper. This review paper was focused on the last decade, representing the 61% of the total cited paper. From these papers, 62% are published during the last 5 years. From the total cited papers, 92% belong to the last 2 decades, and few references before that are also included for completeness.

B. CONTRIBUTIONS

The main contributions of this overview paper, compared to similar publications, are summarized in Table 1, i.e.: (i) it presents a comprehensive review of advanced four-leg topologies, (ii) it provides a detailed description of all types of input/output filters used for four-leg topologies, (iii) unlike previous surveys, this paper present a comprehensive revision of applications that require the use of four-leg topologies and (iv) a detailed description of the most relevant modulation strategies proposed for four-leg converters are presented. All these topics are coherently presented and discussed in this paper.

The rest of this paper is structured as follows: Section II presents a review of the four-leg converter topologies and passive filter configurations, Section III shows a summary and discussion of modulation strategies for four-leg converters. In Section IV the control strategies and requirements for regulating voltage and currents in unbalanced and non-linear systems are discussed, including signal conditioning, linear and non-linear controllers. Section V discusses the applications of four-leg converters. Finally, conclusions and future challenges for four-leg converters are discussed.

II. FOUR-LEG CONVERTER AND OUTPUT FILTER TOPOLOGIES

This section summarizes the reported four-leg converter topologies and output filter configurations. It is divided into three main sub-sections: A) Four-leg converters topologies derived from three-leg converters, which are mainly extended topologies from its thee legs version, B) Advanced Four-Leg Converter Topologies, which are interesting new and uncommon topologies and C) a comprehensive summary of the output filters configurations used for four-leg topologies.

A. FOUR-LEG CONVERTERS TOPOLOGIES DERIVED FROM THREE-LEG CONVERTERS

The simplest alternative to develop a four-leg converter is to incorporate an extra leg to topologies originally presented as thee-leg converters in the literature. The semiconductors used in the fourth leg have to be designed to withstand the same voltage and peak current (transient operation) as the other three legs of the converter, however, the RMS current through the fourth leg (the unbalanced current) is usually lower than the nominal RMS current of each phase of the converter [72]. Therefore, the nominal power of the fourth leg can be designed smaller than the other three legs which rated power depends on the specific application [61], [73]. Furthermore, the incorporation of this new leg introduces new challenges and concepts, which are summarized in this section:

1) FOUR-LEG TWO-LEVEL CONVERTER

The typical topology of a four-leg two-level VSI is shown in Fig. 1. As seen, it is formed by 8 power switching devices coupled to free-wheeling diodes and a dc-link composed of a single capacitor. The converter allows 2^4 switching combinations, with two combinations that generate zero voltage in all PTN output voltages (double redundancy). It supplies three voltage-levels at the output PTN and PTP voltages, namely v_{dc}, 0, $-v_{dc}$, same as the PTP voltages in a three-leg converter. Since its introduction in the early 90's [28], it has been proposed for several applications, mainly for compensating unbalanced and harmonic components of stand alone and grid-connected applications, such as: UPS [63], [74]–[76], APF [32], [77]–[79], UPQC [80]–[82], DVR [83], [84], stand-alone power supply for 50/60Hz operation [85]–[89] and 400Hz operation as GPU for aerospace applications [28] or grid connected power supply applications for utility and microgrids [31], [65], [90]. In addition, it has been proposed in variable speed drives for elimination of common-mode voltage which causes unwanted bearing currents and ground fault relays operation [69]. The same common-mode voltage reduction principle has been used to minimize leakage current in PV applications [91]. Also it has been proposed

TABLE 1. Summary of the content of recently published surveys related to four-leg converters.

Ref.	Year	Standard Four-leg Topologies	Advanced Four-leg Topologies	Input/Ouput Filters	Modulation Strategies	Linear Controllers	Nonlinear Controllers	Applications
[24]	2015	yes	no	no	no	yes	yes	only MGs
[63]	2016	no	no	no	no	yes	yes	only UPSs
[71]	2017	yes	no	no	only PWM	no	no	only SAPFs
[32]	2017	yes	no	no	no	yes	no	only SAPFs
[49]	2018	yes	no	no	only SVM	no	no	no
[72]	2019	yes	no	no	no	yes	yes	only MGs
Proposed Survey	2022	yes	yes	yes	yes	yes	yes	yes

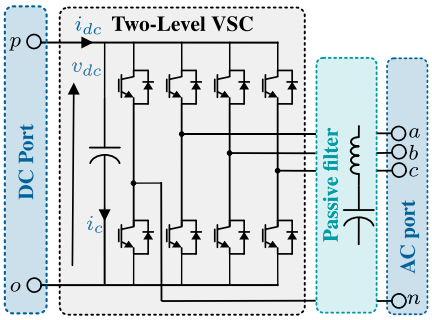

FIGURE 1. Four-leg two-level converter topology.

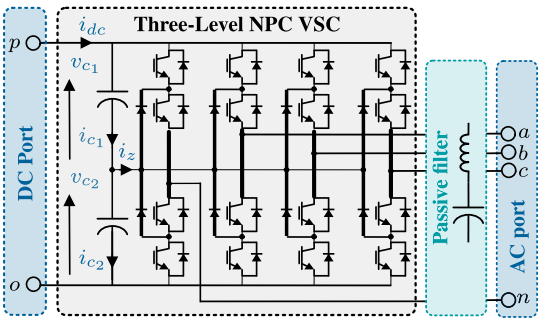

FIGURE 2. Four-Leg NPC converter topology.

for multiple drive configuration, where the converter legs are grouped into two pairs to drive simultaneously two AC motors [92] and as fault-tolerant converter using the fourth leg as redundancy in three-phase systems [93].

2) FOUR-LEG NPC CONVERTER

The typical topology of a four-leg NPC converter is shown in Fig. 2. The converter is composed of 16 power switching devices coupled to free-wheeling diodes and 8 clamping power diodes. Its dc-link voltage is naturally split by two dc-capacitors, which provide a mid-point for clamping the 8 power diodes. Note that this mid-point remains floating in this topology, and does not provide the output fourth wire of the converter, which is obtained by its fourth leg. Early presented in [94], this converter possesses 81 admissible switching combinations, which generates 50 non-redundant combinations, 14 active redundant combinations and 1 zero voltage combination with triple redundancy [95].

The converter provides five voltage levels at the output PTN voltages whose dominant harmonic component is twice the switching frequency of the individual power devices. This higher effective switching frequency allow to reduce the output filter size, increasing the power density of the solution. It also improves the efficiency, and allows the converter to synthesize voltages with a higher fundamental frequency compared to that synthezised by a two-level VSI. Thereby, the converter becomes a good alternative for the integration of renewable energy in unbalanced distribution systems [96], in GPU for aerospace applications where 400Hz output voltage and high order harmonic distortion compensation are required [61] or for high power quality energy supply [97]. To maintain the dc-link voltages balanced, an active control over the mid-point current i_z has to be implemented either with vectorial [44], [98] or scalar modulation schemes [99]. Both approaches successfully achieve balancing of the floating voltages, but vectorial methods provide more flexibility to implement different switching patterns and achieve balancing even in cases where the output current possesses some dc component [95]. Although this converter can be scaled for higher voltages by increasing the number of levels, for more than 3 levels the topology becomes complex, difficult to implement, and to balance its floating capacitor, not being attractive as a real solution [100]. Thereby, the 3-level NPC is attractive as a high-efficiency solution in LV applications or as an alternative for MV applications in the range of 2-6kV [100].

3) FOUR-LEG T-TYPE NPC CONVERTER

The typical topology of a four-leg T-Type NPC converter is shown in Fig.3. In its three-level version, the converter possesses 16 power switching devices, without clamping diodes. Each leg has two switching devices designed to withstand the full dc-link voltage (one of its major drawbacks) and the other two devices, connected to the mid-point of the dc bus handle only half of the full dc-link voltage each [36]. The two switches connected to the mid-point of the dc-link

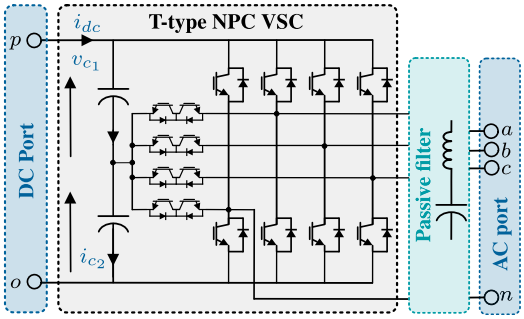

FIGURE 3. Four-leg T-type NPC converter topology.

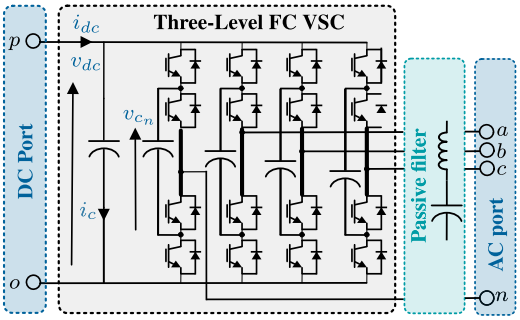

FIGURE 4. Four-leg flying capacitor converter topology.

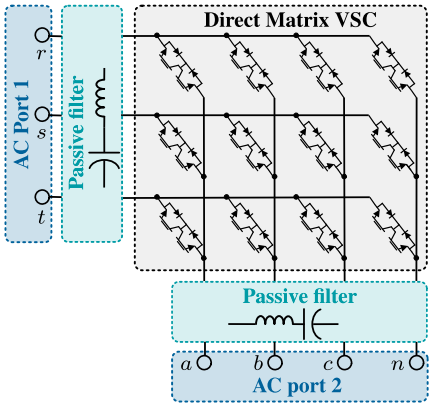

FIGURE 5. Four-leg matrix converter topology.

form a bidirectional switch, which is normally configured as a common-collector to reduce the number of isolated gate drives [101], [102]. These two devices can be also replaced by a single bidirectional Reverse Blocking (RB)-IGBT to reduce conduction losses [103]. The converter has 81 admissible switching combinations, providing high-quality five voltage-levels at the PTN output voltages.

This four-leg topology performs better power quality than two-level VSC and better efficiency compared to standard NPC converter [104], mainly because load currents do flow permanently through two series-connected devices, reducing considerably the conduction losses [104]. Thereby, this topology is a good alternative for low-voltage, high efficiency, and/or high power quality applications, such as motor drives using the fourth leg to provide fault-tolerant capability [105] or as stand-alone power supply for unbalanced and distorted systems [36].

4) FOUR-LEG FLYING CAPACITOR CONVERTER

The typical topology of a four-leg flying capacitor converter is shown in Fig.4. In its three-level version, the converter has 16 power switching devices coupled to free-wheeling diodes and 4 flying capacitors. Similar to a four-leg NPC converter, the flying-capacitor converter has been originally designed to operate in MV levels, thereby series-connected devices are used to allow each device to withstand a maximum of half of the dc-link voltage at the cost of increasing conduction power losses. Thereby, each floating capacitor voltage is set to half of the dc-link voltage, allowing each leg of the converter to provide half of the dc-link voltage to the load with two redundant switching combinations, which are used to maintain the floating voltage controlled to its set point. This leads to 4 admissible switching combinations on each leg, which results in 256 switching combinations for the converter. The high number of redundant switching combinations improves the capability to balance the voltage on the flying capacitors compare to its three-leg version [35]. However, extended algorithms for balancing the voltage on flying capacitors schemes are required to maintain the converter stable under distorted and unbalanced operation which due to the high number of redundant vectors increases its complexity [35]. The converter becomes a good alternative for integration of Renewable Energy Sources in distribution networks [106], [107] and also as active power filters [35], [108].

5) FOUR-LEG MATRIX CONVERTER

Presented in Fig.5, this converter can provide bidirectional power flow directly between three-wire and four-wire AC systems. The converter is implemented using 24 common-emitter-connected power semiconductors coupled to free-wheeling diodes which form 12 bidirectional power switches [37], [109]–[115]. The converter has 81 switching states, where three states provide zero voltage. All these 81 states can be used to control output voltages when controllers without modulation stage, such as predictive control, are used [116]. However, when a linear modulation stage is implemented, such as SVM, only 45 switching states are useful, namely stationary vectors, and 33 are discarded as they rotate in the $\alpha\beta 0$ space [114].

An input LC filter is also required for the operation of the converter, it provides a path for switched pulsating currents avoiding large di/dt on inductors which could damage the power semiconductors due to over-voltage. In addition, the filter is also implemented to decouple fast transitory disturbance between both AC ports. To design the input LC filter, the converter and its load can be considered as a transitory negative resistor when a voltage sag occurs at the input port of the converter, which could cause instability. Thereby, the input LC filter design is a compromise between input power

quality and its stability margin [117]. Damping resistors parallel connected to the filter inductors can be also incorporated to overcome this issue [45]. A bidirectional diode clamp absorption circuit is also required in this topology. It is composed of two three-phase rectifiers and a dc-link capacitor, connected to the three phases of the input AC system and to three of the four wires of the output AC system [118].

Although the absence of a dc-link capacitor limits the achievable modulated output PTN voltages of the converter to only 87% of the input voltage [37], it also enables its major advantages, such as greater power density, higher reliability, and higher operating temperature range of the converter. Thus, the converter has become an attractive solution for applications that require strength operational conditions, such as utility power source for unbalanced systems in military applications [114], for the aerospace industry, where the plane can be considered as a small unbalanced microgrid, as GPU [37] or as a wing ice protection system [118]. It has been also presented as a stand-alone power supply for interfacing diesel generators for improving efficiency [45]. The fourth leg of the converter has been also proposed for disturbance-free operation in three-phase systems to improve reliability [119].

Most of the advantages of the four-leg Matrix Converter are related to the lack of a bulky dc-link capacitor, which increases the reliability and the power density of the topology. However, the lack of a dc-link capacitor produces several disadvantages for heavily unbalanced operation at the four-leg output [60]. For instance, assuming that an unbalanced load is fed with a frequency ω_o at the output, then the negative/zero sequence load current component may produce double frequency ($\pm 2\omega_o$) power pulsations at the load. Considering the conservation of the instantaneous power (see [120]) and the lack of a dc-link capacitor buffer, then at the MC input side, fed by a balanced voltage supply of frequency ω_i, harmonic distortion in the current is produced with frequency components of $\omega_i \mp 2\omega_o$. To compensate the harmonic distortion at the MC input side, the *LC* power filter has to be redesigned, increasing the size of the capacitance and/or inductance. However, in this case, the advantages of the matrix converter to increase the power density, could be lost.

If a very reduced input current harmonic distortion of a four-leg converter is required, then the direct and the indirect four-leg matrix converters are not suitable topologies to provide electrical energy to loads with high levels of imbalance and/or harmonics.

6) FOUR-LEG INDIRECT MATRIX CONVERTER

The typical topology of a four-leg indirect MC is shown in Fig.6. This converter comprises two stages; a current source rectifier (CSR) and a voltage source inverter (VSI). The CSR stage of the converter is typically composed of 12 common-emitter-connected power switches coupled to free-wheeling diodes which form 6 bidirectional semiconductors, while its two-level VSI stage is composed of 8 power switching devices also coupled to free-wheeling diodes. Compared to

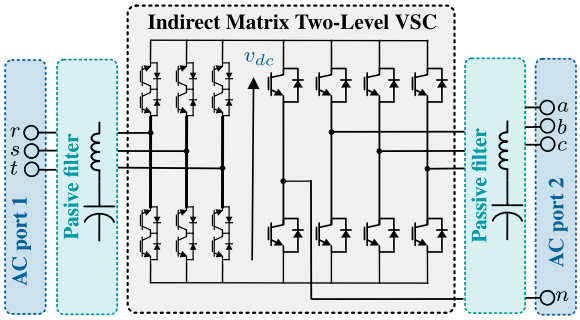

FIGURE 6. Four-leg indirect matrix converter topology.

the direct MC, the IMC has fewer switching devices, opens the application of multilevel operation at the VSI stage [121], which can be useful for handling unbalances and high-order harmonic components, and it also provides a dc-bus which can be used to connect multiple independent output ports through several VSIs (see [122]). The lack of a dc-link capacitor to filter out the instantaneous power oscillations produced by unbalanced/non-linear loads generate harmonic distortion in the IMC input current. This problem is similar to that produced in the four-leg direct MC (see the discussion above). Again, one the possible solution, is to redesign the *LC* input filter, increasing the power filter size and reducing the power density and specific power density of the topology [123].

Several applications have been reported for the IMC. It has been suggested as a suitable alternative for common-mode voltage minimization in motor drives [124], also as current power supply to provide balanced currents to unbalanced loads [125]–[127] or voltage power supply [128]. In [129] a four-leg indirect matrix converter is used to transform a single-phase system to a dual single-phase system to independently control two open-end windings of a single-phase machine. Furthermore, in [130], the converter has been proposed for Hybrid Electric Vehicle (HEV) applications, to provide both, three-phase AC voltage for motor drives and also a single-phase output voltage to provide electrical energy to the power compressors of the vehicle.

7) FOUR-LEG CURRENT SOURCE CONVERTER (CSC)

The typical topology of this converter is shown in Fig. 7. This converter is composed of 8 IGBTs each of them with a series-connected power diode. Additionally, the converter requires two dc-link inductors for its operation. The converter performs 16 different switching combinations, each one simultaneously closing only two switches of the converter, maintaining a constant current on the dc port of the converter. This topology becomes a good alternative for unbalanced and distorted current compensation. In [78], [131] the converter is proposed as active filter for unbalance and harmonic compensation. The CSC has also been proposed for minimizing common-mode output voltage using an innovative SVM technique, which takes advantage of the additional zero vector to effectively reduce the common-mode voltage and eliminates

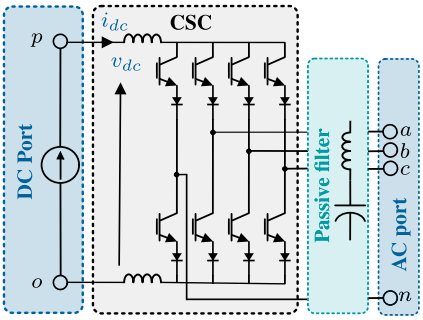

FIGURE 7. Four-leg current source converter topology.

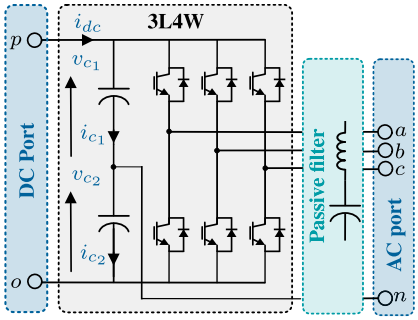

FIGURE 8. Three-leg four-wire converter topology.

undesirable bipolar current pulses generated in 3L4W CSIs (see [132]).

8) THREE-LEG FOUR-WIRE CONVERTER

Three-leg four-wire (3L4W) converters can be considered the first-generation technology to provide a circulation path for zero-sequence current in unbalanced and/or distorted systems. These converters are characterized for providing the fourth wire of the converter by splitting the dc-link voltage with two series-connected capacitors, generating a mid-point used for providing the output neutral wire of the converter. The most common example is shown in Fig. 8. Although this configuration is very simple, avoiding the implementation of an extra leg, it has two major drawbacks which limit its application: a) the capacitors used to create the dc mid-point must handle the full zero-sequence current, forcing the oversizing of the dc-link capacitance in order to maintain low dc-link voltage ripple oscillations [133]–[135] or the introduction of an additional inductance in the neutral wire [136]. This not only increases the footprint and cost of the converter but also reduces the lifetime of the capacitors reducing the reliability of the converter [137]–[139] and b) the output PTN voltages generated by the converter are physically limited to be 15,5% less than in four-leg converters [133] (no zero-sequence injection is allowed), under-utilizing the dc-link voltage of the converter and forcing the capacitors and semiconductors of the converter to handle larger voltage magnitudes to modulate nominal output voltages. Furthermore, any 3L4W converter topology produces less number of levels at its output PTN voltages compared to its four-leg version topology. To maintain power quality, the reduced number of could produce an increase in the output filter footprint.

Despite its drawbacks, the converter still can be a good alternative for some applications where the zero-sequence current is reduced and the power density of the converter is not critical. Thereby, the converter has been successfully implemented as UPS [140]–[142], STATCOM [143], [144] APF [26], [27], [145]–[152], UPQC [153]–[155] and DVR [156], [157]. In addition, it has also been proposed for other applications, such as compensator for balancing and eliminating harmonic distortion in electrical power generators [158], photovoltaic applications for reducing leakage ground current in PV panels [159] or as a power rectifier [160], [161].

Several 3L3W power converters, such as two-level converter [151] and three-level flying capacitor converter [162] have been modified by splitting the dc-link voltage by two series-connected dc capacitors to obtain the fourth wire of the converter. Other topologies, such as: three-level NPC converter [143], [149], [163]–[166], five-level NPC converter [167] and T-Type NPC converter [168] achieve the same goal by utilizing the natural split dc-link voltage of the topology. Although no additional series capacitors are required for these topologies, its capacitance has to be increased to handle the increase in voltage ripple produced by the zero-sequence current. Moreover, dc-link voltage utilization is still reduced in $\approx$ 15% [133] and the number of levels at the output PTN voltages is not increased when a split dc-link capacitance is utilized to obtain the fourth wire.

In order to modulate a three-leg four-wire converter, extended modulation schemes in a three-dimensional frame have been proposed. In [169]–[172] SVM methods in $\alpha\beta 0$ reference frame for two-level 3L4W converter are proposed. In [166] a similar technique is proposed using cylindrical coordinates. Later on, in [173] the technique is extended for multi-level converters. In addition, three-dimensional hysteresis control has been also proposed as an alternative [174], however this technique produces a higher current ripple at the zero-sequence output current. Also, carrier-based PWM methods have been successfully implemented in [161], [175].

B. ADVANCED FOUR-LEG CONVERTER TOPOLOGIES

Special modifications of standard four-leg topologies or innovative interconnections can be implemented to create new topologies four-leg converter topologies, which are studied in this section.

1) FOUR-LEG ACTIVE SPLIT DC-LINK CONVERTER

This topology is presented in Fig. 9, early presented in [176], the two-level four-leg split dc-link converter is composed of 8 power semiconductors. Unlike the standard two-level four-leg topology presented in Fig. 1, in this topology, the dc-bus is split through two capacitors connecting its neutral

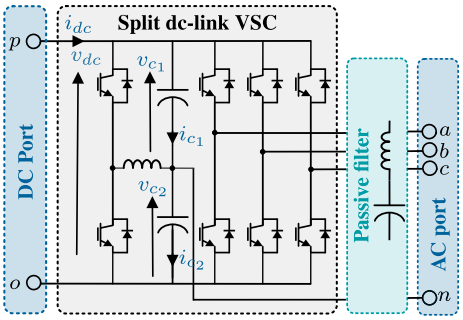

FIGURE 9. Four-leg active split dc-link converter topology.

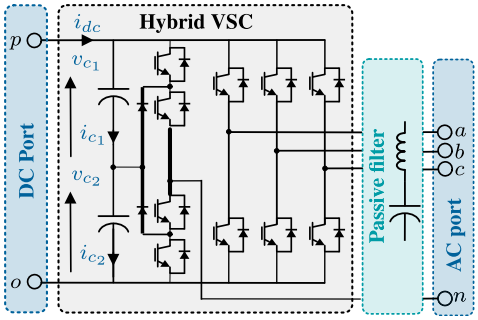

FIGURE 10. Four-leg hybrid-Legs converter topology.

point through an inductor to the output of the fourth-leg. The converter provides full dc-link voltage utilization by actively introducing third harmonic components into the dc-bus [177]. Clamping the mid-point of the dc-link voltage to the output neutral wire, greatly reduces the magnitude of the high-frequency voltage between the parasitic capacitance formed between positive/negative dc-bus poles and ground terminals, reducing leakage common-mode current [133]. In addition, the dv/dt produced in the fourth leg is also minimized which greatly reduces associated Electromagnetic Interference (EMI) problems. Despite these advantages, this converter requires a choke neutral inductor designed to handle nominal zero-sequence current, a pair of series-connected dc capacitors, and its associated balancing algorithm which are its major drawbacks. It must be highlighted that this converter is suitable for low-voltage distribution applications, such as vehicle-to-grid applications [178], active power filter [176] or balanced power supply for unbalanced loads [179].

2) FOUR-LEG HYBRID-LEGS CONVERTERS

A Four-leg hybrid-legs converter is shown in Fig. 10. As seen, this topology comprises three two-level legs and one three-level NPC leg used as its fourth-leg [180]. Thereby, the converter utilizes 10 power semiconductor devices with their corresponding free-wheeling diodes and 2 additional clamping power diodes. Due to the nature of the three-level NPC converter, it also requires two series-connected capacitors. Similar to the previously shown active split dc-link converter, this topology arises as an alternative to reduce large dv/dt and EMI problems associated with the commutation at the neutral leg of the converter [180]. The voltage between the fourth wire and ground connection oscillates between $\pm v_{dc}$ for a two-level leg. Alternatively, also an additional flying capacitor fourth-leg has been added to a three-level NPC converter to increase reliability in fault-tolerant four-leg converters [181]. Note that unlike the actively split dc-link topology or 3L4W converter, this approach does not require splitting the dc-bus, thereby, for instance, an FC leg can be also an alternative to be used as the fourth leg.

3) FOUR-LEG DUAL-OUTPUT CONVERTER

As an alternative to driving multiple loads simultaneously, a 12 switches four-leg dual-output converter was proposed in [182]. This converter is presented in Fig. 11, it provides two independent sets of three PTN voltages with independently regulated frequency and magnitude. The converter is modulated using a special PWM algorithm which, according to the output frequency of each port can operate in equal frequencies (EF) or different frequencies (DF) operation modes [183]. Also, [184] proposed a space-vector modulation based on the *abc* frame for this converter, achieving a minimum THD and switching losses. The maximum achievable modulation index on each port depends on the phase shift between both sets of PTN output voltages and their frequencies. Thereby, in EF mode the converter can provide a maximum modulation index of $3/\sqrt{2}$ and it fully utilizes the dc-link voltage if the phase-shift between both sets of PTN voltages is 0°. This range is limited when the phase shift is not 0°. For instance, the modulation index is restricted to 0,97 for a phase shift of 12° between both sets of PTN output voltages. The maximum modulation index is even more restricted for DF operation mode [182]. Thus, the operational point of each port of the converter, i.e. its frequencies and phase-shift between them, determines the dc-link voltage utilization and the dc-link voltage magnitude, and the rating of the semiconductor devices. This converter becomes a good alternative when operated at equal frequency in both ports, because it reduces by 25% the total number of devices required, providing similar performance to that obtained using two independent two-level four-leg converters. However, its performance is reduced when signals of different frequencies and/or phase-shift are modulated in each output port. More research is required to improve its performance in DF operation mode.

4) INTERCONNECTION OF FOUR-WIRE CONVERTERS

The connection of several converters to interface four-wire networks have been also explored [42]. The main advantage of this methodology is to use the simple control and modulation of each independent converter, the possibility to increase the number of levels, and also the capability to provide power modularity and scalability. The most popular manner of interconnecting several converters is in parallel, as shown in Fig.12(a). In this figure, a set of two or three converters, each of them comprised of two, three, or four legs,

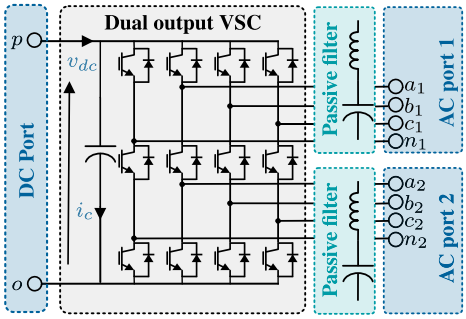

FIGURE 11. Four-leg dual-output converter topology.

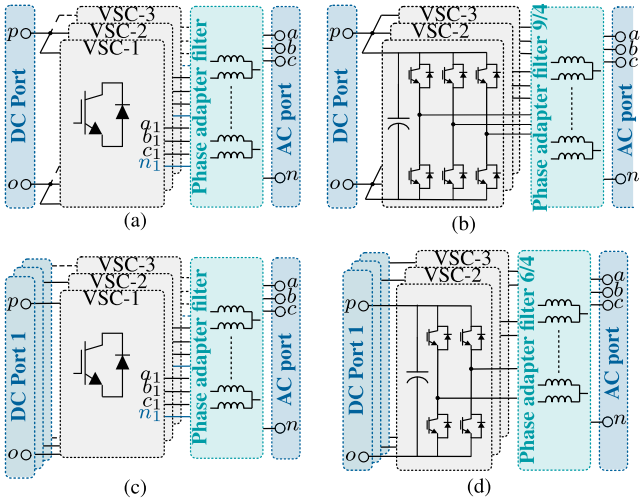

FIGURE 12. Generalized interconnected four-wire converters topology: (a) Parallel VSC, (b) 3 parallel-connected two-level inverters, (c) cascade VSC, (d) 3-cascade H-bridge converter.

share the same dc-link port and their outputs are interconnected to interface a four-wire network [32]. Fig. 12(b) shows an example of three parallel-connected three-leg converters. As they share the same dc-link, the direct interconnection between outputs poles is not allowed, as it shall cause a short circuit, and specially designed filters are required to adapt the 6, 8, 9, or 12 output phases of the converter outputs to the 4 wires required at the PCC (see Fig. 15). The dc-port of Fig. 12(b) can be either floating (as for APF or UPFC applications [185]), connected to a power source (as for voltage power supply [40], [186]) or linked to another AFE Converter forming a back-to-back configuration [42]. The maximum number of voltage levels produced by the converter is calculated as 2^n, with n being the number of parallel-connected converters. This is one of the major advantages of this configuration. Hence, usually, the converters are modulated as multilevel, using level-shifted PWM [187], with the references being obtained from synchronized controllers.

Alternatively, a similar approach can be achieved for interconnecting several converters without sharing the same dc-link, as illustrated in Fig. 12(c) [41]. In this case, it is possible to interconnect the dc-bus of each converter to a different isolated power supply, AFE converter or leave them as floating voltages (for APF applications). Thereby, in this configuration it is possible to interconnect directly the output phases among different converters, providing more flexibility. In [41], as presented in Fig. 12(d) (and Fig. 13), a Y interconnection of three converters, each of them formed by two legs, is presented. The isolated dc-bus allows direct interconnection of converter output phases to form the output neutral wire, avoiding the use of transformers at the output filter. In [188], each dc-port of the converter presented in Fig. 12(d) is obtained by connecting a bidirectional buck converter to each of phase of an AC system, achieving a series-connection of the converter with the grid and providing regulated AC current to an unbalanced four-wire system. In [43], different configurations for interconnecting converters with isolated dc-bus using two-leg and three-leg based converters are proposed. Reference [43] also explores the use of hybrid legs for each of the interconnected converters, using two-level and three-level NPC legs in the same converter to increase voltage levels and reduce EMI problems. Interconnecting converters can also result in modular multilevel converters (MMCs), in [189] the author proposes a four-leg MMC for STATCOM applications, extending the advantages of this types of converters, such as low dv/dt, reliability, and scalability, to unbalanced loads.

Tab. 6 summarizes the features of each topology comparatively. It also highlights some of its applications.

C. FOUR-WIRE FILTER CONFIGURATIONS

Output filters used in four-leg converters can be mainly divided into two groups: 4-to-4 phases filters and N-to-4 phases filters. The first group interconnects a single four-leg converter to a point of common coupling (PCC), while the second interconnects several converters that form N phases to a four-wire PCC.

1) 4-TO-4 PHASES PASSIVE FILTERS

Fig. 13 summarizes the filter topologies reported for a 4-to-4 passive filter, which input-output variables are defined as:

$$\boldsymbol{v}_{a_1b_1c_1} = \begin{bmatrix} v_{a_1n_1} \\ v_{b_1n_1} \\ v_{c_1n_1} \end{bmatrix}, \quad \boldsymbol{v}_{abc} = \begin{bmatrix} v_{an} \\ v_{bn} \\ v_{cn} \end{bmatrix}, \boldsymbol{i}_{abc} = \begin{bmatrix} i_a \\ i_b \\ i_c \end{bmatrix} \quad (1)$$

Fig. 13a shows the simplest first-order L filter for output current control, while Fig. 13b to Fig. 13e show different configurations for: i) LCL third-order filter for output current control, if the output inductor L_2 is considered or ii) LC second-order filter for output voltage control, if the output inductor L_2 is neglected. These filters are usually designed to have the same parameters in the three phases (a-b-c), but the design of the neutral inductor and capacitor (L_n and C_n) has to be done separately and would depend on the load unbalance [190] and the non-linearities of the system.

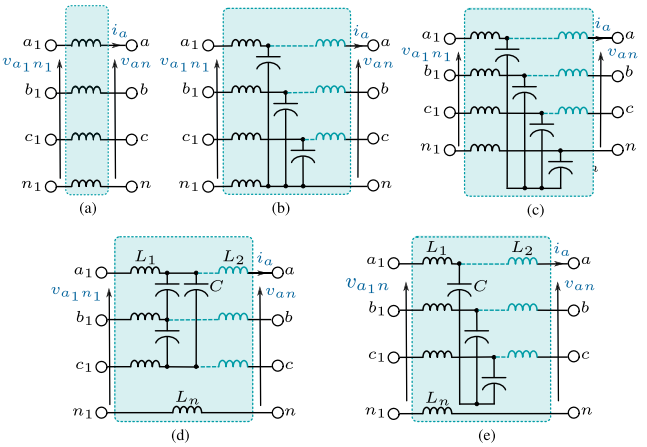

FIGURE 13. 4-to-4 phases passive filters configurations. (a) First order L filter, (b) LC or LCL filter with Y connected capacitors, where the neutral-point of the capacitors is directly connected to neutral-wire, or (c) neutral-point connected to neutral-wire through a capacitor C_n. Also is possible to obtain LC and LCL filter connecting capacitors in (d) Δ or (e) floating star connection, without any connection to the neutral-wire.

a: FILTERS FOR CURRENT CONTROL

The first-order L filter, and third-order LCL filters are commonly implemented for current control in grid-connected applications, or any application where output current needs to be controlled. Although the L filter is very simple, robust, and does not possess any resonance frequency, the LCL filter provides higher attenuation of high order harmonics and a higher power density, allowing a smaller footprint and better performance [191]. However, its resonance frequency has to be carefully selected to avoid overlapping with the harmonic spectrum of the modulated output voltage of the converter which causes large resonance currents. This is especially challenging in four-wire applications, as it is connected to unbalanced and non-linear loads [192]. Alternatively, methods based on state variable feedback, for instance active damping or virtual impedance algorithms could be used for the control of lightly damped power filters (see [193], [194]).

Considering that the L or LCL filter depicted in Fig. 13, is connected to an unbalanced passive load, as depicted in Fig. 14a, the dynamic model of the system can be derived by:

$$\boldsymbol{v}_{a_1b_1c_1} = \mathbf{Z}_{eq}\boldsymbol{i}_{abc} \tag{2}$$

$$\mathbf{Z}_{eq} = \mathbf{Z}_f + \mathbf{Z}_{Load} \tag{3}$$

where matrix $\mathbf{Z}_f$ stands for the dynamic of filters and $\mathbf{Z}_{load}$ represent the unbalanced load, which can be expressed as:

$$\mathbf{Z}_f = \begin{bmatrix} Z+Z_n & Z_n & Z_n \\ Z_n & Z+Z_n & Z_n \\ Z_n & Z_n & Z+Z_n \end{bmatrix} \tag{4}$$

$$\mathbf{Z}_{load} = \begin{bmatrix} Z_a & 0 & 0 \\ 0 & Z_b & 0 \\ 0 & 0 & Z_c \end{bmatrix} \tag{5}$$

the parameters of matrix $\mathbf{Z}_f$ for each L or LCL filter of Fig. 13 are known and are presented in Table 2. If the load impedance matrix $\mathbf{Z}_{load}$ is known and unbalanced, the dynamic between the output voltage and current, defined by (2), can not be decoupled and multiple-input multiple-output (MIMO) control or complex state variables control need to be implemented [195]. Usually, the load impedance matrix is unknown and varies during converter operation. In this case, the output $\mathbf{v}_{abc}$ can be measured and considered as an external perturbation, which is feed-forwarded into the control loop, to obtain a plant independent of the load impedance parameters [32], [153]. This approach is equivalent to consider that the filter is connected to a grid (balanced or unbalanced), as presented in Fig. 14c. Thus, the dynamic relation can be described as:

$$\boldsymbol{i}_{abc}(s) = \mathbf{Z}_f^{-1}(s) \cdot \Delta\boldsymbol{v}_{abc}(s) \tag{6}$$

$$\Delta\boldsymbol{v}_{abc} = \boldsymbol{v}_{a_1b_1c_1} - \boldsymbol{v}_{abc} \tag{7}$$

Applying $\alpha\beta0$ transformation to (6), and due to the parameters symmetry of filters, it is possible to decouple the system, leading to three independent SISO systems:

$$\Delta v_{\alpha\beta0} = \underbrace{T_{\alpha\beta0}\mathbf{Z}_f T_{\alpha\beta0}^{-1}}_{\mathbf{Z}_{\alpha\beta0}} \mathbf{i}_{\alpha\beta0} \tag{8}$$

$$\mathbf{Z}_{\alpha\beta0}^{-1}(s) = \begin{bmatrix} Z_\alpha^{-1}(s) & 0 & 0 \\ 0 & Z_\beta(s)^{-1} & 0 \\ 0 & 0 & Z_0(s)^{-1} \end{bmatrix} \tag{9}$$

$$\frac{i_j(s)}{\Delta v_j(s)} = Z_j^{-1}; \quad j = \{\alpha, \beta, 0\} \tag{10}$$

TABLE 2. Dynamic coefficients of $\mathbf{Z}_f$ for the first and third-order L and LCL filters of Fig. 13.

	Z	Z_n
Fig. 13a	sL	sL_n
Fig. 13b	$s^3CL_1L_2 + s(L_1+L_2)$	$s^3CL_2L_n + sL_n$
Fig. 13c	$s^3CL_1L_2 + s(L_1+L_2)$	$-s^3L_2\frac{C^2L_1-CC_nL_n}{3C+Cn} + sL_n$
Fig. 13d	$3s^3CL_1L_2 + s(L_1+L_2)$	$-s^3CL_1L_2 + sL_n$
Fig. 13e	$s^3CL_1L_2 + s(L_1+L_2)$	$-\frac{1}{3}s^3CL_1L_2 + sL_n$

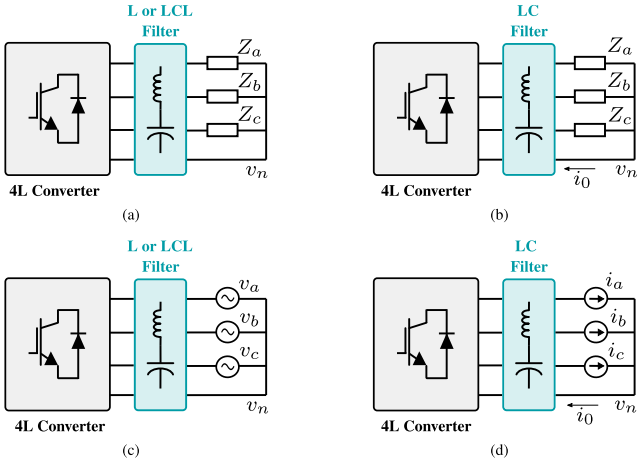

FIGURE 14. Four-wire system considered for dynamic transfer function. a) L or LCL filter with unbalance load, b) LC filter with unbalance load, c) L or LCL filter with high-impedance load or voltage sources, d) LC filter with short-circuit load or current sources.

TABLE 3. Dynamic coefficients of $\mathbf{Z}_{\alpha,\beta,0}$ for the first and third-order L and LCL filters of Fig. 13.

	$Z_\alpha(s)$=$Z_\beta(s)$	$Z_0(s)$
Fig. 13a	sL	$(sL+3sL_n)/2$
Fig. 13b	$s^3CL_1L_2+s(L_1+L_2)$	$s^3CL_2(L_1+3L_n)/2+$ $s(L_1+L_2+3L_n)/2$
Fig. 13c	$s^3CL_1L_2+s(L_1+L_2)$	$s^3CL_2(L1-3\frac{CL_1-C_nL_n}{3C+Cn})+$ $s(L_1+L_2+3L_n)$
Fig. 13d	$3s^3CL_1L_2+s(L_1+L_2)$	$s(3L_n+L_1+L_2)/2$
Fig. 13e	$s^3CL_1L_2+s(L_1+L_2)$	$s(3L_n+L_1+L_2)/2$

which parameters are summarized in Table 3 and enable independent controller design for each coordinate.

In four-wire systems, the voltage $\Delta \boldsymbol{V}_{abc}$ is usually unbalanced. Therefore, (10) can be directly used when resonant controllers are implemented. However, if PI controllers in dq frame are used instead, it is convenient to derive the positive, negative and zero sequences. Applying Fortescue transformation (T^{+-0}) [196] to (6):

$$\Delta \boldsymbol{v}^{+-0} = \underbrace{T^{+-0}\boldsymbol{Z}_f T^{+-0^-}}_{\boldsymbol{Z}^{+-0}} \boldsymbol{i}^{+-0} \tag{11}$$

$$\boldsymbol{Z}^{+-0^{-1}}(s) = \begin{bmatrix} Z^{+^{-1}}(s) & 0 & 0 \\ 0 & Z^{-^{-1}}(s) & 0 \\ 0 & 0 & Z^{0^{-1}}(s) \end{bmatrix} \tag{12}$$

which also represents a decoupled system, leading to independent SISO systems to relate input voltage with output current. The positive ($Z^+(s)$) and negative ($Z^-(s)$) sequence filter transfer function have the same coefficients as $Z_\alpha(s)$ and $Z_\beta(s)$.

From Table 3, it is straightforward to show that the zero-sequence plant is different to the $\alpha\beta$ dynamic plants, and therefore controllers for each of them should be tuned differently. Moreover, it is observed that L_1 and L_2 line inductors are always present at the zero-sequence dynamics. Thereby, although the neutral-wire inductor L_n is not implemented, an equivalent, different from zero, zero-sequence plant is present, which gives the dynamic to the zero-sequence current. Notice that when L_n (and C_n) is not implemented, the $Z_0(s)$ present the same dynamic as the terms $Z_\alpha(s)$ and $Z_\beta(s)$ for filters of Fig. 13a to Fig. 13c (most common configurations). Thus, no special considerations for the zero-sequence controllers are required. However, this is not true for configurations of Fig.13d and Fig.13e, which $Z_0(s)$ term is always different to $Z_\alpha(s)$ and $Z_\beta(s)$ terms and independent controllers should be implemented regardless of the value of L_n.

A common practice to implement current controllers in the filter configurations of Fig. 13b to Fig. 13e is to split the third-order LCL filter equation into three first-order equations and implement nested controllers [197], [198]. Also, if the capacitor voltage dynamic is considered much slower than the current dynamic at L_1, it would be equivalent to consider that L_1 is directly connected to a grid. Thus, the capacitor voltage is controlled by the current through L_1. This voltage controls the current through the line inductor L_2, and acts as a controlled voltage source.

b: FILTERS FOR VOLTAGE CONTROL

Neglecting the output inductor L_2 from filters depicted in Fig.13(b) to Fig.13(e), second-order LC filters, aimed to control output voltages $\boldsymbol{v}_{abc}$ are obtained.

Due to its neutral-wire connection, Fig. 13(b) and Fig. 13(c) are the best choices for voltage source converters such as UPS, GPU and programmable power supplies [61], where each of the PTN voltages has to be controlled independently. Note that configurations shown in Fig. 13(d) and Fig. 13(e) can be implemented to control PTP output voltages for three-phase loads, using the fourth leg to control neutral-to-ground voltage for reducing or eliminating the leakage currents (or ground-loop currents), usually present in MV machine drives or PV applications [69], [179]. It is important to notice that the delta connection of Fig. 13(d) can provide a smaller footprint compared to Fig. 13(e) (as the equivalent capacitance required is three times smaller), however, configuration of Fig. 13(e) provides an extra connection point, which can be used for equipment grounding.

The modulation of the four-leg converter and harmonic content of non-linear loads has to be regulated to avoid harmonic content close to the resonance frequency of the LC filers [44]. A typical design rule is to tune the resonance frequency of the filter at least ten times higher than the fundamental frequency of the voltage or currents that are being controlled and ten times lower than the dominant harmonic component of the converter output [199]. However, when several harmonics are being compensated, a more accurate design is needed and the study of stability margins is required [44].

From Fig. 14(b), the dynamic between the output voltage of the converter and the output voltage of the LC filter, considering the unbalanced load, can be obtained as:

$$\boldsymbol{v}_{a_1b_1c_1}(s) = \boldsymbol{A}_{eq}(s)\boldsymbol{v}_{abc}(s) \tag{13}$$

where $\boldsymbol{A}_{eq}(s)$ is a matrix formed by the terms of the unbalanced load and the filter. When filter and load parameters are known, (13) could be used to control the output voltage, however, it can not be decoupled and multiple-input multiple-output (MIMO) control or complex state variables control need to be implemented [195]. Usually, the load impedance is unknown and varies during converter operation. Therefore, it is convenient to neglect the output load into the dynamic and measure the output current $\boldsymbol{i}_{abc}$ instead (see Fig. 14(d)). This current is considered a perturbation and feed-forwarded into the control scheme [200]. Thus, the following relationship between the output voltage of the converter and the output voltage of the LC filters, i.e voltage plant, can be obtained:

$$\boldsymbol{v}_{a_1b_1c_1} = \boldsymbol{A}\boldsymbol{v}_{abc} \tag{14}$$

where $\boldsymbol{A}$ represents the dynamic of each LC filter (without including the load parameters). Similarly to (10), applying

TABLE 4. Dynamic coefficients of A for the second-order LC filters of Fig. 13.

	$A_\alpha(s)$=$A_\beta(s)$	$A_0(s)$
Fig. 13b	s^2CL_1+1	$1+s^2C(L_1+3L_n)$
Fig. 13c	s^2CL_1+1	$1+s^2C(L_1+3\frac{(CL_1-C_nL_n)}{3C+C_n})$
Fig. 13d	$3s^2CL_1+1$	1
Fig. 13e	s^2CL_1+1	1

TABLE 5. Dynamic coefficients of Z' for the first-order C filters of Fig. 13.

	Z'
Fig. 13b	sC
Fig. 13c	$sCC_n/(C_n+C)$

$\alpha\beta0$ transformation to (14),

$$\boldsymbol{v}_{\alpha\beta0_1} = \underbrace{T_{\alpha\beta0}\boldsymbol{A}T_{\alpha\beta0}^{-1}}_{\boldsymbol{A}_{\alpha\beta0}}\boldsymbol{v}_{\alpha\beta0} \tag{15}$$

$$\frac{I_j(s)}{\Delta V_j(s)} = A_j^{-1}; \quad j=\{\alpha,\beta,0\} \tag{16}$$

where $\boldsymbol{A}_{\alpha\beta0}$ possesses the same structure as (9) and its parameters can be found in Table 4. In presence of unbalanced load currents, the system can be expressed in its symmetrical components, where positive and negative sequence transfer functions, $A^+(s)$ and $A^-(s)$, are equal, and equal to $A_\alpha(s)$ (or $A_\beta(s)$).

Although the second-order transfer function can be directly used to control the output voltage with linear controllers [110], [201] A common practice is to split the second-order plants (see table 13) into two first-order plants, i.e. current control at L_1 and the voltage control at C, implementing a voltage and current nested control scheme.

The first order plant that relates the voltage at the capacitors with the currents can be obtained by KCL at the capacitor, where the capacitors voltage gets related to the converter current and load current as follows:

$$\Delta\boldsymbol{i}_{abc}(s) = Z'^{-1}(s)\cdot\boldsymbol{v}_{abc}(s) \tag{17}$$

$$\Delta\boldsymbol{i}_{abc}(s) = i_{a_1b_1c_1} - i_{abc} \tag{18}$$

Without the coupling terms seen by the current plant, the voltage sees the same dynamic at every line:

From Table 4, it is straightforward that LC filter of Fig. 13(b) and Fig. 13(c) provide a second-order dynamic for the zero-sequence component. This is paramount, as this provides the capability to control the output zero-sequence voltage of the filter. Although for Fig. 13(d) and Fig. 13(e), the magnitude of the output zero-sequence voltage can still be controlled (as it is a degree of freedom of the converter), it is not filtered, leading to a switched signal with high dv/dt. For a dq representation of (8) and (16), the operator "s" must be replaced by "$s+j\omega$", as presented in [110], being ω the rotational frequency of the dq frame.

2) N-TO-4 PHASES PASSIVE FILTERS

The generalized four-wire converters from Fig. 12 requires passive filters that have N number of inputs connectors. For this reason, the passive filters presented in Fig. 13 can not be used. The N-to-4 phases passive filters topologies are presented in Fig. 15.

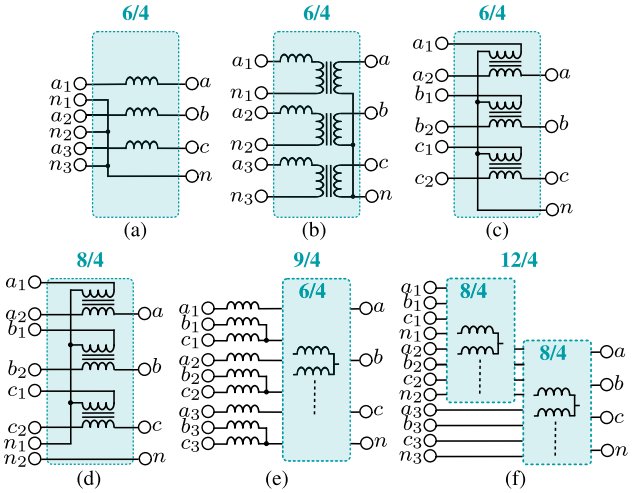

FIGURE 15. 6-to-4 phase reduction filters, using three independent single-phase voltages as input system, and (a) without using transformer, (b) using transformer and generating the output neutral-wire in the secondary side, or (c) using two three-phase input systems (without neutral-wire), and generating the output neutral-wire at the primary side of transformers, similarly (d) 8-to-4 phase reduction filter, but with the input system including neutral-wire, (e) 9-to-4 filter transformer and (f) use of 8-to-4 phase reduction filters to generate 12-to-4 phase reduction filter.

In [202], the influence of circulating currents on 6-to-4 poles adapter filter is discussed. Filter in Fig. 15(a) is the simplest solution to avoid a short-circuit from sub-converters that share the same DC-Link, but it leads to large zero-sequence circulating currents [203]. An improved solution is to use a transformer as Fig. 15(b) where those zero-sequence circulating currents are eliminated. A similar principle is shown in Fig. 15(c), where the neutral wire is obtained from the primary winding of the transformer, and the input of the transformer is formed by two three-phase systems without a neutral wire. Same approach is showed Fig. 15(d), but the input system now contains the neutral wire, leading to a 8-to-4 filter [43]. The previous interconnection, before facing the filter, can also be implemented to reduce the number of input phases, as presented in Fig. 15(e). In this case, using a previous interconnection of phases it is possible to use a 6-to-4 filter to transform 9 to 4 phases. To continue scaling the number of phases, the arrangement of previous filters can be used, as presented in Fig. 15(f), which uses two 8-to-4 filters to achieve 12-to-4 phases transformation, notice that the output of the first 8-to-4 filter is used as the input for the second 8-to-4 filter.

III. FOUR-LEG CONVERTERS: MODULATION TECHNIQUES

The incorporation of a fourth leg, and the requirement of zero-sequence control, has generated new modulation strategies. These strategies, extensions of developed modulation techniques for three-leg converters [204], can be mainly divided

TABLE 6. Qualitative summary of features and comparison of the reported four-leg topologies and their application. All topologies have full utilization of dc-link, except for the two-level 3L4W topology.

Topology	Mature Technology	Topology Complexity	Power Level	Filters size	Zero-Sequence Volt/Curr Control	Applications Applications
4L 2LVSI	High	Low	Low	Medium	High	Drives [69], [92] UPS [63], [74]–[76] GPU [28] APF [32], [77]–[79] UPQC [80]–[82] DVR [83], [84]
4L NPC	Medium	Medium	Medium-High	Small	Medium-High	RES [96] GPU [61] MV UPS [100] P. supply [97]
4L T-Type	Low	Medium	Medium-High	Small	Medium-High	Drives [105] P. supply [36]
4L FC	Medium	High	Medium-High	Small	Medium-High	RES [106], [107] APF [35], [108]
4L MC	High	High	Low	Small	Medium	UPS [114] GPU [37]
4L IMC	Low	High	Low	Small	Medium	Drives [124], [129], [130] P. supply [125]–[128]
4L CSC	Low	Low	Low		High	APF [78], [131]
3L 2L4W	High	Low	Low	Large	Low	APF [26], [27], [145]–[152] UPS [140]–[142] STATCOM [143], [144] UPQC [153]–[155] DVR [156], [157]
4L Active Split DC-Link	High	Low	Low	Medium	Medium	V2G [178] APF [176] P. supply [179]
4L Hybrid Legs	Medium	Medium	Low	Small	Medium-High	RES [180], [181]
4L Dual-Output	Medium	Medium	Low	Large	Medium-Low	Drives [182], [183]
4L Interconnected	Medium	Medium	Medium	Large	High	APF [185], [188]

into three main groups of methods: a) 3D Space Vectors PWM (3D-SVPWM) methods in $\alpha\beta 0$ frame, b) 3D-SVPWM methods in *abc* frame and c) Carrier-based PWM methods (CPWM).

Similarly to standard 2D-SVM techniques, to modulate a reference voltage vector in a 3D space, the following steps have to be considered:

- To identify the nearest *stationary vectors* that enclose the reference vector (represented as one point in $\alpha\beta 0$ or *abc* plane).
- To calculate the *dwell-time* for each of the selected stationary vectors.
- To define a sequence pattern for the selected stationery vectors, that achieves the *minimum switching transition principle* [48].
- Apply the selected vectors with the associated *dwell-times* during the next sampling time.

The sequence pattern to arrange these vectors through the sampling time T_s can be classified by the use of redundancies on a sampling time, as: *Full-Redundancy Sequence* and *Single-Redundancy Sequence*. The first group uses all redundancies of the redundant vectors while the second group uses only one redundancy. Also, they are classified by the symmetry on T_s as: Symmetric or Asymmetric. The first increases the switching frequency but improves the harmonic spectrum, while the second reduces the switching losses at the cost of a higher distortion [205], [206]:

On the other hand, carrier-based PWM methods for balanced systems are simpler than SVM methods, as they just compare a high-frequency triangular carrier signal with the reference signal to directly control the devices that modulate the output phase voltages in a VSI. However, unbalanced systems increase the difficulty of controlling the fourth leg; Moreover, in the carrier-based PWM, the redundant vectors cannot be used as degrees of freedom as in SVM [207].

A. SPACE VECTOR MODULATION IN $\alpha\beta 0$ REFERENCE FRAME

The most common modulation technique in three-leg converters is the Space Vector Modulation (SVM) in $\alpha\beta$ coordinate frame [205], [206]. In four-leg converters, a zero-sequence voltage and current have to be also controlled, leading to the extension of typical SVM in $\alpha\beta$ coordinates frame to a three-dimensional $\alpha\beta 0$ [79]. Thereby, the voltage vectors generated by the four-leg converter create a three-dimensional modulation space, it was first proposed in [208]–[210] for a two-level VSI and then extended for multilevel converters in [211]. Fig. 16 shows the three-dimensional available modulation space for a four-leg VSI. Different topologies of four-leg VSI generate a different number of stationary vectors inside this

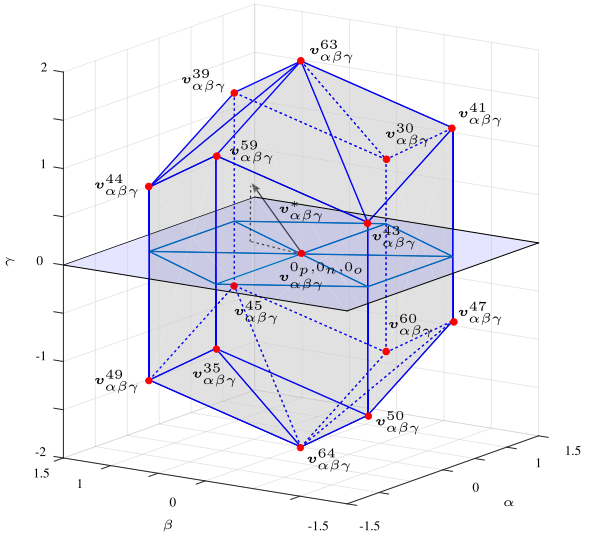

FIGURE 16. Outer three-dimensional boundaries for a four-leg inverter. Red points indicates the 16 vectors for a two-level inverter.

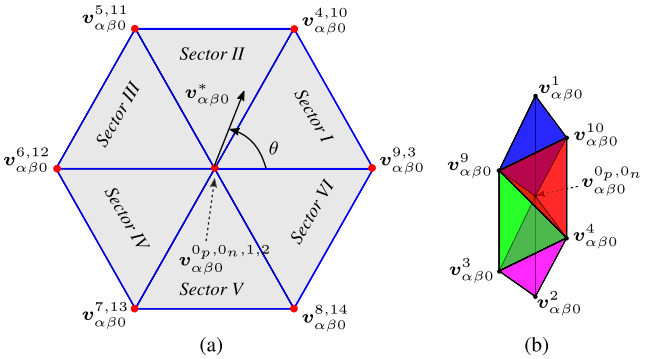

FIGURE 17. (a) Intersection with the $\alpha\beta$ plane. (b) Sector I in the $\alpha\beta\gamma$ space for a two-level four-leg VSI.

region, which allows a finer resolution to modulate output voltages, i.e. voltage levels. However, the three-dimensional boundaries are the same for any topology and it is defined by the magnitude of the dc-link voltage.

To identify the region formed by the four nearest *stationary vectors* that enclose the reference vector, a three-dimensional search must be done on the space depicted in Fig. 16, which determines the pentahedron formed by the four *stationary vectors* that contains the reference vector. This search can be done by look-up tables [205]. Although this method is robust and has been proven successfully, it is not practical for implementation in converters with more than three levels, as look-up tables are too extensive and the search process demands high computational effort [212]. A simplified tetrahedron identification method, which does not require look-up tables, is presented in [48]. In this method, for each sampled reference vector a two-level modulation space is generated and the tetrahedron is selected as shown on Fig. 17. Thereby, the method can be implemented regardless of the number of levels of the converter. Alternatively, the computational burden can be reduced by avoiding the trigonometric functions required in most methods using barycentric coordinates [213] or the first-order equations of the curve fitting technique to reduce calculation time [214].

Once obtained the four *stationary vectors* $\boldsymbol{v}^{s1}_{\alpha\beta0}$, $\boldsymbol{v}^{s2}_{\alpha\beta0}$, $\boldsymbol{v}^{s3}_{\alpha\beta0}$ and $\boldsymbol{v}^{0}_{\alpha\beta0}$ that enclose the reference vector, their *dwell times* can be calculated as:

$$\begin{bmatrix} d_1 \\ d_2 \\ d_3 \end{bmatrix} = T_s \begin{bmatrix} v^{s1}_{\alpha} & v^{s2}_{\alpha} & v^{s3}_{\alpha} \\ v^{s1}_{\beta} & v^{s2}_{\beta} & v^{s3}_{\beta} \\ v^{s1}_{0} & v^{s2}_{0} & v^{s3}_{0} \end{bmatrix}^{-1} \begin{bmatrix} v^{*}_{\alpha} \\ v^{*}_{\beta} \\ v^{*}_{0} \end{bmatrix} \tag{19}$$

$$d_0 = T_s - d_1 - d_2 - d_3 \tag{20}$$

where T_s represents the sampling time and d_0 to d_3 the *dwell time* for the corresponding *stationary vectors*. To avoid the calculation of the inverse matrix at (19) at each sampling time, a preset look-up table with the values of the inverse matrix for each tetrahedron is usually employed [215]. Another method is to use the already calculated determinants of the baryocentric coordinates to obtain the dwell times [216].

This implementation of the modulation presents several advantages compared to its analogue *abc* reference frame, such as: a) avoid transformation from $\alpha\beta\gamma$ to *abc* coordinate system of the control references given by external controllers, b) direct control and visualization of the zero-sequence component, important in numerous applications [52], [152], [154], [208]–[210], c) simple implementation of overmodulation algorithms, specially important in power quality conditioners [217], [218] and d) straight implementation of even harmonics elimination, specially important in grid-connected applications [205]. In addition, it can be applied in matrix converters decoupling the input from the output variables [45]. A generalized linear transformation for arbitrary number of phases and voltage levels has been presented in [219], [220], the method has low computational effort and has been implemented in FPGA, however, it has been validated in five-phase drive application.

B. SPACE VECTOR MODULATION IN abc REFERENCE FRAME

Instead of using the $\alpha\beta0$ transformation, a Space Vector based modulation technique implemented in an orthogonal system corresponding with the three phases of the inverter *abc*, form the *abc* reference frame, it was firstly introduced in [211] for two-level converters. This technique was later extended for multilevel converters in [221]. This modulation is very similar to SVM in $\alpha\beta0$. However, it avoids mathematical calculation related to the $\alpha\beta0$ transform, and the search for vectors that enclose the reference vector can be easily achieved. Fig. 18 shows the modulation space created in *abc* coordinate frame.

Similarly to standard $\alpha\beta0$ SVM technique, to modulate a reference voltage vector which is inside this region, the closest *stationary vectors* and corresponding *dwell times* need to be found.

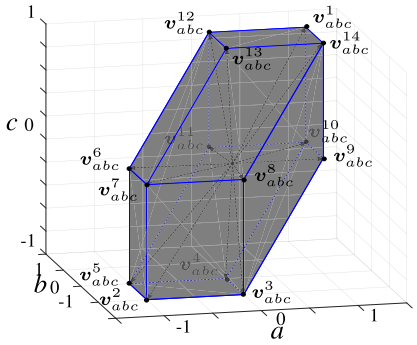

FIGURE 18. Modulation region for a two-level four-leg converter in *abc* coordinate frame.

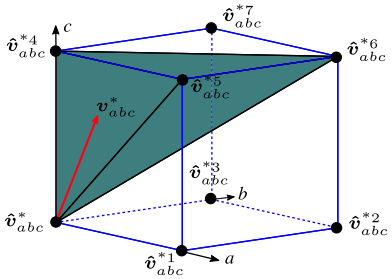

FIGURE 19. Six tetrahedrons are formed by the vertex of the cube from the pivot vector, here just one is shown containing the reference vector in red.

Assuming a reference vector:

$$\boldsymbol{v}^*_{a_1b_1c_1} = \left[v_{an}, v_{bn}, v_{cn}\right]^T \tag{21}$$

Calculating the smallest following integer of each coordinate of (21) with the floor function $\lfloor\ \rfloor$ as:

$$\hat{\boldsymbol{v}}^*_{abc} = \left[\lfloor\hat{v}^*_{an}\rfloor, \lfloor\hat{v}^*_{bn}\rfloor, \lfloor\hat{v}^*_{cn}\rfloor\right]^T \tag{22}$$

where $\hat{\boldsymbol{v}}^*_{abc_f}$ is one of the *stationary vectors* that can modulate $\boldsymbol{v}^*_{abc_f}$, and will work as a pivot vector to find the others. Thereby, in a four-leg two-level inverter, $\hat{\boldsymbol{v}}^*_{abc_f}$ represents one of the 16 switches combinations available. Based on this pivot a cube that contains the reference vector is created (see Fig. 19), where each of the eight vertexes is a potential *stationary vector*, but just four are needed. Thereby, in order to identify these four vertexes, that contains the reference vector, a three dimensional search must be done.

The algorithm for the three dimensional search in [221] achieves simple identification of the *stationary vectors* and calculation of their *dwell times* by basic operations. However, it does not recognize whether the reference vector remains inside the region presented in Fig. 18 or not. This could result in selecting a set of *stationary vectors*, which do not belong to the allowable modulation space. To assure proper operation of the converter under all conditions, avoiding the erroneous selection of *stationary vectors* or *dwell times* calculation, identi?cation of these non-feasible switching combinations is required, which would increase the computational burden. For the best knowledge of the authors, a solution for this issue or an overmodulation method for limiting the reference vector to the interior of the polygon presented in Fig. 18 has not been reported yet.

C. CARRIER-BASED PWM

This method uses the comparison of a triangular carrier with a modulating waveform to directly control the devices that modulate the output phase voltages in a VSI. Accordingly, the SPWM method was introduced as the simplest method to achieve modulation of a three-leg VSI. Considering that the voltages v_{az}, v_{bz} and v_{cz} are the phase voltages, referred to the middle point of the dc-link (z), to be modulated in a three-leg four-wire converter, the SPWM method can be directly applied in this topology [161].

Unlike the three-leg four-wire converter, when a four-leg converter is implemented (see for example Fig.2), the voltages to be modulated are no longer referenced to the middle point of the dc-link, but to the fourth leg of the converter. Thereby, the output phase-voltages in a four-leg VSI are represented as:

$$v_{an} = v_{az} - v_{nz} \tag{23}$$
$$v_{bn} = v_{bz} - v_{nz} \tag{24}$$
$$v_{cn} = v_{cz} - v_{nz}, \tag{25}$$

where each voltage is limited by the dc-link magnitude as:

$$-v_{dc} \leq v_{az}, v_{bz}, v_{cz} \leq v_{dc} \tag{26}$$
$$-2v_{dc} \leq v_{an}, v_{bn}, v_{cn} \leq 2v_{dc}, \tag{27}$$

From these equations, four voltages respect to the middle point of the converter are obtained, namely v_{az}, v_{bz}, v_{cz} and v_{nz}. Therefore, if both components of any of the pairs (v_{az}, v_{nz}), (v_{bz}, v_{nz}) and (v_{cz}, v_{nz}) change in the same magnitude, it would not be noticed in the output voltages v_{an}, v_{bn} or v_{cn}, but it allows to modulate output phase-voltages with a higher fundamental component and common-mode control [50].

Let us consider a set of reference phase-voltages v^*_{an}, v^*_{bn} and v^*_{cn}, given by an external controller. In order to be able to implement a carrier-based PWM algorithm, a suitable set of reference voltages v^*_{az}, v^*_{bz}, v^*_{cz} and v^*_{nz} have to be obtained to latter be compared with a triangular carrier waveform. This comparison should modulates the reference phase-voltages and maximize the utilization of the dc-link voltage. Hence, using (23) to (25), the reference values can be written as:

$$v^*_{az} = v^*_{nz} + v^*_{an} \tag{28}$$
$$v^*_{bz} = v^*_{nz} + v^*_{nn} \tag{29}$$
$$v^*_{cz} = v^*_{nz} + v^*_{nn} \tag{30}$$

Considering that v^*_{an}, v^*_{bn} and v^*_{cn} remain constant for a small sampling time and using v^*_{nz} as the abscissa and v^*_{az}, v^*_{bz}, v^*_{cz} as the ordinate of a Cartesian plane, each equation of (28) to (30) can be represented as a line with unitary slope over the planes: (v^*_{az}, v^*_{nz}), (v^*_{bz}, v^*_{nz}) and (v^*_{cz}, v^*_{nz}). This is shown in Fig.20, where the three lines are represented as L_1, L_2 and L_3 in the terms of v_{min}, v_{mid} and v_{max}, which represent

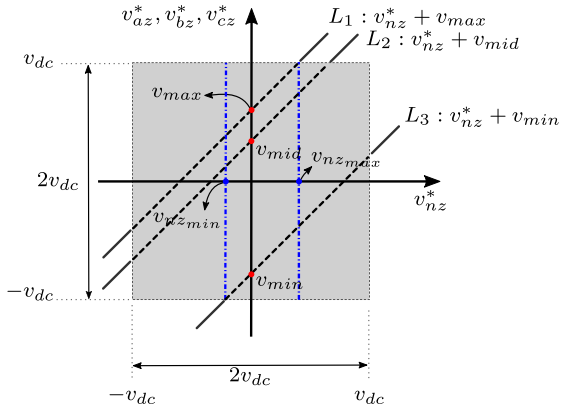

FIGURE 20. Limitation region for identification of the references voltages v^*_{az}, v^*_{bz}, v^*_{cz} and v^*_{nz}. v_{max}=*max*$\{v^*_{an}, v^*_{bn}, v^*_{cn}\}$, v_{mid}=*middle*$\{v^*_{an}, v^*_{bn}, v^*_{cn}\}$, v_{min}=*min*$\{v^*_{an}, v^*_{bn}, v^*_{cn}\}$.

the maximum, middle and minimum value of the reference phase-voltages v^*_{an}, v^*_{bn} and v^*_{cn}. From this figure, it can be seen that the black dotted line represent the pairs (v^*_{az}, v^*_{nz}), (v^*_{bz}, v^*_{nz}) and (v^*_{cz}, v^*_{nz}) that generate constant phase-voltages v^*_{an}, v^*_{bn} and v^*_{cn} inside a feasible modulation region. Thereby, as v^*_{nz} is the common coordinate for the three coordinate pairs (v^*_{az}, v^*_{nz}), (v^*_{bz}, v^*_{nz}) and (v^*_{cz}, v^*_{nz}), the intersection of a vertical line with L_1, L_2 and L_3 gives a possible solution for modulating v^*_{an}, v^*_{bn} and v^*_{cn}. Fig.20 shows, marked as three red points, this intersection for v^*_{fz}=0. This intersection points are obviously equal to the reference phase-voltages v^*_{an}, v^*_{bn} and v^*_{cn}, denoted as v_{min}, v_{mid} and v_{max} (see (28) to (30)). As the solution for v^*_{az}, v^*_{bz}, v^*_{cz} and v^*_{nz} must remain inside the feasible modulation region, the sector for placing this vertical line, i.e. the reference value of v^*_{nz}, is limited by:

$$v^*_{nz_{min}} \leq v^*_{nz} \leq v^*_{nz_{max}}, \tag{31}$$

denoted with blue dotted lines in Fig.20 and calculated as:

$$v_{nz_{min}} = -v_{dc} - v_{min} \tag{32}$$

$$v_{nz_{max}} = v_{dc} - v_{max} \tag{33}$$

In order to obtain a switching pattern equivalent to the *Single-Redundancy Symmetric* sequence, the following criteria must be used for selecting v^*_{nz}:

$$\begin{aligned} v^*_{nz} &= -\frac{v_{max}}{2}; \quad \text{for } v_{min} > 0 \\ v^*_{nz} &= -\frac{v_{min}}{2}; \quad \text{for } v_{max} < 0 \\ v^*_{nz} &= -\frac{v_{max} + v_{min}}{2}; \quad \text{Otherwise} \end{aligned} \tag{34}$$

Once obtained v^*_{nz}, the references v^*_{az}, v^*_{bz} and v^*_{cz} are obtained from (28) to (30). Afterwards, this constant values are compared with one period of a triangular carrier during the next sampling time T_s, generating, for example, the trigger signals for the eight devices of the two-level four-leg VSI [50], [172]. This process is repeated at each sampling time.

For multilevel VSIs with N-levels there will be $N-1$ carriers per leg to modulate the converter and an extended version of (34), but following the same idea of injecting a zero-sequence component by min-max functions [51].

Another method uses a linear transformation to obtain three-phase components from the four phases of the converter [**?**], [223], resulting in a regular three-phase system that can be easily controlled by, for example, symmetrical components. After controlling the system variables in the $\alpha\beta 0$ space, the four-leg references can be obtained by inverting the transformation in (35). In addition a zero sequence injection, like the one in (34), can be also be done to extend the DC-Voltage utilization [223], [224].

$$\begin{bmatrix} v_{az} \\ v_{bz} \\ v_{cz} \\ v_{nz} \end{bmatrix} = \begin{bmatrix} 1 & 0 & \frac{1}{2\sqrt{2}} \\ \frac{-1}{2} & \frac{\sqrt{3}}{2} & \frac{1}{2\sqrt{2}} \\ \frac{-1}{2} & -\frac{\sqrt{3}}{2} & \frac{1}{2\sqrt{2}} \\ 0 & 0 & \frac{-3}{2\sqrt{2}} \end{bmatrix} \begin{bmatrix} v_\alpha \\ v_\beta \\ v_0 \end{bmatrix} \tag{35}$$

The main advantage of SPWM relies on the simple calculation of the references leg voltages and the straight acquisition of the duty cycles of each device, obtained directly by comparison of the calculated references with a triangular carrier at each sampling time T_s. Equivalent SPWM methods have been proposed to obtain equivalent results as SVM methods [225]. However, the calculation of v^*_{fz} to perform different switching patterns [206], [226] or to successfully accomplish overmodulation methods become complex. Additionally, the utilization of the redundant switching combinations is very limited, as reported in its extension to multilevel converters [51], [227]. This become important in multilevel converters, where the shape of the harmonic spectrum, the balance of the voltages on the dc-link capacitors or distribution of the switches' power losses are important issues.

D. HYSTERESIS PWM CURRENT CONTROL

As a natural extension of the current controllers for the three-phase VSIs, the closed-loop Hysteresis PWM Current controllers were the first strategy used for accomplishing control of the output voltages in converters for four-wire applications, mainly three-leg four-wire VSIs.

The diagram of Fig.21 shows the control scheme of the Hysteresis PWM Current control for the three-leg four-wire VSI presented in Fig.8. This scheme accomplishes the control of the output currents i_a, i_b, and i_c by directly comparing the measured line currents with its arbitrary references, i^*_a, i^*_b and i^*_c, provided by an external controller. Note that these references can be non-sinusoidal; for instance, the reference currents of an active filter are non-sinusoidal. Thereby, the output of each hysteresis controller directly trigger the devices of each leg of the converter through the signals $g_{a,\bar{a}}$, $g_{b,\bar{b}}$ and $g_{c,\bar{c}}$. The width of the hysteresis band is denoted as ϵ and it is dynamically regulated by an additional controller, called

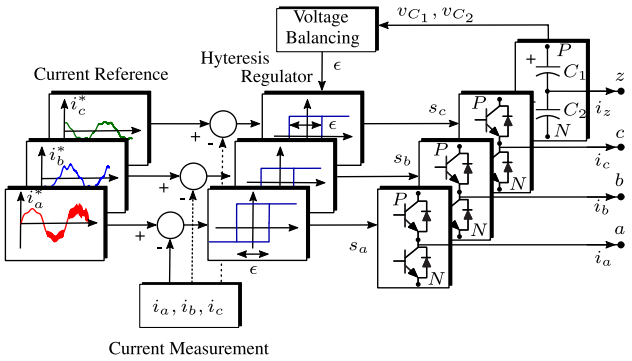

FIGURE 21. Control scheme for hysteresis modulation for four-leg converters.

Voltage Balancing. This controller regulates the width of the hyteresis band (ϵ) for actively balance the voltages v_{C_1} and v_{C_2} [152], [154]. This controller performs the same features reported for three-phase converters, namely: high transient response, high-frequency ripple in the controlled currents, and a non-fixed switching frequency, i.e. spread voltage and current harmonic spectrum.

A method that uses four hysteresis comparators applied to four-leg VSI is presented in [228]. Although this method performs good control of the line currents, the current through the neutral wire is not being directly controlled. This results in a neutral current i_z with a ripple up to three times higher compared to the line currents [26]. To solve this problem, Verdelho et. al. [26], [52], [151], proposed the hysteresis PWM current controller in $\alpha\beta\gamma$ coordinates. This controller uses the Clarke transformation to separate the zero-sequence of the reference currents from its $\alpha\beta$ active components. Thus, direct control over the *abc* currents and over the current through the neutral wire i_z is achieved. This results in four currents, namely i_a, i_b, i_c and i_f, that perform the same ripple [52].

A three-dimensional Hysteresis PWM Current controller was also introduced in [149], [166], [174]. This generates a cubical hysteresis region implemented directly in $\alpha\beta\gamma$ space. This method was implemented in cylindrical coordinate frames to facilitate the three-dimensional comparisons, required to identify when the reference vector is out of the hysteresis cube. As result, the method behaves similarly to the already presented method that uses independent hysteresis controllers in $\alpha\beta\gamma$ coordinates. Additionally, it gives more flexibility for implementing switching sequences. The method is successfully implemented in a two-level converter and also in a three-level three-leg four-wire NPC converter.

The major problem of hysteresis-based strategies is the generation of variable switching frequency, which complicates the filter design [77]. As a result, some authors have proposed strategies to achieve nearly constant switching frequencies [229] or constant frequencies [230], at the cost of increasing the implementation complexity and reducing the dynamic response of the controller.

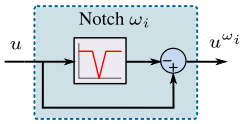

FIGURE 22. Frequency separation for generic variable *u*.

IV. CONTROL STRATEGIES FOR FOUR-LEG CONVERTERS

This section presents general voltage and current control schemes used on four-legs converters. First, the fundamental schemes for signal conditioning are analyzed, as signal filters, sequence separation, and changes on the reference frame. Then, a discussion about electrical power theory to compensate four-wire networks is reviewed. Later, virtual schemes as active damping and virtual impedance are analyzed. Afterward, the most commonly used linear and non-linear controller loops are revised, focusing on how they control the zero-sequence component. Finally, most reported control schemes for four-leg converters are grouped into single and cascaded loops are presented, showing the difference among implementations in SRF and RRF.

In this section, the "u" variable is used as a general variable that can represent either voltage or current.

A. FUNDAMENTAL SIGNAL CONDITIONING

Four-leg converters usually are connected to networks composed by linear and non-linear, balanced and unbalanced loads, which affect grid voltages and especially currents, adding harmonics to electrical signals, along with zero and negative sequence [231]. To simplify the control of four-leg converters, the following tasks are usually performed: i) isolation of specific frequencies, e.g. in the presence of harmonic distortion and ii) separation of electrical sequences from the measured currents and voltages.

In abc-frame or SRF (Static Reference Frame), it is advantageous to use a narrow pass-band filter (notch filter) to isolate the frequencies to be compensated by controllers, which can be achieved with notch filters [232]. The basic transfer function for the notch filter is shown in (36).

$$H(s) = \frac{s^2 + \omega_i}{s^2 + 2\xi\omega_i s + \omega_i^2} \tag{36}$$

In [233] different structures for notch filters are presented, analyzing its transfer function with bode-plots. The selection of the proper implementation depends mainly on the required bandwidth (associated with the level of harmonic contamination of the original signal) and the number of bits of the digital platform for its implementation. Multiple Notch filters can be also implemented to extract n different frequencies from the original signal, as shown in Fig. 22.

The accurate selectivity of notch filters has to be designed as a trade-off with its dynamic response. Therefore, if the filter is too narrow it can have a slow dynamic response to fast perturbations. Conversely, if the filter is not very narrow, the output may contain several frequency components [234].

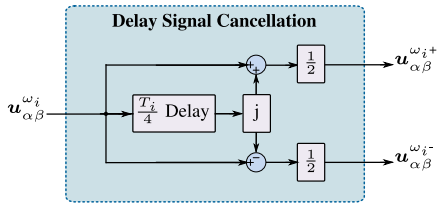

FIGURE 23. Sequence separation in SRF for arbitrary frequency ω_i.

It is common to control four-leg converters in abc reference frame when unbalanced loads are connected, where three-phase signals can be controlled independently thanks to the neutral wire connection [235]. This control approach avoids linear transforms [236], however, its zero-sequence can not be controlled directly. In addition, for achieving accurate control of unbalances, sequence separation can be applied in the abc reference frame, to control the converter considering its symmetrical components using Fortescue transformation [196], controlling each sequence component separately [237].

To decouple the zero sequence, Clarke transformation can be applied to 3-phase signals in abc-frame as shown in (37).

$$\begin{bmatrix} u_\alpha \\ u_\beta \\ u_0 \end{bmatrix} = \frac{2}{3} \begin{bmatrix} 1 & -\frac{1}{2} & -\frac{1}{2} \\ 0 & \frac{\sqrt{3}}{2} & -\frac{\sqrt{3}}{2} \\ \frac{1}{2} & \frac{1}{2} & \frac{1}{2} \end{bmatrix} \begin{bmatrix} u_a \\ u_b \\ u_c \end{bmatrix} \tag{37}$$

In SRF, positive and negative sequences are contained into $\alpha\beta$ components. To decouple those sequences, the delay signal cancellation (DSC) technique can be applied [238], where quadrature signals for both α and β components are emulated, as shown in Fig. 23. The DSC technique is a simple solution, but it exhibits poor transient response caused by the quarter period delay; furthermore, high memory usage is needed to store the data points required for the quarter period delayed signals. In some cases, the digital implementation of the quarter period cannot be achieved perfectly because the division between sampling and fundamental frequencies is not an integer value [239]. However, improvements on DSC have been implemented in [240], where the setting time is reduced significantly, reaching 1/40 of the fundamental period at the cost of higher overshoot during transient events.

To avoid the implementation of controllers in SRF (usually resonant controllers), the Park transformation, using a rotating reference frame (RRF) with d-q axes, can be implemented. Thus, DC signals are obtained when d-q axes rotate at the grid frequency, enabling the implementation of PI controllers. However, this is only valid for balanced and harmonic-free systems. The relationship between SRF and RRF signals is shown in (38).

$$\begin{bmatrix} u_d \\ u_q \\ u_0 \end{bmatrix} = \frac{2}{3} \begin{bmatrix} \cos\theta & \sin\theta & 0 \\ -\sin\theta & \cos\theta & 0 \\ 0 & 0 & 1 \end{bmatrix} \begin{bmatrix} u_\alpha \\ u_\beta \\ u_0 \end{bmatrix} \tag{38}$$

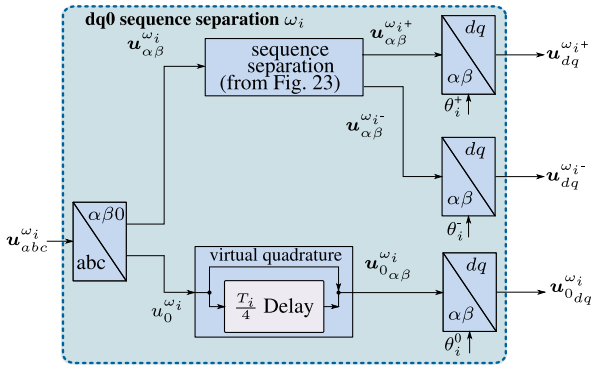

FIGURE 24. Sequence separation in RRF [243] considering zero sequence in RRF.

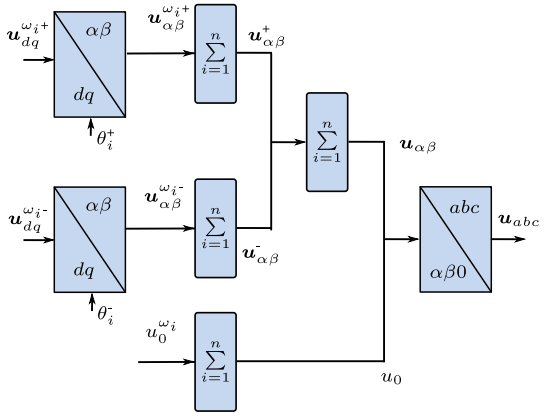

FIGURE 25. Sequence composition from RRF to abc SRF. For simplicity zero-sequence is considered directly in SRF, but it can be also composed form virtual component $u_{0_{dq}}^{\omega_i}$ (see Fig. 24).

In unbalanced scenarios it is advantageous to separate the positive and negative sequences before applying park transformation, to avoid double fundamental frequency harmonics on the d-q signals. On the other hand, the zero-sequence signal is not a vector and it cannot be transformed into an RRF without further processing. A solution is to use a quadrature generator; for instance, to delay the homopolar signal by a quarter of the period creating a virtual quadrature component. After that, the park transform can be applied to obtain the corresponding d-q fictitious signals, as shown in Fig. 24. Alternatively, an all-pass filter to emulate the quadrature signal can be used [241], which possesses a better transient response [242]. When harmonics are presented in the abc signals, they must be filtered out before passing to RRF, leading to one d-q system for each frequency as depicted in Fig. 24. Fig. 25, shows the inverse process.

In RRF, d-q components could be affected by incorrect estimation of the grid frequency θ angle. This is especially important in unbalanced and distorted networks. The three-phase synchronous (or Rotating) Reference Frame phase-locked loop (RRF-PLL) is one of the most used PLL on three-phase converters due to its simplicity, but it is not suitable for distorted and unbalance grids because inaccuracy

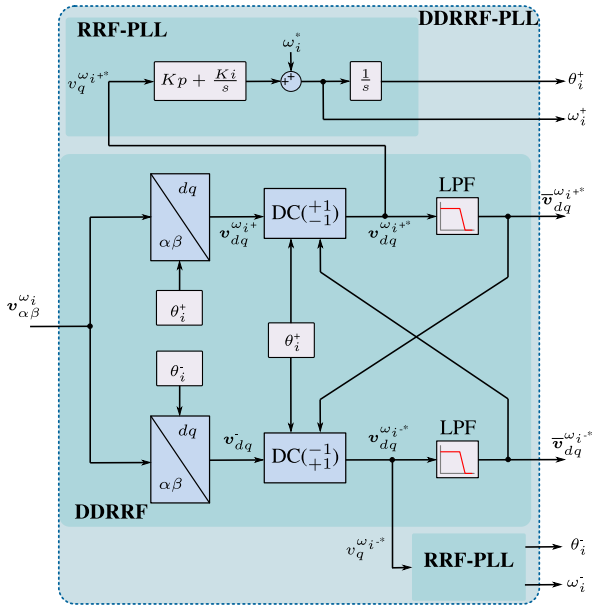

FIGURE 26. Decoupled double rotating reference frame PLL where.

on phase estimation, which leads to an increase of current THD [244].

A simple synchronization strategy for unbalanced systems is presented in [245], where a DSC algorithm is used to separate the positive sequence from grid voltages and then uses the RRF-PLL to obtain the grid angle, where a good synchronization tracking is achieved in steady-state, but on transient events, the quarter fundamental period delay of DSC affects its performance. Reference [246] proposes another approach with decoupled double rotating reference frame PLL (DDRRF-PLL) which exploits two rotating reference frames, one for positive sequence and the other for negative sequence, both rotating at the calculated angle from the positive sequence with the classical RRF-PLL, as shown in Fig. 26.

The DDRRF scheme provides the positive and negative sequences in RRF which is another solution to obtain these signals. The blocks named *DC* represent a "decoupling cell" which eliminate the double fundamental frequency oscillation on the d-q signals produced by the positive and negative sequences of the $\alpha\beta$ signals. The equations for *DC* $(+1, -1)^\intercal$ are presented in (39)-(40), and for *DC* $(-1, +1)^\intercal$ in (41)-(42).

$$u_d^{+*} = u_d^+ - \left(\bar{u}_d^- \cos(2\theta^+) + \bar{u}_q^- \sin(2\theta^+)\right) \quad (39)$$

$$u_q^{+*} = u_q^+ - \left(\bar{u}_q^- \cos(2\theta^+) - \bar{u}_d^- \sin(2\theta^+)\right) \quad (40)$$

$$u_d^{-*} = u_d^- - \left(\bar{u}_d^+ \cos(2\theta^+) - \bar{u}_q^+ \sin(2\theta^+)\right) \quad (41)$$

$$u_q^{-*} = u_q^- - \left(\bar{u}_q^+ \cos(2\theta^+) + \bar{u}_d^+ \sin(2\theta^+)\right) \quad (42)$$

Due to the presence of low pass filters in DDRRF, the method perform poor dynamics, hence authors in [247] proposed using a reduced-order generalized integrator (ROGI) as a pre-filter for the RRF-PLL, which increases the open-loop bandwidth of PLL to improve the dynamic performance of synchronization when perturbations occur.

If independent control for each PTN phase is desired, single-phase PLL (SP-PLL) can be used to obtain the grid-angle for each phase separately. This can be achieved by generating a quadrature signal for each phase using all-pass filters [31] or $T/4$ delay, where the transient events affect the synchronization with the grid angle. A comparison between SP-PLLs was presented in [248] where authors evaluated their steady-state and dynamic response, concluding that faster dynamics could be achieved but at the cost of oscillations in steady-state. In addition, line notching, line dips, phase loss, and frequency variations on power networks worse the correct functionality of PLLs, hence extra conditioning stages are needed [249].

Notice that when the converter is connected to weak grids, and the bandwidth of the PLL is large, the control of the converter, i.e. injected power, affects the frequency of the grid, which can lead to unstable operation and loss of synchronization [250], [251]. This issue can be overcome by improving the PLL design considering the weakness of the grid and/or adding compensation terms [252].

1) ELECTRICAL POWER THEORIES

Large implementation of microgrids and smart grids, and different power loads inherently unbalanced and distorted in distributions systems, has promoted the need for power new theories, which can handle distorted and unbalanced systems [120], [253]–[260]. Time-domain-based theories, which use instantaneous quantities to define the current decompositions and power terms has been widely explored in the literature [261]. The most popular theory is the so-called pq theory [120], [253]. Later on, in [153], [254], [257], [261], [262], this theory was extended to the zero sequence components, under the name of the modified p-q theory. This theory gives a generalized definition of active and reactive power, which can be used for sinusoidal or non-sinusoidal, balanced or unbalanced, three-phase power systems with or without zero-sequence currents and/or voltages [254]. It must be pointed out that the pq theory (and its modified versions) has been widely used in the literature for active power filter applications [263]–[267]. However, in recent years, the conservative power theory (CPT) [258], [268] has got attention from researchers. Indeed, in [260], it is claimed that the CPT is one of the major power theories of electrical systems with non-sinusoidal and unbalanced currents. The high number of contributions based on the CPT support this claim: [65], [269]–[277], which have been also implemented in four-wire active power filters [268], [278].

Fig. 27 show the implementation of the modified pq theory for an four-leg active power filter.

The grid voltage and the unbalanced-distorted load current are converted into $\alpha\beta 0$ components. Then the instantaneous power variables are obtained using the p-q theory

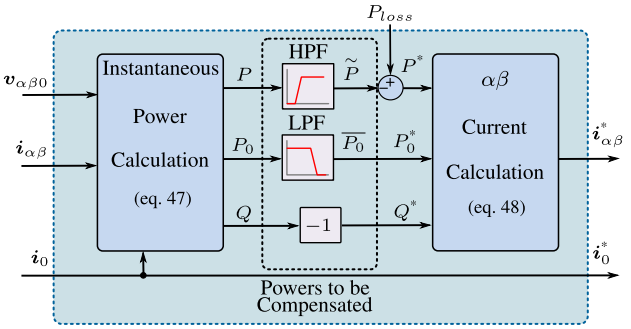

FIGURE 27. Instantaneous reactive p-q theory. Active power filter application example.

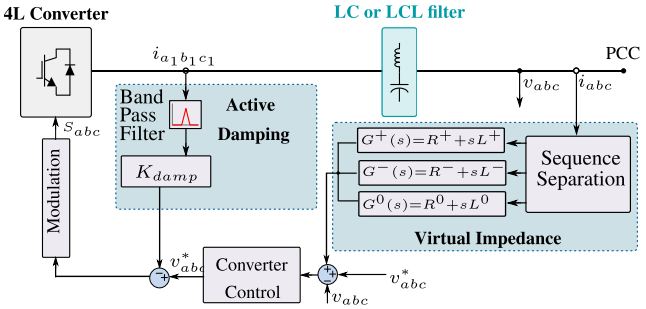

FIGURE 28. Active damping and virtual impedance reference schemes.

equations (43).

$$\begin{bmatrix} P_0 \\ P \\ Q \end{bmatrix} = \begin{bmatrix} v_0 & 0 & 0 \\ 0 & v_\alpha & v_\beta \\ 0 & v_\beta & -v_\alpha \end{bmatrix} \begin{bmatrix} i_0 \\ i_\alpha \\ i_\beta \end{bmatrix} \tag{43}$$

Now the power signals to be compensated are selected, which usually are all of them except the active power variable, in order to compensate only reactive power as active power filter applications. After this, the reference currents are obtained using the inverse equations of p-q theory, as described in (44).

$$\begin{bmatrix} i_\alpha \\ i_\beta \end{bmatrix} = \frac{1}{v_\alpha^2 + v_\beta^2} \begin{bmatrix} v_\alpha & v_\beta \\ v_\beta & -v_\alpha \end{bmatrix} \begin{bmatrix} P^* + P_0^* \\ Q^* \end{bmatrix} \tag{44}$$

The obtained 3 current references are completely independent due to the neutral connection of the four-leg converter. It is worth mentioning that implementing other theories have a similar structure as Fig. 27 but with their corresponding power and current calculation equations.

2) ACTIVE DAMPING

Resonance frequency on LC or LCL passive filters must be designed to avoid power system instability, due to the integration of its resonance frequency with voltage harmonics produced by modulation or non-linear loads. During transient responses, resonance modes can be also exited and cause large voltage fluctuations on the filter capacitor [279]. To avoid fluctuations, resistors can be placed in the filter to damp the resonant frequency, but this leads to extra losses and a larger filter footprint [280]. An alternative is to emulate this damping effect on the controller using the active damping technique.

A simple implementation of an active damping method is to measure the capacitor current and feed-forwarded it into the controller converter voltage reference. This emulates a series resistor with the filter capacitor. This requires measuring the filter capacitor currents which are not typically measured, hence extra current sensors are required [281]. Unlike using the capacitor currents, the capacitor voltages (typically measured) can be used to estimate the capacitor current. However, special derivative methods must be implemented to avoid noise amplification [282].

Alternatively, to avoid capacitor current measurement or estimation, the converter output current can be used instead. This approximation is accurate only if the load impedance is relatively large compared with the filter impedance [30]. Also, it is possible to directly emulate a series resistor with the inductor tight to the converter on LC or LCL passive filters [31]. Those solutions effectively damp the filter resonant but also magnifies the output impedance of the converter which deteriorates the output voltage quality [193]. Hence, selective active damping can be achieved by filtering only the resonant frequency from the measured converter currents, as shown in Fig. 28 (see active damping block). The gain K_{damp} represents the size of the emulated series resistor to the L_1 inductor is added to damp the oscillations.

3) VIRTUAL IMPEDANCE

The output impedance of a converter is relatively low compared with grid line impedance, making it difficult to accurately distribute power capacity when several converters are connected to a CCP. To overcome this problem, a virtual impedance loop on the converter controller can be implemented [283].

When the load is unbalanced, the current is composed of positive, negative, and zero sequence components. If the voltages supplied by the converter are balanced, then it is hardly possible to share the unbalanced components of the load currents between converters [65]. Therefore, using the unbalanced components of the output current (i.e. negative and zero sequence currents), virtual impedances are implemented in the control system to unbalance the output voltages references adding negative and zero sequence voltage components [90], as shown in Fig. 28.

Typical power grid lines are mainly inductive, which allows to decouple the control of frequency and voltage magnitude through the control of active and reactive power respectively. In low-voltage microgrids, the grid impedance coould be mainly resistive, coupling the control of power flows within the MG. In this case, the virtual impedance loop transforms the resistive line impedance to inductive, allowing the use of the classic droop controllers [284], [285]. Furthermore, virtual impedance can be implemented with droop controllers to enhance the current sharing capability in

MG [286], and/or to compensate imbalances and harmonics at some point of the MG [287]. Note that the value of the required virtual impedance could be dependent on the MG operating point. Because of that, in the literature, this magnitude is usually adjusted in real-time by a secondary controller. In [16], a comprehensive description of the virtual impedance control loop along with its main applications is provided.

B. CONTROLLERS

Linear and non-linear controllers commonly used on four-leg converters are analyzed in this section. The controllers are presented generically, to be implemented for either voltage or current control (input variable defined as u), the system plant, usually filter plants of (16) or (10) for current or voltage control correspondingly, are represented as $G(s)$ and the controller output is represented as y.

1) PROPORTIONAL INTEGRAL

The proportional-integral controller (PI) achieves zero steady state error at DC signals, due to it pole is located in the origin of the s plane. The PI transfer function is shown in (45).

$$C(s) = K_p + \frac{K_i}{s} \tag{45}$$

The PI controller is a simple control structure used in RRF. The Fig. 29(a) and (b) shows the implementation of PI controller for positive (a similar control topology is required for the negative sequence component) and zero sequences for a L filter Fig. 13(a). The RRF zero-sequence has been obtained based on a virtual quadrature scheme shown in Fig. 24. Fig. 29(c) shows the implementation of a resonant controller or the zero sequence. This is an alternative to controlling the zero sequence avoiding RRF transformation.

The positive and negative sequence control loops are identical, the cross-coupling terms can be feed-forwarded to decouple the dynamics between d and q axis, the same cross-coupling can be used for an LC filter as the one at Fig. 13b [110], for other filters a more complex decoupling could be necessary.

It is worth noticing that the control scheme presented in Fig. 29 is valid only for a single frequency ω_i, hence under distorted grid conditions, several equivalent loops must be implemented to compensate harmonics. Furthermore, measurements must also be filtered and transformed into RRF for each frequency (see Fig. 24) and then into SRF for modulation (see Fig. 25), increasing significantly the overall controller complexity [288].

2) PROPORTIONAL RESONANT

The proportional-resonant (PR) controller achieves zero steady state error at AC signals with a frequency equal to resonant PR frequency, due to it complex-conjugated poles located at the resonant frequency [113], [289]. The multi-resonant PR controller, for compensation of multiple

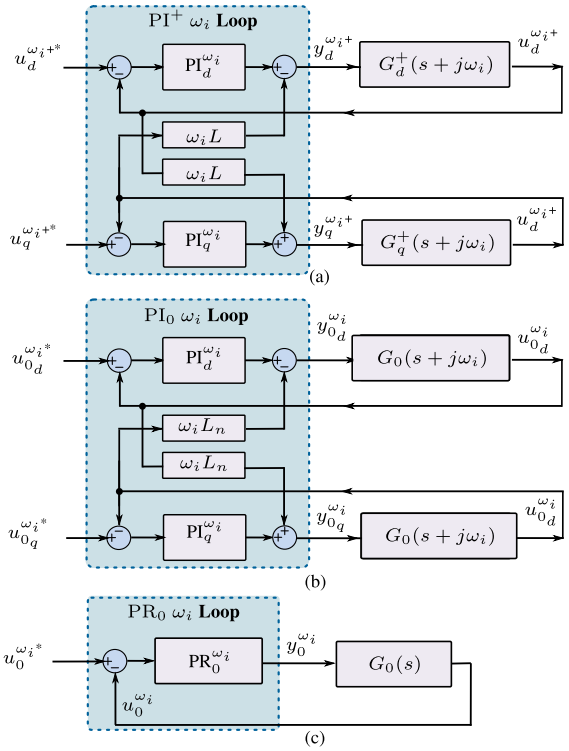

FIGURE 29. Proportional-integral controller loops for (a) positive sequence in RRF, (b) zero sequence in RRF and (c) zero sequence in SRF for arbitrary frequency ω_i.

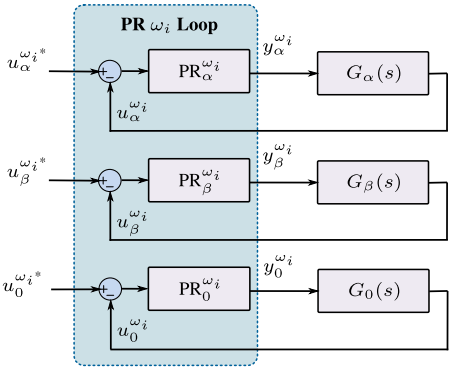

FIGURE 30. Proportional-resonant controller loops for α, β and 0 sequence in SRF for arbitrary frequency ω_i.

frequencies is shown in (46) [76], [113].

$$C(s) = Kp + \sum_{i=1}^{n} \frac{Ki_i s}{s^2 + w_i^2} \tag{46}$$

Fig. 30 shows the implementation of PR controller in SRF, considering that the plant behavior can be decoupled (see section II-C).

The α and β must not be separated into positive and negative sequences, because the PR controller can naturally control both terms independently. The PR controller can be also implemented in *abc* reference frame [61].To maintain an accurate resonance frequency, and phase of the controller

after discretization, it is important to consider tustin with prewarping [290]. In addition, to maintain the controller stability when high order harmonics are being compensated, as in four-leg active power filters or power supply for unbalanced loads, it is important to compensate the phase-shift introduced by the plant [61]. In this case, the extended structure of the resonance controller of (47) is used to compensate the phase-shift introduced by the plant at ω_i, i.e. ϑ (see (48)) [291].

$$R^c(s) = \sum_{i=1}^{k} R_i^c(s) = \sum_{i=1}^{k} K_i \frac{s\cos\vartheta_i - \omega_i \sin\vartheta_i}{s^2 + \omega_i^2} \quad (47)$$

$$\vartheta_i = -\angle P(j\omega_i) \quad (48)$$

Each controller $R^c(s)$ injects an angle of $\frac{\pi}{2} + \vartheta_i$ and $-\frac{\pi}{2} + \vartheta_i$ at each resonance frequency ω_i, giving an extra degree of freedom for the design of the controller used to increase its stability margins. Note that for $\vartheta_i = 0$ the controller presented in (47) is equivalent to (46).

In order to implement a resonant controller as in (46) in a digital system, its discretization has to fulfill two important requirements: (i) To maintain the resonant frequencies ω_i (ii) To have the largest gain at the resonant frequencies ω_i. This can be achieved using tustin with prewarping approximation [290], [292], which implementation in (46) leads to

$$\sum_{i=1}^{k} R_i^{tpw}(z) = \sum_{i=1}^{k} K_i \frac{\sin(\omega_i T_s)\left(1 - z^{-2}\right)}{2\omega_i\left(1 - 2z^{-1}\cos(\omega_i T_s) + z^{-2}\right)} \quad (49)$$

where T_s is the discretization sampling time and the prewarping frequency has been selected as the resonance frequency of each resonant controller ω_n. Similarly, using other discretization methods or adding the angle compensation as in (47) other discrete representations can be obtained [290], [292].

3) REPETITIVE CONTROL

The repetitive controller (RC) ensures zero steady-state error for all harmonic frequencies, due to its several number of poles in the unit circle of Z-plane. Additionally, the controller needs compensators to improve its stability, as can be seen in the complete transfer function of (50).

$$C(z) = \frac{K_{RC} L(z)}{1 - Q(z) z^{-N}} \quad (50)$$

The $Q(z)$ is a zero-phase low-pass filter, and $L(z)$ is a lag network, both compensators reduce the controller gain at high frequencies, improving the stability. The K_{RC} corresponds to the gain of the controller. The N value is the integer value of ω_{samp}/ω_1, where ω_{samp} is the sampling frequency, and ω_1 the fundamental frequency to be regulated.

The plug-in topology is shown in figure Fig. 31, although other topologies have been proposed as the direct type [74] or parallel type [293].

In steady-state condition, RC shows a robust performance against known periodic disturbances with zero error, however, unlike PR controllers, RC experiences poor dynamics during transients, due to the long learning time. Furthermore, RC is difficult to stabilize for unknown loads disturbances [112], [294]. RC can be a good alternative for applications where several unknown harmonics have to be compensated, such as four-wire active power filters.

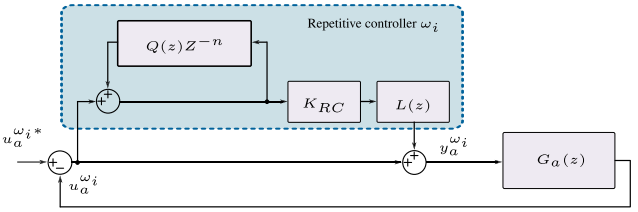

FIGURE 31. Plug-in repetitive controller loops in abc-frame for one phase. Equivalently it can be also applied in SRF.

4) FINITE-SET-MODEL PREDICTIVE CONTROL

The Finite-Set-Model Predictive Control (FS-MPC) computes all the possible power switch combinations at sample time (k), which would minimize a determined cost function evaluated in the $(k+1) - th$ sampling time. The switch combination that minimizes the cost function is selected and then applied for the whole (k+1) sampling time. An example of cost function is shown in (51).

$$g(k+1) = \lambda_1 |v_o^*(k+1) - v_o(k+1)|^2 + \lambda_2 |i_o^*(k+1) - i_o(k+1)|^2 + \ldots \quad (51)$$

The cost function could have one or more objectives, depending on the application. Notice that the incorporation of more control goals makes it difficult to tune the weighting factors (λ_i) [53], which determine the importance of one control goal over the others. To determine a specific magnitude of each weighting factor to obtain the desired performance is not a simple task and is still under investigation [295], [296].

Fig. 32 shows the basic scheme for FS-MPC, where the voltage of the output filter capacitor represents the controlled variable. Using the model and measurements in time (k), the voltage is predicted for the sampling time (k+1). The cost function is calculated by evaluating all the possible switching combinations, then the combination (S_{abc}) which minimizes the cost function is applied to the converter in the next sampling time. Further step predictions can be implemented to improve the response of the converter at the cost of a higher computational burden [297].

The main advantage of FS-MPC is the fast transient dynamic due to the selection of the optimal switch combination to accomplish the control objective and it is also a very simple control technique, which eliminates the complex modulation of four-leg converters [56]. Also, the non-linearities of the system can be easily incorporated. However, the method does not provide a deterministic procedure to define different weighting factors, it can generate high switching frequency in steady-state operation, and it requires a high computational burden when implemented in multilevel converters or for

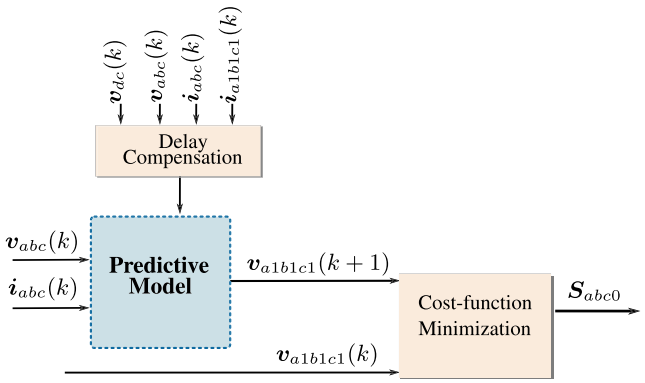

FIGURE 32. Predictive controller.

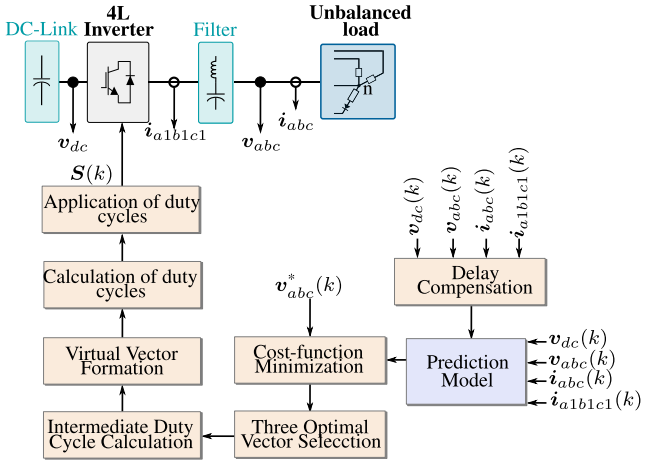

FIGURE 33. Modulated FS-MPC [59].

more than two steps prediction and also generates a variable switching frequency spectrum in the modulated waveform (which compromises the filter design) [298]. In four-leg converters, the neutral leg experience more switching frequency than the other 3-phase legs if this is not addressed in the controller formulation [299].

5) MODULATED FS-MPC

Modulated FS-MPC is a variant of FS-MPC which is able to set a constant switching frequency and reduced ripple at steady-state, incorporating a modulator stage after the prediction of duty cycles, instead of the switch combinations calculated in the classic FS-MPC. This technique is well documented on three-leg converters [300] but its implementation in four-leg converters is rather new due to the complexity of the modulator in 3D state-vector geometry. One common approach to four-leg converters is to find 3 optimal voltage vectors to be associated with its temporary duty cycles, to perform a virtual vector which can be used in 3D-SVM [55].

$$V_{virtual} = d_1 V_{op1} + d_2 V_{op2} + d_3 V_{op3} \tag{52}$$

In Fig. 33, it is shown some of the stages of the Modulated FS-MPC based on the solution proposed by authors in [59].

Fig. 33 and Fig. 32, share the delay compensation, prediction model and cost-function minimization stages, however, unlike FS-MPC, the modulated FS-MPC evaluates the cost function with stationary vectors of the modulation strategy, calculating the duty cycles to be applied in the converter, fixing the switching frequency [59], [301], [302]. Modulated FS-MPC fixes the switching frequency, performs a fast transient response and good THD against compared to FS-MPC. However, it requires a high computational burden and it is sensitive to system parameter mismatches [303].

6) DEAD-BEAT CONTROLLER

The dead-beat controller is a discrete time control which places all their closed-loop poles in the origin of the z-plane, achieving the fastest possible dynamic performance. This condition relies in the accurate system model. A simple dead-beat equation for a converter connected to the grid through a first-order filter is presented in (53). (Presented for one phase, equivalent for other phases)

$$v_{a_1 n_1}(k) = v_{grid_{an}}(k) + \frac{L}{T_s}\left(i_a^*(k) - i_a(k)\right) \tag{53}$$

with T_s as the controller sampling period. The reference voltage to be modulated is obtained from (53). In case LC or LCL filters are implemented, (53) changes according to the models presented in section II-C and the same procedure is implemented to obtain the control law [88], [304].

Dead-beat controllers perform a fast transient response and it is very simple to implement, however, it is highly sensitive to parameter variations, loading uncertainties, disturbances, and consequently to steady state error, since there is no inherent integral component in it [63]. Complementary strategies to improve its robustness, such disturbance observer [305] or to recalculate the system parameters [306] are typically implemented.

7) LINEAR QUADRATIC REGULATOR

Linear Quadratic Regulator (LQR) is a multivariable controller which minimizes the desired cost function. To achieve this, the system is modeled into state variables where it is augmented to add the controller states. The resulting state vector ($\mathbf{x}$) is used with the controller actuator vector ($\mathbf{u}$) to be optimized into a function J, which searches for the quickest possible way to achieve a new equilibrium point. A common LQR cost function is shown in (54).

$$J_p = \frac{1}{2}\int_0^\infty \left[u^\intercal \boldsymbol{R} u + x^\intercal \boldsymbol{Q} x\right] dt \tag{54}$$

The $\boldsymbol{R}$ and $\boldsymbol{Q}$ matrices represent the penalty coefficients (weighting factors) which tuning is a non-deterministic process, some general guidelines to select their values are presented in [307], where a detailed description of LQR applied to four-leg converted was presented.

In [308], integral and oscillatory controllers are used to regulate the desired variable (current or voltage) in a four-leg converter. Then the augmented state variable vector is formed

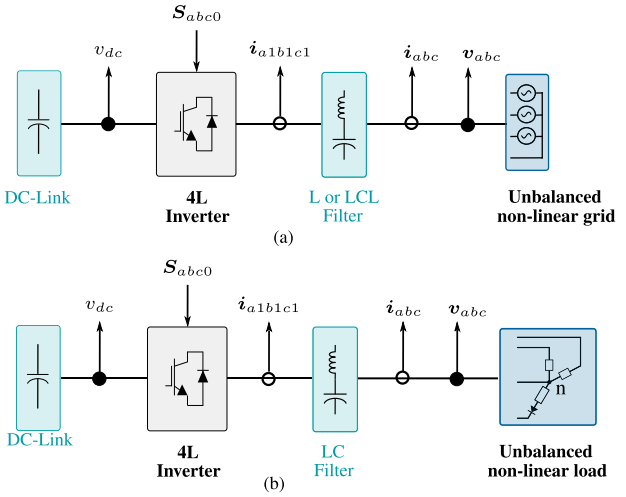

FIGURE 34. Four-wire configurations: (a) in current control mode and (b) in voltage control mode.

to interact with the K gain obtained from the before-hand optimization (using Ricatti equations). Finally, the converter voltage references are generated.

The complexity of the LQR method relies in the tuning of the $\boldsymbol{R}$ and $\boldsymbol{Q}$ matrices. Also, the system model mismatches deteriorate the control dynamics and its performance. For heavily distorted systems, authors in [309] add a feed-forward disturbance rejection, reducing the oscillatory terms in the controller and obtaining a lower load current THD.

C. CONTROL SCHEMES

Typical single-loop and nested control schemes for four-leg converters are presented in this section. The controlled variable is either the current at the output inductor of L or LCL filter, as in Fig. 34a, or the voltage at the capacitor output LC filter, as in Fig. 34b. Single-loop control schemes are a natural alternative for current control in L filters, and can also be implemented for higher-order transfer functions, such as voltage control in LC filters and current control in LCL filters. However, in these cases, internal currents (for LC and LCL filters) and internal voltages (LCL filter) are not controlled, which can lead to a dangerous operation. When the switching frequency and controllers bandwidth are compatible with the maximum sampling time of real-time controllers, nested-loop control schemes are preferred for both voltage control in LC filters [140], [310], [310], [311] and current control in LCL filters, which allows to control and limit the output current of the converter and internal capacitor voltage in the LCL filter [197], [198], [282], [312].

1) SINGLE-LOOP CONTROL SCHEME

A single-loop control scheme is simple and easy to implement, it is the only alternative for current control in L filters, and it is a possible alternative for current control in LCL filters and voltage control in LC filters. For LC and LCL filters, the use of a single-loop controller disables the control and limitation of internal variables, such as converter currents in LC filters or converter current and capacitor voltage in LCL filters. In addition, the (linear) controller is hard to tune, due to the high order of the filter transfer function [145]. Fig. 34(b), shows a four-leg converter with an output LC filter connected to an unbalanced and non-linear load. In Fig. 35(a)-(c), a single-loop voltage controller in abc and $\alpha\beta 0$ SRF and dq RRF for controlling the output PTN voltages is presented.

In Fig. 35(a), v_{an}, v_{bn} and v_{cn} are directly regulated. The implementation of three independent resonant controllers are a good alternative for this purpose (see section IV-B2), but also repetitive control (see section IV-B3) or non-linear controllers, such as: dead-beat (see section IV-B6), FS-MPC (see section IV-B4) or modulated FS-MPC (see section IV-B5) (as presented in previous section) can be used instead. In Fig. 35(a), the zero sequence is controlled indirectly. As presented in (13), voltages and currents of phases a, b and c are coupled, which makes difficult to define a decoupled dynamic plant between $v_{a_1n_1}$ and v_{an}. When this control scheme is implemented, usually the neutral inductor L_n is neglected ($Z_n = 0$), decoupling the dynamic of the filter. Thus, a simple LC branch is used to tune each resonant controller and the same controller is used in the three phases [313]. Similarly, Fig. 35(b) presents the control scheme in $\alpha\beta 0$ SRF. Also resonant controllers arise as the most reported alternative to control the output voltage [24], [72], [201], however, in this case the zero sequence is directly controlled. As discussed in Section II-C, the same transfer function is obtained for α and β coordinates, while a different dynamic is found for the zero sequence, which allow to design proper controllers for each variable.

Fig. 35(c) shows the control diagram for a four-leg converter in $dq0$ RRF. In this case, it is mandatory to previously separate positive and negative sequences of the measured signals and also to separate the system in different frequencies, leading to a set of several symmetric and balanced three-phase systems which can be then transformed into a $dq0$ reference frame [314]. The dq signals are controlled by PI controllers, however, the zero-sequence can be either directly controlled by a resonant controller or transformed to an additional dq_0 frame using a virtual quadrature signal, as presented in Fig. 24, and be controlled by PI controllers [111]. Thereby, two sets of dq signals are controlled for each frequency component. The output of the controllers is then transformed to obtain the modulated signal as presented in Fig. 25.

Same control schemes as showed in Fig. 35(a)-(c) can be implemented for current control of first-order L filter. However, grid voltage are feed forwarded to mitigate the current control of grid voltage disturbances (instead of active damping block) and equations of table 3 are implemented as control plant [235], [315].

In the case of non-linear loads, it is necessary to control the current harmonics to improve the THD, which is accomplished using the controllers described for voltage control, such as multi-resonant PR controller or repetitive

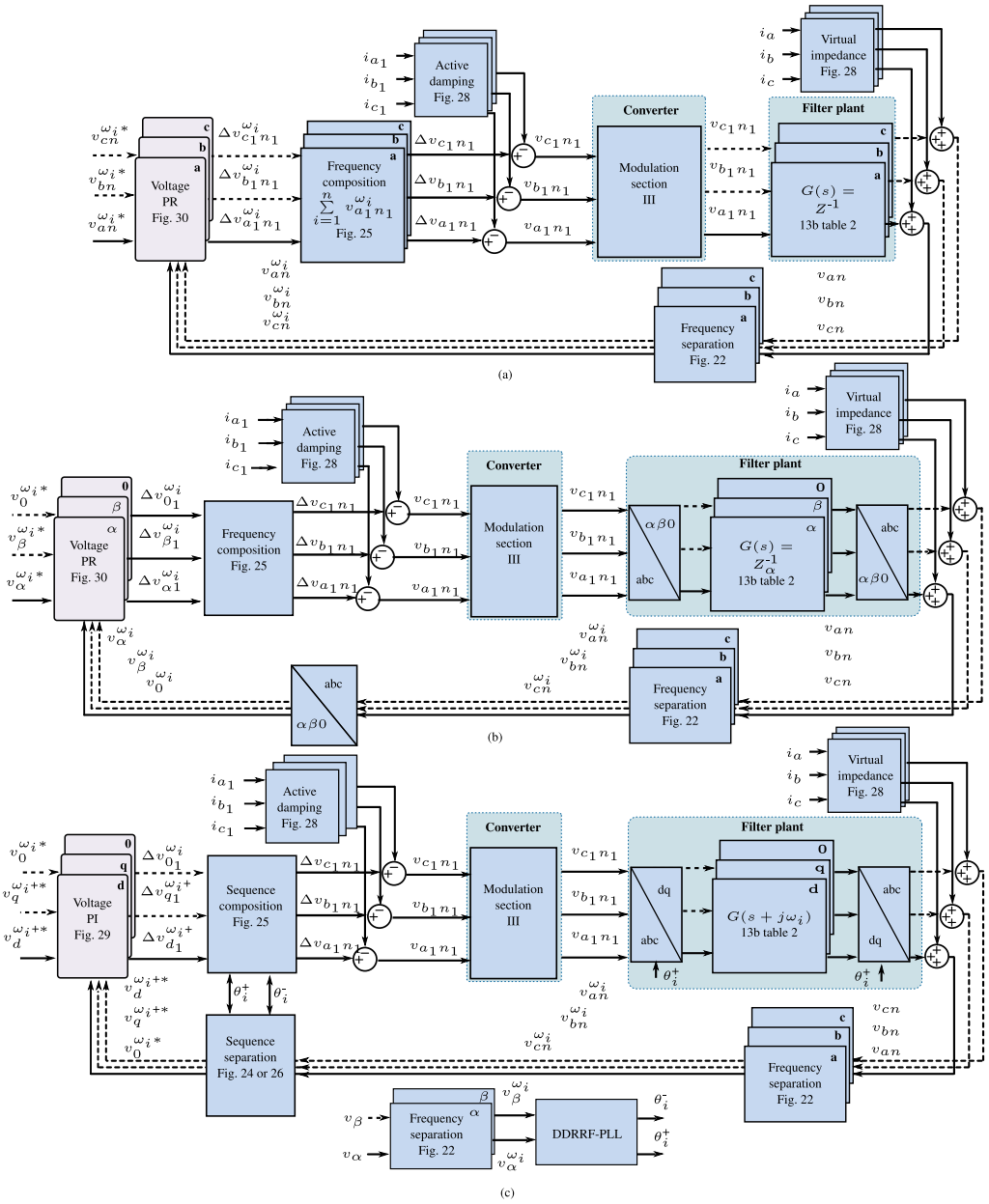

FIGURE 35. Single loop voltage control of a four-leg converter with an LC filter for a frequency ω_i with implementation active damping and virtual impedance. The converter plants are shown as seen by the SISO controllers. (a) In abc-frame, (b) SRF and (c) RRF for the positive sequence. The negative sequence is controlled in a similar way. In RRF, the zero sequence is controlled by a PR or by a PI controller with a virtual vector in RRF.

control [316]. The use of RRF is possible but it needs n controllers as shown in Fig. 29 per each frequency to be controlled and sequence separation, which increases the complexity of the overall control system. For this reason Fig. 35 is showed for frequency ω_i

2) NESTED-LOOP CONTROL SCHEMES

This configuration is widely used by its robustness against parameter mismatches and to obtain a better overall performance [25], [293]. In Fig. 36, the cascaded loop scheme for voltage control in abc, $\alpha\beta0$ and dq0 reference frames are shown. It considers controllers that handles positive, negative and zero sequences and compensation of ω_i frequencies for four-leg converter connected to an unbalance and non-linear load [317] and [237], [318].

Similar structure as Fig. 36 can be used for LCL filters. A nested control loop is used, for the inner part of the filter, the LC filter (as shown on Fig. 36), while an additional outer loop controls the L_2 output current. However, this structure has just been reported for three-wire converters [197]. To simplify the control, usually the capacitor dynamic is neglected and the converter with a LCL filter is controlled as a simple L filter, with a single loop control [243], [279], [312], [319].

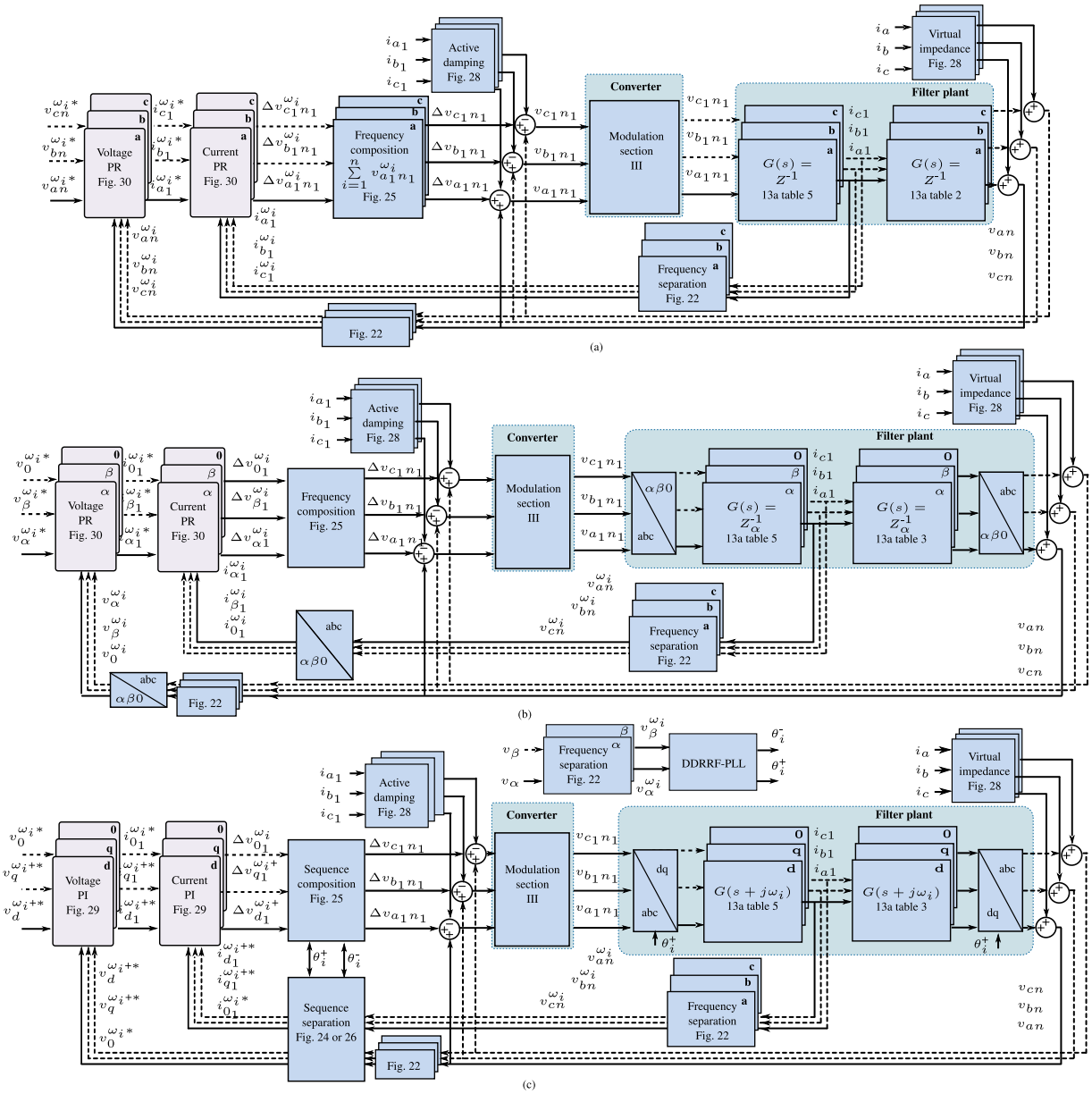

FIGURE 36. Nested voltage and current loop controllers of a four leg converter with a LC filter for a frequency ω_i with active damping and virtual impedance. The converter plants are shown as seen by the SISO controllers. (a) In abc-frame (b) In SRF (c) In RRF for the positive sequence.

The FS-MPC controller has been also used to control voltage and current as with a cascaded scheme, but due to its nature, it can not be considered as a cascaded control loop, because all reference variables are evaluated at the same time in the cost function [320]. Simplified, FS-MPC has been used in cascaded control just to implement the inner current loop (due to its fast dynamics), leaving the external controller as a linear controller [302], [321].

V. FOUR-LEG CONVERTERS OPERATION MODES AND APPLICATIONS

A. STAND-ALONE APPLICATIONS

Four-leg converters can be used for feeding stand-alone loads in applications, such as: (i) Uninterruptible Power Supply (UPS), (ii) Stand-Alone Power Supply, and (iii) Ground Power Unit (GPU). It must be noted that the UPS feeds loads when the main power grid fails, while a stand-alone power supply (also known as remote area power supply) provides power supply to off-the-grid loads, i.e., to loads that are not connected to the main power grid. Finally, a GPU unit is in charge of supplying power to airplanes while they are parked on the ground. The main reported works that belong to these applications and are based on four-leg converters are discussed in the following subsections.

1) UPS

Due to its ability to work with unbalanced voltages, four-leg converters have been applied as Uninterruptible Power

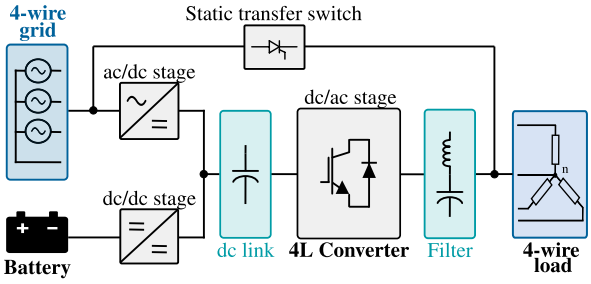

FIGURE 37. UPS system along with its typical control system—only the control scheme associated with the four-leg converter is shown.

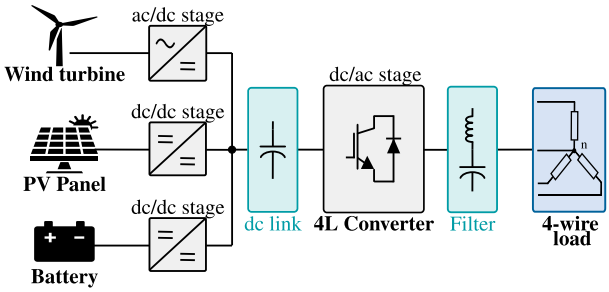

FIGURE 38. Stand-alone photovoltaic-wind energy-based hybrid power supply.

Supplies [63], [75], [76], [168], [322]. Fig. 37 illustrates a typical UPS system. The system is composed of one (or more) energy storage system (ESS), a DC/DC converter, usually responsible for regulating the voltage at the dc-link, and a four-leg converter with output LC filter. Note that, four-wire transformerless UPS is a mature technology with patents [322] and up to 600kVa commercial products (Toshiba Mitsubishi) for 3-phase 4-wire power systems [168].

Single-loop or nested loop controllers, including the active damping loop to improve the stability (see Fig. 28) are typically implemented to regulate the output voltage. In [75], [76], PR controllers in the abc reference frame have been reported for this application, where parallel PR controllers are implemented (see Fig. 30) to handle the fundamental frequency and the main harmonics present in the system (3rt, 5th, etc.). Also, de RRF has been considered for control of the system with PIs and state-space variables [323]. In addition, in [63], an overview of different UPSs configurations for three/four-wire applications is presented.

In a similar application, a battery energy storage system (BESS), can be directly used to supply energy to isolated loads using four-leg converters (the scheme is the same as the one shown in Fig. 37 but neglecting the four-wire grid) [324]. For instance, in [34], a four-leg NPC is proposed to interface a BESS to an unbalanced AC microgrid. In this reference, PI controllers in the dq0 reference frame, similar to those shown in Fig. 29, are implemented. The PWM scheme is used as the modulation technique. The proposed control system has been experimentally validated with excellent performance.

2) STAND-ALONE POWER SUPPLY

This is one of the most reported applications of four-leg converters, supplying energy to unbalanced and/or non-linear loads [60], [61], [74], [85], [86], [88], [111], [113], [180], [195], [262], [325]. Fig. 38 shows an example of a stand-alone four-leg power supply with different energy sources. Note that, in some cases, the neutral inductance (L_n in Fig. 13) is not considered. However, this solution is not recommended as the L_n increases the impedance seen by the zero-sequence voltage components (see Table 3), present in the voltage synthesized by the modulation algorithms utilized for four-leg converters [195], [236]. This is important when several four-leg converters are interconnected to avoid large peaks on the neutral currents [277].

A four-wire VSI based on a split capacitor configuration (see Fig. 8) was proposed in [87] for stand-alone PV applications. This topology avoids an extra leg and generates reduced EMI problems compared to its four-leg counterpart (due to reduced magnitude of the modulated voltage level), however, it has low voltage utilization and reduced power density because bulkier dc-link capacitors are required to handle the increased ripple [133].

The four-leg two-level converter (see Fig. 1) is the most reported topology for stand-alone applications. In this topology, a 4^{th} leg is included, providing some advantages such as better utilization of the dc-link and less ripple in the capacitors. A 60kW two-level four-leg VSI topology has been selected for the Consolidated Utility Base Electrical (CUBE) system developed by NREL USA to replace the delta-star transformer used in the previous version CUBE-V1 [326]. The four-leg three-level NPC converter [99] and four-leg flying capacitor topology [35], have been also proposed as stand-alone power supply to reduce the harmonic content of the modulate voltage and reduce the switching frequency of each proposed for harmonic cancellation and increase the equivalent switching frequency of the modulated voltage, which allows for smaller filters and lower losses.

The direct four-leg matrix converter (see in Fig. 5) has been also proposed as stand-alone power supply [110], [111], [113]. The main advantages of the matrix converter topologies are their higher power densities (both measured in power/volume and power/weight) and reliability due to the elimination of bulky dc-link capacitors. It is estimated that the volume saved with matrix converters, when compared to a similar back-to-back topology based on two-level VSC, is increased by a factor of at least 3 [327]. Therefore, with these converters, it is even possible to implement the converter embedded in an electrical generator [328]. However, the oscillations in the instantaneous power absorbed by the load, which is typically a consequence of the imbalances and non-linearities [120], yield distortions in the input currents, being its major drawback. Fig. 39 shows the control systems proposed for four-leg matrix converters feeding stand-alone linear unbalanced loads. In this case, the control system is

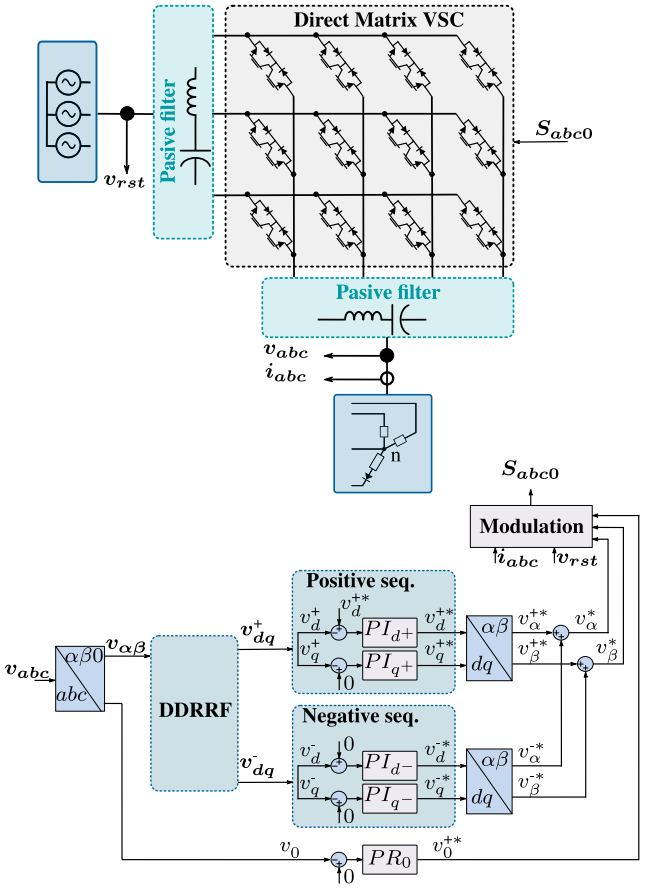

FIGURE 39. A direct matrix converter and associated control system [111]. In this case it is assumed that separate controllers are required for the regulation of the positive, negative and zero sequence components in the load voltages.

based on separating the positive, negative, and zero sequences components of the load voltage. PI controllers (see section IV-B-1) and one resonant-based control system (for the zero-sequence voltage) can be used to regulate the load voltage if sinusoidal but unbalanced voltages are considered. In [110], [113], [201], implementation of three independent resonant controllers (see section IV-B-2) regulates the voltages in the case of unbalanced linear loads. In this implementation, L_n has been neglected and the same transfer function for the three sequences (i.e., positive, negative, and zero sequences) has been used. Note that multi-resonant (see Fig. 30) and repetitive controllers (see Fig. 31) are also good options for matrix converters feeding unbalanced non-linear loads [37], [61], [290], [292].

Indirect matrix converters (see in Fig. 6) share same advantages of matrix converters in terms of power density and reliability [109], [329] (see Fig. 6). According to [122], one of the advantages of the indirect matrix converter is that several inverting stages can be connected to a single pulsating rectifying stage. Regarding the control system of this topology, in [128], an FS-MPC strategy (see section IV-B-4) is proposed for controlling a four-leg indirect matrix converter. The proposal was validated through simulations and experimental assessment, showing a good performance [330]. Alternatively, the load side converter could be replaced by a multilevel convertertopology, for instance, using a four-leg three-level NPC VSC [121].

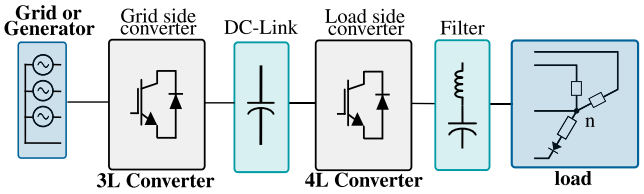

FIGURE 40. A 7-leg back-to-back converter proposed for variable speed generation in [60].

Additional topologies for power conversion from a 3-phase power supply to a four-leg system are based on back-to-back systems, as shown in Fig. 40. The grid or generator side is connected to an electrical generator that could be operating under a maximum power point tracking algorithm (MPPT) (e.g., in the case of wind turbines) or a maximum efficiency point tracking algorithm as, for instance, in the case of a variable speed diesel generator. Because of the boost capability of the topology shown in Fig. 40, it is possible to operate the generator at a relatively low speed achieving a better speed operating range than that achieved with matrix converters.

Control systems for the topology shown in Fig. 40 are presented and extensively discussed in [60]. The control methodology proposed in [60] is based on resonant controllers and a feed-forward compensation term relating the power-current at the load side to the torque-current component at the generator side. In this case, the control system on the generator side is similar to that shown in Fig. 35 for voltage (single-loop current control scheme), but without the active damping and virtual impedance; whereas the control scheme on the load side converter is the one shown in Fig. 35 (single-loop voltage control scheme). Another application of back-to-back topology is reported in [85]. In this case, the back-to-back converter is used to interface a doubly fed induction generator (DFIG) to a stand-alone unbalanced load (see Fig. 41). The three-leg VSI is connected to the rotor of the DFIG, and the four-leg VSI is connected to the stator. The control system is designed to regulate the magnetizing and power components of the rotor currents using the three-leg rotor-side converter. The four-leg stator-side converter is controlled to achieve two control targets. To maintain the dc-link voltage constant as well as to compensate the zero and negative sequence currents of the load, maintaining the DFIG stator current balanced. In [85], a combination of resonant and PI controllers is used to achieve these two control goals.

In [88], a deadbeat controller (see section IV-B-6) is proposed to regulate the output voltages in the four-leg power supply. Additionally, in this work, an algorithm to eliminate the coupling effects among different phases produced by the

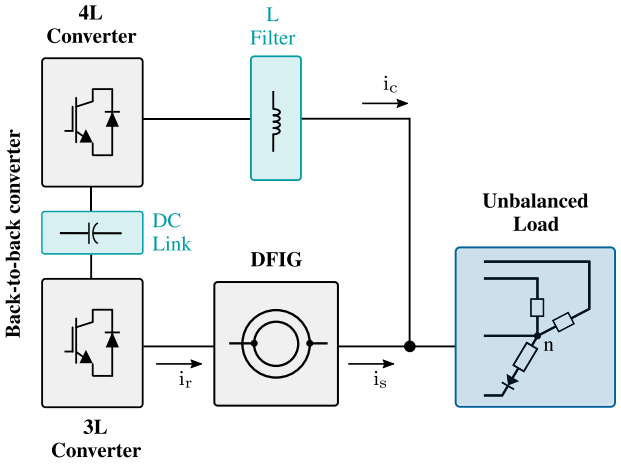

FIGURE 41. A topology proposed in [85] for the control of a doubly-fed induction generator (DFIG) feeding four-wire loads.

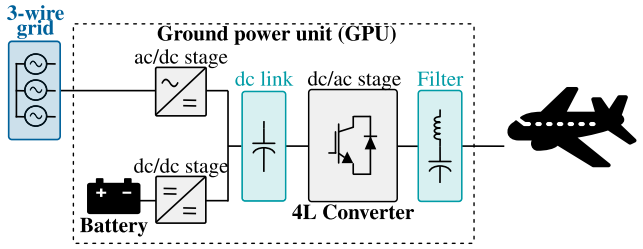

FIGURE 42. Example of an aircraft group power unit.

neutral inductor is considered. In [74], a repetitive control system (see section IV-B-3) is proposed and experimentally validated. A zero phase-shift algorithm is presented in this paper to compensate the phase delays typically introduced by the discretization algorithm and measurements in the feedback signal. As mentioned before, repetitive control systems have a relatively low dynamic response (see [86], [112]). Therefore, in [86], a combination of deadbeat for a fast dynamic response, with repetitive control, is proposed. It is claimed that this control methodology reduces the total voltage harmonic distortion to less than 0.5% when highly unbalanced non-linear loads are fed by the four-leg VSI. A control system in the RRF has been also been proposed [331] using PIs. Also, in [309], an LQR controller (see section IV-B-7) is proposed and validated with fast recovering times and small voltage drops in [332].

The model predictive control (see section IV-B-4 and section IV-B-5), has also been proposed for four-leg converters in stand-alone applications [299], [308], [333]–[335]. In [333], [334], a simple model current predictive control strategy is proposed for controlling a four-leg converter (similar to that shown in Fig. 1) feeding an unbalanced and distorted load. The proposal was validated through simulation and experimentally, showing a good performance. A similar approach is proposed in [335], but for controlling a three-level four-leg NPC converter.

Recently, in [336], a new control system based on the differential flatness theory [337] and the Grey Wolf optimization method [338] has been proposed. A two-level four-leg VSI is used to control balanced output voltages under unbalanced loads. The proposal is experimentally validated, showing a good performance. However, only unbalanced resistive loads have been used and no harmonics have been compensated. In [24], an extensive review of control schemes of four-leg converters used in stand-alone applications is presented.

Additional applications of four-leg converters acting as stand-alone power supply have been also reported. For instance, to eliminate the common-mode voltage in an induction machine motor drive. As it is well-known, common-mode currents have the potential to produce damage to the machine or undesired tripping of the protections [339]. Therefore, in [69], it is proposed the use of a five-wire four-leg two-level VSI for the elimination of the common-mode voltage by modifying the modulation strategy of the four-leg converter. The design of the control systems and experimental results to validate the proposed methodology are discussed in the paper. Authors in [92] propose a methodology to drive two ac motors independently with only one four-leg inverter (Multi-machine drives). The proposed methodology considers the use of two legs of the inverter to drive each machine (u-v and u'-v'), while the remaining phase of both motors (w and w') is connected to the neutral point of a capacitor bridge. A theoretical analysis of the harmonics in the output voltage using an expanded two-arm modulation scheme is also performed in [92]. Simulation tests show the effectiveness of the proposed strategy.

3) GROUND POWER UNIT

Fig. 42 shows the diagram for a Ground Power Unit (GPU). A GPU can be considered a particular case of a stand-alone power supply for aerospace applications, which typically use 400Hz and must accomplish stringent safety and power quality regulations [62], [340]. The GPU is connected to the aircraft after landing to provide electrical energy to the electronic equipment available on the plane. In the past, energy was provided by motor-generation systems. However, nowadays, this configuration has been replaced by static converters because of the advantages associated with this technology [114], [341], [342].

An aircraft can be considered as an isolated three-phase four-wire unbalanced electrical system, with single-phase linear/non-linear loads being fed by the static converter. The standard solution for a power electronic-based GPU is typically implemented using three H-bridge converters [186], like that shown in Fig. 12(d), with power operation ranges between 32-200kVA, being 90kVA the most typical power rate. In this case, three H-bridges sharing the same dc-link are used to control each of the output phase-to-neutral voltages independently. Also, topologies based on four-leg matrix converters have been proposed in the literature [113], [343]. The higher reliability of this converter is a great advantage

on these applications, however, under highly distorted loads the converter suffers from low power quality and power oscillation. Recently three-level four-leg NPC multilevel converters have been proposed for GPU applications [44], [61]. As reported in these publications, the NPC has several advantages for this sort of application, considering the higher effective switching achievable with a three-level converter, which makes it possible to utilize smaller filters at the load-side (see [61]), reducing the reactive power consumption. This is of particular importance in this application as the fundamental frequency is 400HZ, and high-order (e.g. up to 13th) harmonic components are being compensated.

It should be highlighted that, the control scheme for GPU applications are equivalent to those discussed for UPS applications (e.g., resonant controllers, repetitive controllers and PI in SRF [75], [76]), but considering that the fundamental frequency at the output voltage is usually 400Hz, instead of 50/60Hz, difficulting to ensure stability of the controllers when high-order harmonics are being compensated (high-order harmonics frequency become close to the Nyquist frequency) [61], [313]. To solve this issue higher order discretization methods, such as Tustin pre-warping, and frequency response methods are used to design the controllers, i.e., Bode plots [186], Nyquist diagrams [61], [292]. Nyquist stability analysis is required when multi-resonant controllers (see Fig. 30) [61], [290], [292], and also repetitive controllers (see Fig. 31) [37], [45].

B. MICROGRID APPLICATIONS

In this section, four-leg converters working in MGs are discussed. For the sake of clarity, the following classification was established: (i) independently controlled converters, (ii) cooperatively controlled converters for imbalance sharing, (iii) cooperatively controlled converters for power quality enhancement, and (iv) converters for power managing in single/three-phase systems. Note that, power converters that belong to the group (i) are characterized by being controlled using a decentralized approach [16], [344], i.e., their control scheme is based on local measures and does not exist any coordination (and communication) with other converters that could be present in the system. In contrast, converters within the group (ii), are controlled coordinately to regulate one or more variables of the system. This is usually performed by a secondary and/or tertiary control level [16], [345]. This approach has been widely used for MG applications, aiming that both active and reactive powers and imbalances and harmonics are cooperatively shared by the four-leg converters that form part of the MG. Regarding converters belonging to the group (iii), they have a similar objective that those in the previous group, but the goal is to compensate (not share) cooperatively voltages and/or currents at some point of the MG. Finally, converters within the group (iv) aim for improving the sharing of single-phase powers in MGs where there are both single-phase and three-phase power generation. It should be noted that almost all the reported works proposing control systems for 4-leg converters for categories (ii)-(iv) are for microgrids applications. In contrast, those proposed for category (i) correspond mainly to 4-leg converters connected to the grid. The main works for each category are discussed in the coming subsections.

1) INDEPENDENTLY CONTROLLED FOUR-LEG CONVERTERS

Four-wire converters have also been applied to eliminate issues such as doubly frequency power oscillations in distribution systems. As discussed in previous publications [40], [242], active power oscillations have negative effects on the lifetime of the dc-link capacitors of converters. Moreover, reactive power oscillations may introduce voltage fluctuations in some points of a microgrid or distribution network. However, when 3-wire voltage source converters are utilized, it is not possible to eliminate the double frequency oscillations in the active and reactive powers simultaneously without introducing harmonic distortion in the converter output currents, which is certainly undesirable (see [346]).

Nevertheless, as discussed in [40], [242], the zero-sequence components provide an additional degree of freedom, which can be used to simultaneously eliminate the power oscillations in the active and reactive powers. For instance, the control scheme presented in [40] eliminates the active power oscillations at the converter output using the zero sequence components of voltage and currents; meanwhile, the reactive power oscillations are eliminated using the positive and negative sequence components. Note that the proposal reported in [40] is based on the single-loop current control scheme shown in Fig. 35 and it is implemented in the RRF, as shown in Fig. 29. On the other hand, the control system presented in [242] eliminates the active power oscillation from the dc-link capacitors using a vector-controlled approach. The proposed control system is based on a single-loop current control scheme (see Fig. 35) implemented in the SRF, as shown in Fig. 30. Experimental results are presented in both works ([40], [242]) validating the proposed methodologies.

Finally, in [347], a low-voltage ride-through (LVRT) scheme for a three-phase four-wire grid-connected converter is proposed. The converter interfaces a distributed generation unit with the main grid. The proposal is composed of primary and secondary control levels [348]. The former includes the cascaded voltage and current control loops (see Fig. 36), whereas the latter controls the reactive power injection during the balanced/unbalanced voltage sags/swells. One advantage of this proposal is the fact that it is developed based on the independent control of each phase and does not require the calculation of symmetrical components. Therefore, the use of a sequence extraction algorithm is not required. This is particularly important since most of the sequence separation algorithms are strongly affected by noise, harmonic distortion, and small variations in the sampling time [239], [240]. The proposal reported in [347] was validated through simulations, showing a good performance. However, experimental validation was not provided.

2) COOPERATIVELY CONTROLLED FOUR-LEG CONVERTERS FOR IMBALANCE SHARING

As reported in several publications [66], [199], [345], [349]–[353], in a typical isolated AC microgrid [354], the Distributed Generators (DGs) (see Fig. 43) have to cooperatively supply the active and reactive powers required by the system [66], [349]. This task is typically achieved using droop control [345], [353], implemented in the control system displayed in Fig. 36. In this case, secondary control systems [345], [351] are used to restore the frequency and/or the voltage at the PCC (or other points) to the nominal values. A full discussion of the control methods utilized in microgrids is considered outside the scope of this paper and the interested reader is referred elsewhere [199], [352].

In a low voltage four-leg microgrid, the converters are connected, as shown in Fig. 43, to feed unbalanced, linear, and non-linear loads, located at the PCC or at other points in the system [65]. At the dc-link side of the four-leg DGs, renewable or conventional energy sources such as photovoltaic panels, wind energy conversion systems (WECs), Battery Energy Storage Systems (BESSs), variable-speed generators, etc., are connected using an additional converter topology when required [60], [108]. Alternatively, conventional diesel generators, gas turbines, etc., can also be directly connected to the PCC, increasing the inertia of the system.

Few papers discuss collaborative control of four-leg microgrids, where the imbalances are produced not only by the presence of negative sequence components but also by the zero sequence [31], [65], [90], [355]. One of the main problems produced by the propagation of the imbalances is the fact that these components are shared unequally between the DGs [65]. Therefore, one or several four-leg converters could have a high current overload in one of the output phases, and this can affect the stability of the whole system if the tripping and disconnection of these units are produced (a similar situation can occur for harmonic distortion) [356], [357]. To avoid this situation, control schemes to achieve the sharing of imbalances and/or harmonics among the converters present in the MG have been proposed in the literature. These sharing control algorithms use the residual current capacity available in the four-leg/four-wire converters [31], [65], [90], [178], [351]. Most of the control systems reported in the literature, for imbalance sharing applications, are based on the utilization of virtual impedances, which was previously described in section IV-A3.

The selection of virtual impedances is not easy to achieve. In most papers, only the resistive components (i.e. R^- and R^0 in Fig. 28) are considered, neglecting the inductances in $G^-(s)$ and $G^0(s)$. If low values of virtual impedances are considered, then the sharing of the imbalances is rather poor [90]. If the values of the virtual impedances are too high, then the imbalances in the voltages could be too large at the PCC or other points in the microgrid [65], [358]. Unfortunately, the sharing of the imbalances is affected by the size of the line impedances connecting the DGs to the PCC, and it is also dependent on the operating point of the microgrid. Therefore, the tuning of the virtual impedances is not a simple task.

To overcome these drawbacks, adaptive systems have been proposed in [90], and tertiary control systems have been proposed in [65]. In [359], it is proposed to divide the microgrid into several buses or areas where the power quality required by the loads is different. A tertiary control system is then implemented, adjusting the compensating efforts in each converter to fulfill the maximum voltage imbalance required in each area. Simulation results are provided, which demonstrate the good performance achieved with this methodology.

A completely new approach for collaborative control of four-leg converters is proposed in [30], [31]. It is based on controlling each phase of the four-leg converters as an independent single-phase voltage source. Therefore, separate and decoupled droop control algorithms can be implemented in each phase. Using three secondary control systems, the load connected at the PCC is well regulated and operating at the nominal frequency during steady-state conditions. The main advantage of this method is that the sharing of the power and unbalanced components is virtually perfect. However, during the transient, each of the phases is operating with a slightly different frequency. Therefore, this control system is suitable for loads that can withstand this condition (heating and lighting of small isolated villages).

All the proposals discussed until now are based on a centralized approach, meaning that a central controller able to communicate with all the four-leg converters is required to perform the secondary control level. This central controller must process all the information of the system and, based on it, implements the secondary control actions. For instance, in [65], a centralized secondary controller is proposed to adaptively regulate the value of the virtual impedances of the converters to regulate the maximum voltage imbalance/distortion at the point of common coupling. Similarly, in [30], [31], a centralized controller is proposed to regulate frequency, voltage and phase at the PCC. The centralized approach has been widely used in the literature; however, the distributed approach to implementing secondary control systems has got attention from researchers in recent years. In this method, a centralized controller is not required because the units work autonomously in a cooperative fashion to reach global objectives [360]. Thus, the control effort is distributed among the converters. Some advantages of the distributed approach over the centralized one are better reliability, flexibility, scalability, plug-and-play operation, and tolerance to failures in communication links [16], [361]–[364].

Distributed control approach applied to four-leg converters has been just recently addressed [277]. In this work, a distributed control scheme is proposed for improving the sharing of imbalances and harmonics in four-wire MGs and, at the same time, regulate the imbalance and distortion in the voltage at the output of the converters, to meet the appropriate power quality standards [365], [366]. This method is based on the concept of a virtual impedance loop (see section IV-A3) and uses the conservative power theory (CPT) [258], [268]

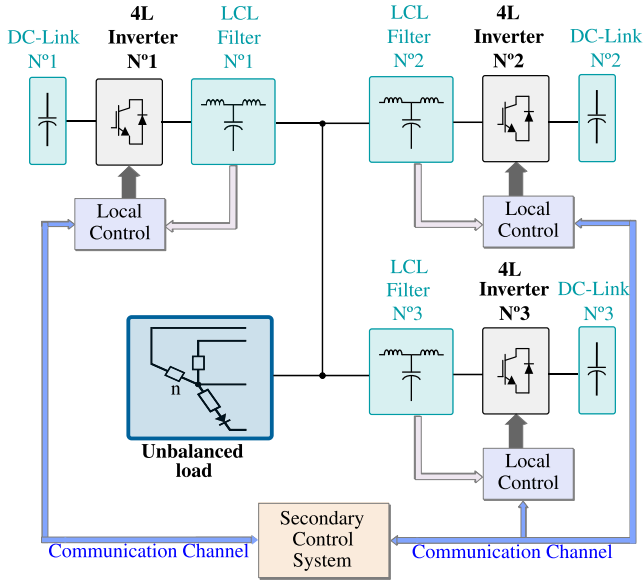

FIGURE 43. A microgrid based on four-leg VSC. Each DC-link could be connected to a renewable or conventional energy source, BESS, variable speed generators, etc.

to identify positive, negative and zero sequence current components in the system. The latter is an advantage since it does not require the use of sequence separation algorithms, which are strongly affected by noise, harmonic distortion, variations in the sampling time magnitude, etc. [239], [240]. One disadvantage of the proposal lies in the complexity of the CPT; thus, its implementation in low-cost control platforms could be difficult to achieve [268].

3) COOPERATIVELY CONTROLLED FOUR-LEG CONVERTERS FOR POWER QUALITY ENHANCEMENT

The imbalance sharing methods discussed in the previous section aims to improve the sharing of unbalanced and/or distorted currents among the converters of the MG to avoid high line currents in some converters, which could lead to a disconnection of some of them due to the activation of their over-current protection systems. In addition, cooperation can be done to compensate voltages and/or current at some PCC of the MG. This approach is similar to the use of APFs but is a more cost-effective solution. Indeed, it is based on embedding imbalance and harmonic compensation capabilities into the control algorithms of the converters that are already available in the MG, thus maximizing the utilization of the hardware.

In this context, reference [**?**] proposes a cooperative control strategy to improve the power quality in four-wire islanded microgrids. In this proposal, a master/slave-based cooperative operation of the converters in the MG is presented. By using the CPT, unwanted currents of the system are calculated, and they are compensated by the slave converters (according to their available power), improving the power quality. A supervisory controller is used to calculate the compensation effort for each slave converter. It should be noted that this proposal was only validated through simulations. Thus, its application in an actual system is not clear as the implementation of algorithms based on the CPT represents a relatively high computational burden for the control platform [268].

As has been stated in this paper, neutral currents are an important concern in four-wire systems. High neutral currents can overload the neutral conductor, producing fire in the most critical situations. For this reason, in [367], [368], a control method to compensate neutral currents by using four-leg converters is proposed. The aim of this proposal is to use the remaining power capacity, which is available after the active and reactive power injection, to compensate neutral currents. The proposal was validated through simulations and experimental tests, showing a good performance in terms of neutral current compensation. It should be noted that the proposal was validated by considering that neutral currents are generated just at the fundamental frequency. Later on, the proposals reported in [367] and [368] were extended in [369], [370] to be applied in four-wire multi-microgrids. In these references, the Internet of Things (IoT) Platform is proposed as a communication network among the microgrids to exchange information and calculate their respective compensation efforts. Simulation results showed a good performance of the proposals in terms of neutral current compensation among the microgrids, even in the case of partial failure in the communication system. However, the effects of latency or data losses in the communications system were not addressed.

4) CONVERTERS FOR POWER MANAGING IN SINGLE/THREE-PHASE MICROGRIDS

Four-leg converters have also been used for power managing in single-/three-phase microgrids, as shown in Fig. 44. In this case, and contrary to the MG illustrated in Fig. 43, the power generation is performed not only for three-phase distributed generation units (DGs) but also for single-phase power generation units. This S/T-MG is inherently an unbalanced system with unequal single-phase distribution among its phases. In this scenario, overloading in some of the DG phases may occur, producing malfunctions in the DG and load shedding, which could affect the overall MG operation security and reliability.

In [371], a decentralized control scheme based on a modified droop scheme is proposed for controlling the power flow among the different phases of the four-leg converters that composes an S/T-MG. In that reference, the studied S/T-MG consists of PV units, battery units and hybrid PV/battery units. The proposal was experimentally validated [371], showing a good performance. However, as it is based on a decentralized approach, there is not any coordination between the four-leg converters, and also the computation of their single-phase powers is not discussed in detail. On the other hand, in [372], a hierarchical distributed control approach is proposed for managing the power flow among the phases of a hybrid AC/DC MG, maximizing its loadability. The proposal was validated through simulation work, showing a good

performance in terms of improving the power balancing of the single/three-phase AC MG and voltage quality enhancement at both the PCC and the output of the four-leg converters. In a later work, this approach even considers single-phase loads and sources [373]. However, experimental verification of the proposal is not provided, and also, the coordination among the four-leg converters and single-phase converters was not considered (see Fig. 44).

In [374], a control system to regulate the power flow among the different phases of a three-phase four-wire distribution power system by means of single-phase converters connected among the phases is proposed. The idea behind this proposal is to improve the voltage quality at the PCC of the MG by controlling the single-phase converters of the system as slave units injecting unbalanced powers to compensate the voltage at the PCC. The unbalanced power that each single-phase converter must supply to the system is calculated by a centralized master controller based on the CPT [258], [268]. Simulation results are provided to validate the proposal. However, experimental validation is not performed. Also, in [374], the coordination between the single-phase and three-phase four-wire DG units is not investigated. Finally, the CPT algorithm could represent a relatively high computational burden for the control platform [29].

Contrary to [374] which aims the voltage compensation at the PCC, in [375], a control system for achieving the compensation of negative and zero sequences of the current in a four-wire distribution system by using single-phase distributed generation units is proposed. The power reference for each single-phase DG unit is calculated based on an optimization problem, where the voltage regulation of the three phases of the system along with the available power rating of DGs are considered as constraints- the optimization problem is solved by using the Karush–Kuhn–Tucker (KKT) method. Simulation results validate the proposal. However, experimental validation is not considered. Moreover, the coordination between the single-phase and three-phase converters that form the system was not addressed.

C. ACTIVE-FILTERING AND REACTIVE POWER COMPENSATION APPLICATIONS

These converters can be classified as: (i) Shunt connected compensators, (ii) Series connected compensators, and (iii) Series-parallel compensators. The main contributions of four-leg converters proposed for these applications are presented and discussed below.

1) SHUNT CONNECTED COMPENSATOR

The diagram of Fig. 45a shows the implementation of a typical four-leg shunt active filter. Usually four-leg two-level topology is used [41], [52], [77], [89], [145], [146], [163], [164], [178], [268], [376], but also four-leg three-level NPC [41], [61], [145], [163] (see Fig. 2) or Y-connected independent converters can be used instead [41], [164] (see Fig. 12) when improved harmonics spectrum, reduced switching frequency or simpler modulation wants to be

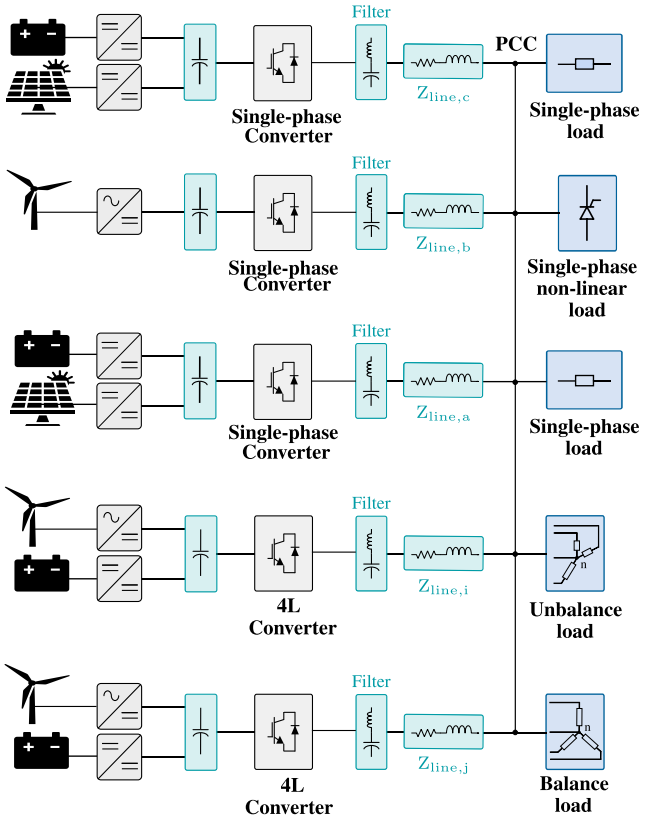

FIGURE 44. Example of a single/three-phase microgrid.

achieved. The converter can be connected to the Point of Common Coupling (PCC) using a first-order L filter or a higher-order filtering topology (see section II-C), commonly third-order LCL proposed in [145], which has a better power to volume ratio and improved rejection of the unwanted signals [145]. The utilization of a four-leg converter as a single-phase APF was reported in [377], where the authors developed two universal APFs configurations for single-phase systems (see also [378]).

A four-wire APF operates by supplying compensating unbalanced and distorted currents to the PCC (see Fig. 45). Several methodologies have been reported to calculate the compensating currents for three and four-wire applications [65], [71], [379]–[383]. For instance, frequency-based methods (see [145], [163], [379]) are usually based on the application of the Fast Fourier Transform, Kalman filters and Wavelet transforms to identify the current components to be compensated. As pointed out in [380], the main problem of the frequency-based methods is the time delay introduced to estimate the compensating current in the presence of fast variations in the load. Other approaches such as the Fryze-Buchholz-Depenbrock (FBD) theory [384]; Lagrange multiplier-based decomposition [385]; the estimation based on neural networks [386], [387] and the use of synchronous frames [388], [389] have been proposed for APF applications. However, it must be noted that the most used methods to determine the compensating currents for the APF are [390]:

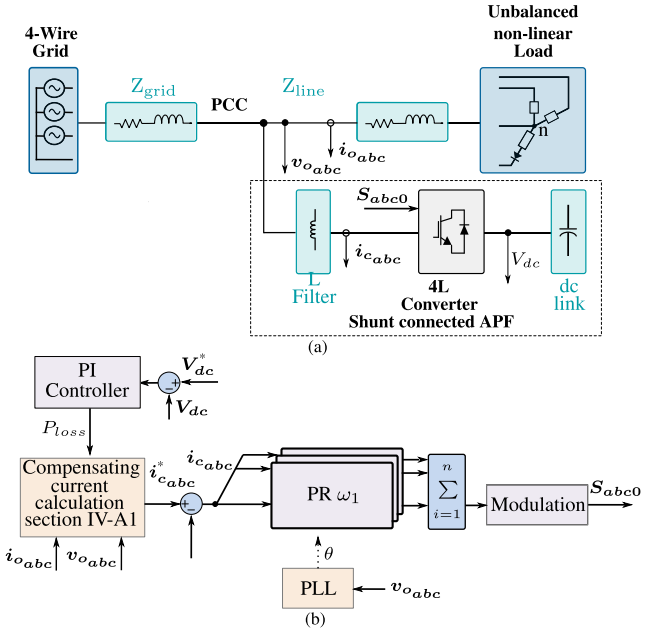

FIGURE 45. Shunt active power filter (a) Connected to a grid. (b) Control system with CPT and PR [268].

the p-q theory [153], [391], [392], the FBD theory [384], and the CPT [268], [278]. In [390], a comparison among these three theories is performed, concluding that their results are very similar under ideal conditions (strong grids). If these power theories are applied to distorted and/or unbalanced grids, it is possible that "hidden currents" could be generated [39], [120], meaning that currents that are not present originally in the load are artificially generated by these theories.

After the compensating current reference is calculated (including its zero sequence component), it has to be regulated using current control loops. There are available several alternatives for the implementation of the digital control system. It is claimed that the simplest alternative is to utilize hysteresis control techniques, which can be used to regulate all the harmonic components in the compensating currents [145], [163], being the first attempts to control four-leg APF [131], [393], [394]. In order to avoid excitation of resonant modes on output filters, caused by the variable switching frequency of hysteresis band current regulators, authors in [77], [395] proposed an optimized design methodology to size passive elements of APF, defining a frequency range for stable operation. The methodology was experimentally validated. Alternatively, the use of three-dimensional vector control was proposed in [79] and a user-defined constant switching frequency control strategy was proposed in [230]. The method still uses hysteresis-band current controllers but uses zero-sequences states to regulate and equalize the switching frequencies of all legs of the converter. However, these approaches are complex and unpractical. Other alternatives are to implement fixed frequency predictive control [33], [58], [396], a control technique that typically requires a high computer burden (see Section IV-B4); control in *d-q-0* coordinates (see IV-B1), which may require multiple *d-q* axis rotating at different sequences and frequencies, and an additional control system to regulate the zero sequence component.

The most established and simplest alternative for compensating distorted current, which includes zero-sequence signals, is to use multi-resonant controllers followed by a modulation stage (see Section IV-B2 and [60], [61]). The performance of this approach is excellent and robust, however only a finite number of harmonics at specific frequencies are compensated. Fig. 45b shows the control diagram for this approach [61], [110], [268]. Some applications require variable electrical frequency, such as microgrids or modern aircraft grids, and the utilization of self-tuning resonant controllers becomesrequired to maintain a good tracking performance in the current control loops. This can be achieved utilizing the dashed line labeled θ in Fig. 45b. A simpler alternative to resonant compensators is obtained using repetitive control or iterative learning control [112]. This approach does not need the design of several single controllers, however, repetitive controllers have poor dynamic response compared to resonant control systems [112].

In addition, in [32], an analysis of the main topologies of four-leg APF is performed in terms of dc-link rating voltage, quality of the output waveforms, and efficiency. This reference names the topologies based on their number of converter legs (*l*) and filter inductors (*L*). According to [32], the four-leg APF topologies most studied and reported in the literature are (i) the three-leg split capacitor converter (3*l*-3*L*), (ii) the 3*l*-4*L* topology, similar to the 3*L*-3*l* but with an additional inductor in the fourth wire (midpoint of dc-link), (iii) the 4*l*-3*L* topology, where the neutral connection is provided for a four-leg converter, the 4*l*-4*L* converter which has an additional inductor at the output of the fourth leg converter, and (v) the 6*l* topology, composed by three isolation transformers, and one six-leg converter (12 switches). This work concluded that topologies 3*l*-4*L* and 4*l*-4*L* have better performance in terms of THD than topologies 3*l*-3*L* and 4*l*-3*L* respectively. However, the former was less efficient in cases with high levels of zero-sequence current components or high imbalance. Finally, it is claimed that topology 6*l* is the most efficient, mainly due to the lowest level of dc-link voltage. However, this topology requires a higher number of switches and also isolation transformers, meaning the most costly solution. Additional topologies, such as two interconnected four-leg converters to compensate voltages and currents when interfacing an MG have been proposed in [376].

2) SERIES CONNECTED COMPENSATOR

Fig. 46 shows the electrical scheme of the dynamic voltage restorer (DVR). As observed, it corresponds to a series-connected four-leg converter whose function is to protect a sensitive industrial load from voltage perturbations. In [83], [84], a control system for a four-leg DVR is proposed and experimentally validated. It is based on the single-loop voltage control scheme shown in Fig. 35(c),

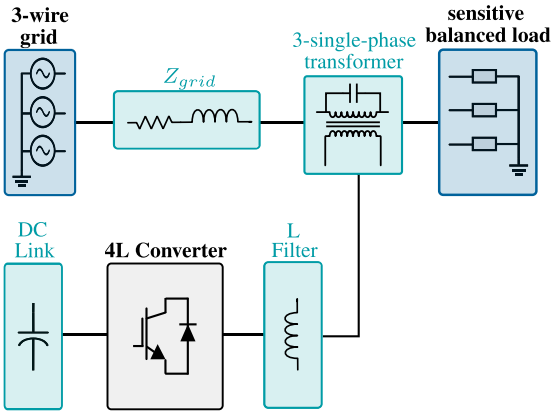

FIGURE 46. Scheme of a four-leg dynamic voltage restorer.

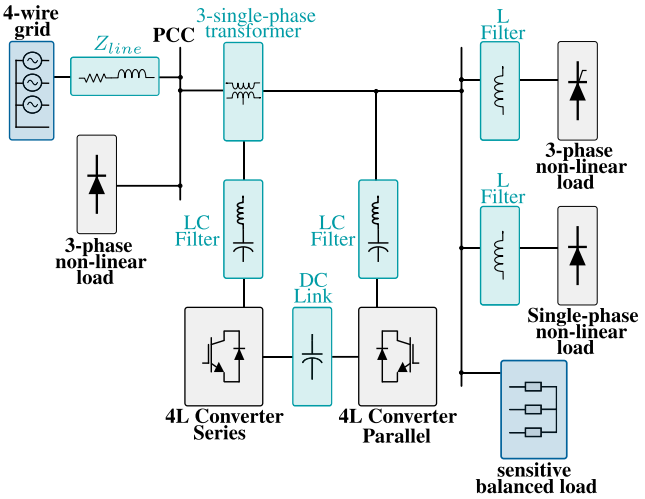

FIGURE 47. Series-parallel active filter.

which is implemented in the RRF. The sequence components theory is used to generate references to the DVR. The performance of the DVR was validated against different types of faults, showing a good performance. Later on, the same authors of [83], [84] proposed a PWM scheme for the four-leg based DVR in [397]–[399]. In those references, it is claimed the proposed PWM method is useful for the generation of unbalanced, 3-phase voltages, including a zero sequence component.

3) SERIES AND PARALLEL COMPENSATOR

Fig. 47 shows a four-leg series-parallel active filter. As seen, it is composed of two converters: one in shunt configuration, and the other in series connection. The shunt four-leg converter compensates the undesired unbalanced and harmonic currents (both negative and zero sequence current components) at the PCC. On the other hand, the series-connected converter aims to compensate both negative and zero sequence voltages to improve the power quality at the PCC. Also, it allows limiting the flow of large currents during voltage sags at the PCC.

It must be highlighted that the series-parallel active filter is less common than the parallel-connected. This is because the series connection of a compensator requires necessarily to intervene the electrical system where the compensator will be placed, which is difficult to achieve for some applications. However, this approach has been proposed for some applications. For instance, in [376], a three-phase four-leg compensator for microgrids applications is proposed: it is composed of two four-leg converters (one series-connected and the other parallel-connected). In [376], both the negative and the zero sequence components of currents and voltages are identified to generate the references for both the series and the parallel four-leg converter. The proposal was verified in simulations and experimentally using a laboratory prototype, showing a good performance. However, its extension for harmonics issues is not discussed.

An extension of [376] for distorted loads is proposed in [81]. According to the authors, the proposed series-parallel compensator allows the harmonic current suppression, reactive power compensation and imbalance compensation. Also, it is claimed that the proposal can be used for single-phase loads. The proposal was validated through simulations, showing good results. However, an experimental validation was not provided.

In [80], a series-parallel active filter is proposed for three-phase four-wire distribution systems. It is composed of a three-phase three-leg series-connected converter along with a three-phase four-leg shunt-connected converter, the performance of the compensator is validated through simulations assuming both unbalanced and distorted loads, showing good behavior. However, an experimental verification was not provided and a three-phase load was implemented. The performance of the proposal in front of single-phase distorted loads was not evaluated.

Finally, in [82], a three-phase four-leg series-parallel active power filter is proposed for compensating both periodic and non-periodic disturbances. This is achieved by controlling the power filter using a control strategy based on the generalized non-active power theory (GNAP) [400]. The performance of the proposal was validated through simulations and experimental results, showing a good performance. The converter can effectively compensate non-sinusoidal and non-periodic currents and voltages. One concern about this proposal is the fact that the implementation of the GPNAP theory produces a relatively high computational burden for the control platform, increasing the cost of this solution.

VI. FUTURE WORK

Four-level converters are appropriate for low voltage microgrid systems where several control issues are still being investigated. In microgrids, it is expected that every distributed generator, interfaced to the grid using power converters, could provide ancillary services, e.g. to share active and reactive and provide frequency and voltage support to the microgrid [16]. Recently, control strategies based on droop control [30],

consensus-based control [16], [29], and model predictive distributed control [401] have been proposed for three and four wire power converters. However, most of the control systems proposed in the literature have been designed and implemented for 3-leg power converters. Therefore, in the authors' opinion, considering that low voltage microgrids are usually 4-wire systems, more research is required to study the control systems required for 4-leg converters to provide ancillary services and cooperative regulation in 4-wire low-voltage microgrids.

There are other issues which can be solved using more advanced control techniques. In systems where loads are unbalanced and highly non-linear, several resonant-based controllers are typically used to regulate harmonics and regulate the positive, negative and zero sequence components of the voltage and/or currents (see Section IV-B2 and Fig. 30). In this case, when several components of the currents are regulated using independent controllers, is challenging to optimally limit the current in each phase to avoid overloading (see the discussion in [402]). Recently the application of Continuous Control Set MPC (or CCS-MPC) with external modulators have been proposed in the literature to achieve optimal limitation of currents and voltages [402] in systems where several components of voltages and currents are independently regulated. The application of these control techniques to 4-wire microgrids has not been investigated yet.

Besides of CCS-MPC [402], there are other model predictive control techniques which can deliver fixed switching frequency, for instance, Modulated Model Predictive Control [303] or M^2PC and Optimal-Switching-Sequence Model Predictive Control (OSS-MPC) [403]. These control techniques are known for their high dynamic performance and have been barely investigated for 4-leg power converter applications.

Finally, in the opinion of the authors of this research effort, four-leg converter of higher power could be important topologies for the implementation of solid-state transformers. Therefore more research is required in four-leg multilevel converters and their control, improving the power density and control performance of solid-state transformers implemented in microgrids and distribution systems.

VII. CONCLUSION

This review summarized the most important contributions in topologies, modulation, control and applications of four-leg converters, given a comprehensive discussion of the state of the art on this technology and providing perspective and unsolved challenges for future works. Compared with previous overview papers, this work discussed virtually all the 4-leg topologies proposed in the literature, including modulation techniques and the control systems required in some relevant fields as for instance microgrids.

Several topologies have been proposed as four-leg converters, being the two-level converter the most simple and utilized topology. However, when high performance, i.e. high effective output switching frequency; relatively low switching frequency in each device and a smaller output power filter is required, multilevel converters such as three-level NPC, T-type NPC, and flying capacitor converters are better alternatives even when these topologies usually require a more complex modulation strategy. If high power density is needed, e.g. for aerospace applications, then direct and indirect 4-leg matrix converters are the best alternatives. Nevertheless, as discussed in this paper, matrix converters are not suitable topologies for feeding highly unbalanced loads because power pulsations at the converter's output produce highly distorted currents at the converter's input.

This paper also discusses 4-leg topologies obtained from the interconnection of several converters (see Section II.B.4). With this converter topology, higher power outputs can be achieved, which could be necessary in future applications as distributed generation is expected to grow.

Modulation methods for 4-leg power converters has also been extensively discussed in this paper. The simplest implementation of modulation methods is the use of hysteresis based PWM current control. However,this method generates a neutral current with a ripple up to three times higher than the line currents and generates variable switching frequency. There are some methodologies to solve the variable switching frequency problem, but increasing complexity and producing a lower dynamic response. Another simple modulation method is the carrier-based PWM augumented with a min-max methodology to increase the maximum modulation index. However, it is more complicated to implement some functions with carrier-based methods, such as balancing the capacitors of a 3-level NPC converter. A more flexible alternative is implementing space vector modulation methods using *abc* or $\alpha\beta0$ coordinate frames.

Output filtering of four-leg converters has also been reviewed in this work. It has been shown that for *L* or *LCL* filters, the line inductances are reflected in the zero-sequence plant, therefore connecting a neutral inductor is not entirely mandatory, However, neutral inductors significantly reduce the neutral current ripple if included. When an LC power filter is placed at the converter's output, connecting the neutral of the star connected capacitances to the 4-leg (neutral) wire is recommended to reduce the high dv/dt on the zero-sequence (or common-mode) voltage.

To regulate the output voltage, resonant controllers arise as the most implemented and effective method to regulate four-leg converter's outputs. Resonant controllers can be implemented in *abc* or $\alpha\beta0$ coordinate frame. However, there are some advantages in implementing a control system in the $\alpha\beta0$ frame, because it allows direct control of the zero-sequence component and a decoupled plant transfer function is usually simpler to obtain. Additional control strategies have been implemented for four-leg converters, such as: repetitive controller, dead-beat, LQR, finite-set predictive control (FS-MPC) and modulated predictive control. Most of these strategies can achieve higher dynamic and are simpler to implement in systems with large distortion compared to linear controllers, however some of them provide

non-fixed switching frequency and could demand a high computer burden. As aforementioned more research is required in this area.

Several applications of 4-leg power converter have been reviewed in this work. One of the most novel and recent applications are in the field of 4-leg microgrid, with a few works reporting applications such as active filtering, droop control and consensus control methods to share positive, negative and zero sequence components of currents and voltages (see Sections V-B-2 and V-B-3). Again, as aforementioned in Section VI, more research is required in this area which is going to be important in the near future.

Regarding four-leg converters used for active filtering and reactive power compensation applications in microgrids and distribution systems. A key element in an active filter implementation is selecting the correct power theory to calculate the compensation efforts. Indeed, some power theories are well defined under sinusoidal operating for linear and balanced symmetrical multiple-phase or even single-phase systems. In contrast, other power theories can work effectively with non-sinusoidal and unbalanced loads. Thus, knowing the characteristics of the waveforms present in the studied system will improve the selection of the best power theory for that application.

REFERENCES

[1] A. Keane, L. F. Ochoa, C. L. T. Borges, G. W. Ault, A. D. Alarcon-Rodriguez, R. A. F. Currie, F. Pilo, C. Dent, and G. P. Harrison, "State-of-the-art techniques and challenges ahead for distributed generation planning and optimization," *IEEE Trans. Power Syst.*, vol. 28, no. 2, pp. 1493–1502, May 2013.

[2] D. Boroyevich, I. Cvetkovic, D. Dong, R. Burgos, F. Wang, and F. Lee, "Future electronic power distribution systems a contemplative view," in *Proc. 12th Int. Conf. Optim. Electr. Electron. Equip.*, May 2010, pp. 1369–1380.

[3] S. C. Ikkurti and H. Prasad Ikkurti, "Proportional multi resonant controller based cascaded voltage control scheme of three phase four leg inverter for nonlinear loads in OFF grid solar photovoltaic applications," in *Proc. Int. Conf. Recent Trends Electr., Control Commun. (RTECC)*, Mar. 2018, pp. 222–227.

[4] L. Dan-Yun, S. Qun-Tai, L. Zhen-Tao, and W. Hui, "Repetitive control of the stator-side four-leg converter in stand-alone DFIG-based wind energy conversion system," in *Proc. 34th Chin. Control Conf. (CCC)*, Jul. 2015, pp. 5795–5798.

[5] G. Pan, W. Gu, Y. Lu, H. Qiu, S. Lu, and S. Yao, "Optimal planning for electricity-hydrogen integrated energy system considering power to hydrogen and heat and seasonal storage," *IEEE Trans. Sustain. Energy*, vol. 11, no. 4, pp. 2662–2676, Oct. 2020.

[6] T. Yun, Z. Wang, Y. Li, Q. Ma, Q. Hui, and S. Li, "Multi-energy storage system model based on electricity heat and hydrogen coordinated optimization for power grid flexibility," *CSEE J. Power Energy Syst.*, vol. 5, no. 2, pp. 266–274, Jun. 2019.

[7] C. R. Stoldt and S.-H. Lee, "All-solid-state lithium metal batteries for next generation energy storage," in *Proc. Transducers Eurosensors XXVII: 17th Int. Conf. Solid-State Sensors, Actuat. Microsyst. (TRANSDUCERS EUROSENSORS XXVII)*, Jun. 2013, pp. 2819–2822.

[8] H. Weiss, T. Winkler, and H. Ziegerhofer, "Large lithium-ion battery-powered electric vehicles—From idea to reality," in *Proc. ELEKTRO*, May 2018, pp. 1–5.

[9] M. Farhadi and O. Mohammed, "Energy storage technologies for high-power applications," *IEEE Trans. Ind. Appl.*, vol. 52, no. 3, pp. 1953–1961, May/Jun. 2016.

[10] C. Burgos-Mellado, M. E. Orchard, M. Kazerani, R. Cárdenas, and D. Sáez, "Particle-filtering-based estimation of maximum available power state in Lithium-Ion batteries," *Appl. Energy*, vol. 161, pp. 349–363, Jan. 2016.

[11] G. D'Ovidio, C. Masciovecchio, A. Ometto, and C. Villante, "On design of hybrid power unit with partitioned fuel-cell and flywheel energy sorage system for city transit buses," in *Proc. Int. Symp. Power Electron., Electr. Drives, Autom. Motion (SPEEDAM)*, Jun. 2020, pp. 287–292.

[12] C. Diaz, V. Quintero, A. Perez, F. Jaramillo, C. Burgos-Mellado, H. Rozas, M. E. Orchard, D. Saez, and R. Cardenas, "Particle-filtering-based prognostics for the state of maximum power available in lithium-ion batteries at electromobility applications," *IEEE Trans. Veh. Technol.*, vol. 69, no. 7, pp. 7187–7200, Jul. 2020.

[13] P. Wheeler and S. Bozhko, "The more electric aircraft: Technology and challenges," *IEEE Electrific. Mag.*, vol. 2, no. 4, pp. 6–12, Dec. 2014.

[14] D. Cervinka, J. Knobloch, P. Prochazka, J. Kadlec, R. Cipin, and I. Pazdera, "Electric powered airplane VUT 051 RAY," in *Proc. 16th Int. Conf. Mechatronics (Mechatronika)*, Dec. 2014, pp. 6–10.

[15] L. Dorn-Gomba, J. Ramoul, J. Reimers, and A. Emadi, "Power electronic converters in electric aircraft: Current status, challenges, and emerging technologies," *IEEE Trans. Transport. Electrific.*, vol. 6, no. 4, pp. 1648–1664, Dec. 2020.

[16] E. Espina, J. Llanos, C. Burgos-Mellado, R. Cardenas-Dobson, M. Martinez-Gomez, and D. Saez, "Distributed control strategies for microgrids: An overview," *IEEE Access*, vol. 8, pp. 193412–193448, 2020.

[17] N. A. Ninad and L. A. C. Lopes, "Control of Δ-Y transformer based grid forming inverter for unbalanced stand-alone hybrid systems," in *Proc. IEEE Elect. Power Energy Conf.*, Oct. 2012, pp. 176–181.

[18] F. H. M. Rafi, M. J. Hossain, and J. Lu, "Improved neutral current compensation with a four-leg PV smart VSI in a LV residential network," *IEEE Trans. Power Del.*, vol. 32, no. 5, pp. 2291–2302, Oct. 2017.

[19] M. Digalovski, K. Najdenkoski, and G. Rafajlovski, "Impact of current high order harmonic to core losses of three-phase distribution transformer," in *Proc. Eurocon*, Jul. 2013, pp. 1531–1535.

[20] D. Wan, K. You, H. Zhou, F. Qi, S. Peng, and T. Peng, "Study on harmonic load loss calculation method of oil-paper insulated distribution power transmission equipment," in *Proc. IEEE 3rd Conf. Energy Internet Energy Syst. Integr. (EI2)*, Nov. 2019, pp. 2746–2749.

[21] A. N. Arvindan and P. Praveenkumar, "Simulation based investigation of harmonics in line and neutral currents of 3-phase utility feeding 2-pulse rectifiers," in *Proc. IET Chennai 4th Int. Conf. Sustain. Energy Intell. Syst. (SEISCON)*, 2013, pp. 144–151.

[22] T. M. Gruzs, "A survey of neutral currents in three-phase computer power systems," *IEEE Trans. Ind. Appl.*, vol. 26, no. 4, pp. 719–725, Jul./Aug. 1990.

[23] H. Jou, K. Wu, J. Wu, and W. Chiang, "A three-phase four-wire power filter comprising a three-phase three-wire active power filter and a zig–zag transformer," *IEEE Trans. Power Electron.*, vol. 23, no. 1, pp. 252–259, Jun. 2008.

[24] M. R. Miveh, M. F. Rahmat, A. A. Ghadimi, and M. W. Mustafa, "Control techniques for three-phase four-leg voltage source inverters in autonomous microgrids: A review," *Renew. Sustain. Energy Rev.*, vol. 54, pp. 1592–1610, Feb. 2016.

[25] E. Heydari, M. P. Moghaddam, and A. Y. Varjani, "Multi-resonant dual loop control of stand-alone four-leg inverter for microgrids applications," in *Proc. 9th Annu. Power Electron., Drives Syst. Technol. Conf. (PEDSTC)*, Feb. 2018, pp. 352–357.

[26] P. Verdelho and G. D. Marques, "Four-wire current-regulated PWM voltage converter," *IEEE Trans. Ind. Electron.*, vol. 45, no. 5, pp. 761–770, Oct. 1998.

[27] T. Thomas, K. Haddad, G. Joos, and A. Jaafari, "Performance evaluation of three phase three and four wire active filters," in *Proc. Conf. Rec. IEEE Ind. Appl. Conf. 31st IAS Annu. Meeting (IAS)*, vol. 2, Oct. 1996, pp. 1016–1023.

[28] T. M. Jahns, R. W. A. A. De Doncker, A. V. Radun, P. M. Szczesny, and F. G. Turnbull, "System design considerations for a high-power aerospace resonant link converter," *IEEE Trans. Power Electron.*, vol. 8, no. 4, pp. 663–672, Oct. 1993.

[29] C. Burgos-Mellado, J. Llanos, E. Espina, D. Saez, R. Cardenas, M. Sumner, and A. Watson, "Single-phase consensus-based control for regulating voltage and sharing unbalanced currents in 3-wire isolated AC microgrids," *IEEE Access*, vol. 8, pp. 164882–164898, 2020.

[30] E. Espina, R. Cardenas-Dobson, M. Espinoza, C. Burgos-Mellado, and D. Saez, "Cooperative regulation of imbalances in three-phase four-wire microgrids using single-phase droop control and secondary control algorithms," *IEEE Trans. Power Electron.*, vol. 35, no. 2, pp. 1978–1992, Feb. 2020.

[31] E. Espina, M. Espinoza, and R. Cardenas, "Active power angle droop control per phase for unbalanced 4-wire microgrids," in *Proc. IEEE Southern Power Electron. Conf. (SPEC)*, Dec. 2017, pp. 1–6.

[32] E. L. L. Fabricio, S. C. S. Junior, C. B. Jacobina, and M. B. de Rossiter Correa, "Analysis of main topologies of shunt active power filters applied to four-wire systems," *IEEE Trans. Power Electron.*, vol. 33, no. 3, pp. 2100–2112, Mar. 2018.

[33] K. Antoniewicz, M. Jasinski, M. Kazmierkowski, and M. Malinowski, "Model predictive control for three-level four-leg flying capacitor converter operating as shunt active power filter," *IEEE Trans. Ind. Electron.*, vol. 63, no. 8, pp. 5255–5262, Aug. 2016.

[34] Q. Tabart, I. Vechiu, A. Etxeberria, and S. Bacha, "Hybrid energy storage system microgrids integration for power quality improvement using four-leg three-level NPC inverter and second-order sliding mode control," *IEEE Trans. Ind. Electron.*, vol. 65, no. 1, pp. 424–435, Jan. 2018.

[35] L. Zhang, M. J. Waite, and B. Chong, "Three-phase four-leg flying-capacitor multi-level inverter-based active power filter for unbalanced current operation," *IET Power Electron.*, vol. 6, no. 1, pp. 153–163, Jan. 2013.

[36] E. Avci and M. Uçar, "SRF based output voltage control of 3-level 3-phase 4-leg AT-NPC inverter," *J. Polytech.*, vol. 21, no. 4, pp. 961–966, Jan. 2018.

[37] W. Rohouma, P. Zanchetta, P. W. Wheeler, and L. Empringham, "A four-leg matrix converter ground power unit with repetitive voltage control," *IEEE Trans. Ind. Electron.*, vol. 62, no. 4, pp. 2032–2040, Apr. 2015.

[38] C. Garcia, M. E. Rivera, J. R. Rodríguez, P. W. Wheeler, and R. S. Peña, "Predictive current control with instantaneous reactive power minimization for a four-leg indirect matrix converter," *IEEE Trans. Ind. Electron.*, vol. 64, no. 2, pp. 922–929, Feb. 2017.

[39] E. H. Watanabe, H. Akagi, and M. Aredes, "Instantaneous p-q power theory for compensating nonsinusoidal systems," in *Proc. Int. School Nonsinusoidal Currents Compensation*, Jun. 2008, pp. 1–10.

[40] K. Ma, W. Chen, M. Liserre, and F. Blaabjerg, "Power controllability of a three-phase converter with an unbalanced AC source," *IEEE Trans. Power Electron.*, vol. 30, no. 3, pp. 1591–1604, Mar. 2015.

[41] E. L. L. Fabricio, C. B. Jacobina, M. A. Vitorino, and M. B. de Rossiter Correa, "Y-connected three-leg converters applied in three or four-wire shunt compensator," *IEEE Trans. Ind. Appl.*, vol. 52, no. 4, pp. 3245–3254, Jul. 2016.

[42] A. C. N. Maia, C. Brandão Jacobina, N. Brandão de Freitas, A. de Paula Dias Queiroz, and E. Roberto Cabral da Silva, "Three-phase four-wire AC–DC–AC multilevel topologies obtained from an interconnection of three-leg converters," *IEEE Trans. Ind. Appl.*, vol. 54, no. 5, pp. 4728–4738, Oct. 2018.

[43] R. P. de Lacerda, E. L. L. Fabricio, C. B. Jacobina, M. B. R. Correa, and I. da Silva, "Y-connected topologies composed of three three-leg converters with two-level and three-level legs," in *Proc. IEEE Energy Convers. Congr. Expo. (ECCE)*, Oct. 2017, pp. 617–624.

[44] F. Rojas, R. Kennel, R. Cardenas, R. Repenning, J. C. Clare, and M. Diaz, "A new space-vector-modulation algorithm for a three-level four-leg NPC inverter," *IEEE Trans. Energy Convers.*, vol. 32, no. 1, pp. 23–35, Mar. 2017.

[45] R. Cardenas, R. Pena, P. Wheeler, and J. Clare, "Experimental validation of a space-vector-modulation algorithm for four-leg matrix converters," *IEEE Trans. Ind. Electron.*, vol. 58, no. 4, pp. 1282–1293, Apr. 2011.

[46] S. Bifaretti, A. Lidozzi, L. Solero, and F. Crescimbini, "Comparison of modulation techniques for active split DC-bus three-phase four-leg inverters," in *Proc. IEEE Energy Convers. Congr. Expo. (ECCE)*, Sep. 2014, pp. 5631–5638.

[47] S. Y. Kim, S. G. Song, and S. J. Park, "Minimum loss discontinuous pulse-width modulation per phase method for three-phase four-leg inverter," *IEEE Access*, vol. 8, pp. 122923–122936, 2020.

[48] F. Rojas, R. Cárdenas, R. Kennel, J. C. Clare, and M. Díaz, "A simplified space-vector modulation algorithm for four-leg NPC converters," *IEEE Trans. Power Electron.*, vol. 32, no. 11, pp. 8371–8380, Nov. 2017.

[49] P. K. Padhmakumar, M. P. Flower Queen, and P. B. Aurtherson, "Three dimensional space vector modulation for three phase four leg inverters—A review," in *Proc. Int. Conf. Emerg. Trends Innov. Eng. Technol. Res. (ICETIETR)*, Jul. 2018, pp. 1–8.

[50] J.-H. Kim and S.-K. Sul, "A carrier-based PWM method for three-phase four-leg voltage source converters," *IEEE Trans. Power Electron.*, vol. 19, no. 1, pp. 66–75, Jan. 2004.

[51] J. H. Kim, S. K. Sul, and P. N. Enjeti, "A carrier-based PWM method with optimal switching sequence for a multilevel four-leg voltage-source inverter," *IEEE Trans. Ind. Appl.*, vol. 44, no. 4, pp. 1239–1248, Jul. 2008.

[52] P. Verdelho and G. D. Marques, "An active power filter and unbalanced current compensator," *IEEE Trans. Ind. Electron.*, vol. 44, no. 3, pp. 321–328, Jun. 1997.

[53] S. Bayhan, H. Abu-Rub, and R. S. Balog, "Model predictive control of quasi-Z-source four-leg inverter," *IEEE Trans. Ind. Electron.*, vol. 63, no. 7, pp. 4506–4516, Jul. 2016.

[54] G. M. Cocco, J. D. A. Borges, M. Stefanello, and F. B. Grigoletto, "Finite set model predictive control of four-leg split-source inverters," in *Proc. 13th IEEE Int. Conf. Ind. Appl. (INDUSCON)*, Nov. 2018, pp. 630–635.

[55] F. Rojas-Lobos, R. Kennel, and R. Cardenas-Dobson, "Current control and capacitor balancing for 4-leg NPC converters using finite set model predictive control," in *Proc. 39th Annu. Conf. IEEE Ind. Electron. Soc. (IECON)*, Nov. 2013, pp. 590–595.

[56] M. Rivera, V. Yaramasu, A. Llor, J. Rodriguez, B. Wu, and M. Fadel, "Digital predictive current control of a three-phase four-leg inverter," *IEEE Trans. Ind. Electron.*, vol. 60, no. 11, pp. 4903–4912, Nov. 2013.

[57] V. Yaramasu, K. Milev, A. Dekka, M. Rivera, J. Rodriguez, and F. Rojas, "Modulated model predictive current control of a four-leg inverter," in *Proc. 11th Power Electron., Drive Syst., Technol. Conf. (PEDSTC)*, Feb. 2020, pp. 1–6.

[58] L. Tarisciotti, A. Formentini, A. Gaeta, M. Degano, P. Zanchetta, R. Rabbeni, and M. Pucci, "Model predictive control for shunt active filters with fixed switching frequency," *IEEE Trans. Ind. Appl.*, vol. 53, no. 1, pp. 296–304, Jan. 2017.

[59] D. Xiao, K. S. Alam, M. P. Akter, S. M. S. I. Shakib, D. Zhang, and M. Rahman, "Modulated model predictive control for four-leg inverters with online duty ratio optimization," *IEEE Trans. Ind. Appl.*, vol. 56, no. 3, pp. 3114–3124, May 2020.

[60] R. Cardenas, E. Espina, J. Clare, and P. Wheeler, "Self-tuning resonant control of a seven-leg back-to-back converter for interfacing variable-speed generators to four-wire loads," *IEEE Trans. Ind. Electron.*, vol. 62, no. 7, pp. 4618–4629, Jul. 2015.

[61] F. Rojas, R. Cardenas, J. Clare, M. Diaz, J. Pereda, and R. Kennel, "A design methodology of multiresonant controllers for high performance 400 Hz ground power units," *IEEE Trans. Ind. Electron.*, vol. 66, no. 8, pp. 6549–6559, Aug. 2019.

[62] *Aircraft Electric Power Characteristics*, Standard MIL-STD-704F, 2004.

[63] M. Aamir, K. A. Kalwar, and S. Mekhilef, "Review: Uninterruptible power supply (UPS) system," *Renew. Sustain. Energy Rev.*, vol. 58, pp. 1395–1410, May 2016.

[64] S. Jiao, K. R. R. Potti, K. Rajashekara, and S. K. Pramanick, "A novel DROGI-based detection scheme for power quality improvement using four-leg converter under unbalanced loads," *IEEE Trans. Ind. Appl.*, vol. 56, no. 1, pp. 815–825, Jan./Feb. 2020.

[65] C. Burgos-Mellado, R. Cardenas-Dobson, D. Saez, A. Costabeber, and M. Sumner, "A control algorithm based on the conservative power theory for cooperative sharing of imbalances in four-wire systems," *IEEE Trans. Power Electron.*, vol. 34, no. 6, pp. 5325–5339, Jun. 2019.

[66] Y. Han, H. Li, P. Shen, E. A. A. Coelho, and J. M. Guerrero, "Review of active and reactive power sharing strategies in hierarchical controlled microgrids," *IEEE Trans. Power Electron.*, vol. 32, no. 3, pp. 2427–2451, Mar. 2017.

[67] K. Gai, C. Li, Q. Zhou, S. Liu, and K. Bi, "Control strategy for three-phase four-leg dynamic voltage restorer based third-harmonic injection," in *Proc. IEEE Transp. Electrific. Conf. Expo, Asia–Pacific (ITEC Asia-Pacific)*, Jun. 2018, pp. 1–5.

[68] M. M. Haque, M. S. Ali, P. Wolfs, and F. Blaabjerg, "A UPFC for voltage regulation in LV distribution feeders with a DC-link ripple voltage suppression technique," *IEEE Trans. Ind. Appl.*, vol. 56, no. 6, pp. 6857–6870, Nov. 2020.

[69] A. L. Julian, G. Oriti, and T. A. Lipo, "Elimination of common-mode voltage in three-phase sinusoidal power converters," *IEEE Trans. Power Electron.*, vol. 14, no. 5, pp. 982–989, Sep. 1999.

[70] C.-C. Hou, P.-W. Wang, C.-C. Chen, and C.-W. Chang, "Common mode voltage reduction in four-leg inverter with multicarrier PWM scheme," in *Proc. 10th Int. Conf. Power Electron. ECCE Asia (ICPE - ECCE Asia)*, May 2019, pp. 3223–3228.

[71] V. Gali, N. Gupta, and R. A. Gupta, "Mitigation of power quality problems using shunt active power filters: A comprehensive review," in *Proc. 12th IEEE Conf. Ind. Electron. Appl. (ICIEA)*, Jun. 2017, pp. 1100–1105.
[72] R. Aboelsaud, A. Ibrahim, and A. Garganeev, "Review of three-phase inverters control for unbalanced load compensation," *Int. J. Power Electron. Drive Syst.*, vol. 10, no. 1, p. 242, Mar. 2019.
[73] L. Zeng, L. Jinjun, and L. Jin, "Modeling, analysis, and mitigation of load neutral point voltage for three-phase four-leg inverter," *IEEE Trans. Ind. Electron.*, vol. 60, no. 5, pp. 2010–2021, May 2013.
[74] A. Lidozzi, C. Ji, L. Solero, F. Crescimbini, and P. Zanchetta, "Load-adaptive zero-phase-shift direct repetitive control for stand-alone four-leg VSI," *IEEE Trans. Ind. Appl.*, vol. 52, no. 6, pp. 4899–4908, Nov. 2016.
[75] A. M. Hava and E. Demirkutlu, "Output voltage control of a four-leg inverter based three-phase UPS," in *Proc. Eur. Conf. Power Electron. Appl.*, 2007, pp. 1–10.
[76] E. Demirkutlu, S. Cetinkaya, and A. M. Hava, "Output voltage control of a four-leg inverter based three-phase UPS by means of stationary frame resonant filter banks," in *Proc. IEEE Int. Electr. Mach. Drives Conf.*, May 2007, pp. 880–885.
[77] N. M. Ismail and M. K. Mishra, "Study on the design and switching dynamics of hysteresis current controlled four-leg voltage source inverter for load compensation," *IET Power Electron.*, vol. 11, no. 2, pp. 310–319, 2018.
[78] M. A. Bou-Rabee, D. Sutanto, M. F. Rahman, and G.-H. Choe, "A three-phase current-fed active power filter by PWM injection method," in *Proc. Rec. 22nd Annu. IEEE Power Electron. Spec. Conf. (PESC)*, Jun. 1991, pp. 112–116.
[79] A. Dastfan, V. J. Gosbell, and D. Platt, "Control of a new active power filter using 3-D vector control," *IEEE Trans. Power Electron.*, vol. 15, no. 1, pp. 5–12, Jan. 2000.
[80] V. Khadkikar and A. Chandra, "A novel structure for three-phase four-wire distribution system utilizing unified power quality conditioner (UPQC)," *IEEE Trans. Ind. Appl.*, vol. 45, no. 5, pp. 1897–1902, Sep./Oct. 2009.
[81] S. A. Oliveira da Silva, R. A. Modesto, A. Goedtel, and C. F. Nascimento, "Compensation algorithms applied to power quality conditioners in three-phase four-wire systems," in *Proc. IEEE Int. Symp. Ind. Electron.*, Jul. 2010, pp. 730–735.
[82] M. Ucar, S. Ozdemir, and E. Ozdemir, "A four-leg unified series–parallel active filter system for periodic and non-periodic disturbance compensation," *Electr. Power Syst. Res.*, vol. 81, no. 5, pp. 1132–1143, 2011.
[83] S. R. Naidu and D. A. Fernandes, "Dynamic voltage restorer based on a four-leg voltage source converter," *IET Gener., Transmiss. Distrib.*, vol. 3, no. 5, pp. 437–447, May 2009.
[84] D. A. Fernandes, S. R. Naidu, and A. M. N. Lima, "A four leg voltage source converter based dynamic voltage restorer," in *Proc. IEEE Power Electron. Spec. Conf.*, Jun. 2008, pp. 3760–3766.
[85] G. Carrasco, C. A. Silva, R. Peña, and R. Cárdenas, "Control of a four-leg converter for the operation of a DFIG feeding stand-alone unbalanced loads," *IEEE Trans. Ind. Electron.*, vol. 62, no. 7, pp. 4630–4640, Jul. 2015.
[86] A. Lidozzi, C. Ji, L. Solero, P. Zanchetta, and F. Crescimbini, "Digital deadbeat and repetitive combined control for a stand-alone four-leg VSI," *IEEE Trans. Ind. Appl.*, vol. 53, no. 6, pp. 5624–5633, Nov. 2017.
[87] S. Ei-Barbari and W. Hofmann, "Digital control of a four leg inverter for standalone photovoltaic systems with unbalanced load," in *Proc. 26th Annu. Conf. IEEE Ind. Electron. Soc. IEEE Int. Conf. Ind. Electron., Control Instrum. 21st Century Technol. Ind. Opportunities (IECON)*, vol. 1, Oct. 2000, pp. 729–734.
[88] M. Pichan, H. Rastegar, and M. Monfared, "Deadbeat control of the stand-alone four-leg inverter considering the effect of the neutral line inductor," *IEEE Trans. Ind. Electron.*, vol. 64, no. 4, pp. 2592–2601, Apr. 2017.
[89] A. Houari, A. Djerioui, A. Saim, M. Ait-Ahmed, and M. Machmoum, "Improved control strategy for power quality enhancement in standalone systems based on four-leg voltage source inverters," *IET Power Electronics*, vol. 11, no. 3, pp. 515–523, Mar. 2018.
[90] X. Zhou, F. Tang, P. C. Loh, X. Jin, and W. Cao, "Four-leg converters with improved common current sharing and selective voltage-quality enhancement for islanded microgrids," *IEEE Trans. Power Del.*, vol. 31, no. 2, pp. 522–531, Apr. 2016.
[91] X. Guo, R. He, J. Jian, Z. Lu, X. Sun, and J. M. Guerrero, "Leakage current elimination of four-leg inverter for transformerless three-phase PV systems," *IEEE Trans. Power Electron.*, vol. 31, no. 3, pp. 1841–1846, Mar. 2016.
[92] A. Furuya, K. Oka, and K. Matsuse, "A characteristic analysis of four-leg inverter in two AC motor drives with independent vector control," in *Proc. Int. Conf. Electr. Mach. Syst. (ICEMS)*, Oct. 2007, pp. 619–624.
[93] F. Meinguet and J. Gyselinck, "Control strategies and reconfiguration of four-leg inverter PMSM drives in case of single-phase open-circuit faults," in *Proc. IEEE Int. Electr. Mach. Drives Conf.*, May 2009, pp. 299–304.
[94] L. G. Franquelo, M. M. Prats, R. Portillo, J. I. León, M. Perales, J. M. Carrasco, E. Galván, and J. L. Mora, "Simple and advanced three dimensional space vector modulation algorithm for four-leg multilevel converters topology," in *Proc. 30th Annu. Conf. IEEE Ind. Electron. Soc. (IECON)*, vol. 3, Nov. 2004, pp. 2285–2289.
[95] F. Rojas-Lobos, R. Kennel, and R. Cardenas-Dobson, "3D-SVM algorithm and capacitor voltage balancing in a 4-leg NPC converter operating under unbalanced and non-linear loads," in *Proc. 15th Eur. Conf. Power Electron. Appl. (EPE)*, Sep. 2013, pp. 1–10.
[96] J. Kortenbruck, T. Premgamone, S. Leksawat, E. Ortjohann, D. Holtschulte, A. Schmelter, and D. Morton, "Multilevel and 4-leg topology for smart grid inverter," in *Proc. IEEE Int. Energy Conf. (ENERGYCON)*, Apr. 2016, pp. 1–6.
[97] M. Sharifzadeh, H. Vahedi, and R. Portillo, "Hybrid SHM-SHE pulse-amplitude modulation for high-power four-leg inverter," *IEEE Trans. Ind. Electron.*, vol. 63, no. 11, pp. 7234–7242, Nov. 2016.
[98] J. I. Leon, L. G. Franquelo, R. C. Portillo, and M. M. Prats, "DC-link capacitors voltage balancing in multilevel four-leg diode-clamped converters," in *Proc. 31st Annu. Conf. IEEE Ind. Electron. Soc. (IECON)*, Nov. 2005, p. 6.
[99] H. Ghoreishy, Z. Zhang, O. C. Thomsen, and M. A. E. Andersen, "A fast-processing modulation strategy for three-phase four-leg neutral-point-clamped inverter based on the circuit-level decoupling concept," in *Proc. 7th Int. Power Electron. Motion Control Conf.*, vol. 1, Jun. 2012, pp. 274–280.
[100] S. Du, A. Dekka, B. Wu, and N. Zargari, *Modular Multilevel Converters: Analysis, Control, and Applications*. Hoboken, NJ, USA: Wiley, 2017.
[101] M. Schweizer and J. W. Kolar, "Design and implementation of a highly efficient three-level T-type converter for low-voltage applications," *IEEE Trans. Power Electron.*, vol. 28, no. 2, pp. 899–907, Feb. 2013.
[102] U.-M. Choi, H.-H. Lee, and K.-B. Lee, "Simple neutral-point voltage control for three-level inverters using a discontinuous pulse width modulation," *IEEE Trans. Energy Convers.*, vol. 28, no. 2, pp. 434–443, Jun. 2013.
[103] P. J. Grbovic, F. Gruson, N. Idir, and P. L. Moigne, "Turn-on performance of reverse blocking IGBT (RB IGBT) and optimization using advanced gate driver," *IEEE Trans. Power Electron.*, vol. 25, no. 4, pp. 970–980, Apr. 2010.
[104] S.-J. Chee, S.-K. Sul, Y. H. Roh, and J. Lee, "Loss comparison of the 3 level topologies for four-leg voltage converters," in *Proc. IEEE Int. Conf. Ind. Technol. (ICIT)*, Feb. 2014, pp. 324–329.
[105] J. He, N. Weise, L. Wei, and N. A. O. Demerdash, "A fault-tolerant topology of T-type NPC inverter with increased thermal overload capability," in *Proc. IEEE Appl. Power Electron. Conf. Exposit. (APEC)*, Mar. 2016, pp. 1065–1070.
[106] M. Sedlak, S. Stynski, M. Malinowski, and M. P. Kazmierkowski, "Power management in four-leg converter interfacing RES with the grid," in *Proc. 15th Eur. Conf. Power Electron. Appl. (EPE)*, Sep. 2013, pp. 1–10.
[107] M. Sedlak, S. Stynski, M. P. Kazmierkowski, and M. Malinowski, "Operation of four-leg three-level flying capacitor grid-connected converter for RES," in *Proc. 39th Annu. Conf. IEEE Ind. Electron. Soc. (IECON)*, Nov. 2013, pp. 1100–1105.
[108] M. Sedlak, S. Stynski, M. P. Kazmierkowski, and M. Malinowski, "Control of three-level four-leg flying capacitor converter with active filtering function for RES," in *Proc. 8th Int. Conf. Exhib. Ecol. Vehicles Renew. Energies (EVER)*, Mar. 2013, pp. 1–7.
[109] F. Yue, P. W. Wheeler, N. Mason, L. Empringham, and J. C. Clare, "A new control method of single-stage 4-leg matrix converter," in *Proc. Eur. Conf. Power Electron. Appl.*, 2007, pp. 1–10.
[110] R. Cardenas, C. Juri, R. Pena, J. Clare, and P. Wheeler, "Analysis and experimental validation of control systems for four-leg matrix converter applications," *IEEE Trans. Ind. Electron.*, vol. 59, no. 1, pp. 141–153, Jan. 2012.

[111] R. Cárdenas, R. Peña, P. Wheeler, J. Clare, and C. Juri, "Control of a matrix converter for the operation of autonomous systems," *Renew. Energy*, vol. 43, pp. 343–353, Jul. 2012.

[112] R. Cárdenas, R. Peña, J. Clare, P. Wheeler, and P. Zanchetta, "A repetitive control system for four-leg matrix converters feeding non-linear loads," *Electr. Power Syst. Res.*, vol. 104, pp. 18–27, Nov. 2013.

[113] R. Cárdenas, C. Juri, R. Peña, P. Wheeler, and J. Clare, "The application of resonant controllers to four-leg matrix converters feeding unbalanced or nonlinear loads," *IEEE Trans. Power Electron.*, vol. 27, no. 3, pp. 1120–1129, Mar. 2012.

[114] P. W. Wheeler, P. Zanchetta, J. C. Clare, L. Empringham, M. Bland, and D. Katsis, "A utility power supply based on a four-output leg matrix converter," *IEEE Trans. Ind. Appl.*, vol. 44, no. 1, pp. 174–186, Jan. 2008.

[115] S. L. Arevalo, P. Zanchetta, and P. W. Wheeler, "Control of a matrix converter-based AC power supply for aircrafts under unbalanced conditions," in *Proc. 33rd Annu. Conf. IEEE Ind. Electron. Soc. (IECON)*, Nov. 2007, pp. 1823–1828.

[116] H. Hua, L. Zhejun, M. Yongmei, W. Hui, D. Hanbing, and W. Meng, "A simple current control strategy for four-leg direct matrix converter," in *Proc. Chin. Autom. Congr. (CAC)*, Nov. 2015, pp. 2174–2179.

[117] D. Casadei, J. Clare, and L. Empringham, "Large-signal model for the stability analysis of matrix converters," *IEEE Trans. Ind. Electron.*, vol. 54, no. 2, pp. 939–950, Apr. 2007.

[118] S. Huang, L. Xu, Y. Guo, Y. Li, and W. Deng, "Research on three-phase four-leg matrix converter based more electric aircraft wing ice protection system," *J. Eng.*, vol. 2018, no. 13, pp. 529–533, Jan. 2018.

[119] S. Kwak, "Four-leg-based fault-tolerant matrix converter schemes based on switching function and space vector methods," *IEEE Trans. Ind. Electron.*, vol. 59, no. 1, pp. 235–243, Jan. 2012.

[120] H. Akagi, E. H. Watanabe, and M. Aredes, "Shunt active filters," in *Instantaneous Power Theory and Applications to Power Conditioning*. Piscataway, NJ, USA: IEEE Press, 2017, pp. 111–236.

[121] M. Y. Lee, P. Wheeler, and C. Klumpner, "Space-vector modulated multilevel matrix converter," *IEEE Trans. Ind. Electron.*, vol. 57, no. 10, pp. 3385–3394, Oct. 2010.

[122] R. Pena, R. Cardenas, E. Reyes, J. Clare, and P. Wheeler, "A topology for multiple generation system with doubly fed induction machines and indirect matrix converter," *IEEE Trans. Ind. Electron.*, vol. 56, no. 10, pp. 4181–4193, Oct. 2009.

[123] Y. Sun, M. Su, X. Li, H. Wang, and W. Gui, "Indirect four-leg matrix converter based on robust adaptive back-stepping control," *IEEE Trans. Ind. Electron.*, vol. 58, no. 9, pp. 4288–4298, Sep. 2011.

[124] C. Garcia, M. Rivera, M. Lopez, J. Rodriguez, P. Wheeler, R. Pena, J. Espinoza, and J. Riedemann, "Predictive current control of a four-leg indirect matrix converter with imposed source currents and common-mode voltage reduction," in *Proc. IEEE Energy Convers. Congr. Expo.*, Sep. 2013, pp. 5306–5311.

[125] C. García, M. Rivera, and M. López, "A simple current control strategy for a four-leg indirect matrix converter," *IEEE Trans. Power Electron.*, vol. 30, no. 4, pp. 2275–2287, Apr. 2015.

[126] T. D. Nguyen and H.-H. Leef, "The control strategy for a four-leg indirect matrix converter with unbalanced load," in *Proc. IET Conf. Renew. Power Gener. (RPG)*, 2011, p. 244.

[127] M. Rivera, I. Contreras, J. Rodriguez, R. Peña, and P. Wheeler, "A simple current control method with instantaneous reactive power minimization for four-leg indirect matrix converters," in *Proc. 14th Eur. Conf. Power Electron. Appl.*, Aug./Sep. 2011, pp. 1–9.

[128] M. Rivera, J. Rodriguez, C. Garcia, R. Peña, and J. Espinoza, "A simple predictive voltage control method with unity displacement power factor for four-leg indirect matrix converters," in *Proc. 15th Int. Power Electron. Motion Control Conf. (EPE/PEMC)*, Sep. 2012, pp. 5–6.

[129] R. Konarik, M. Pridala, M. Jarabicova, J. Sedo, and T. Laskody, "Topologies of converters for two-phase AC motors," in *Proc. 18th Int. Sci. Conf. Electr. Power Eng. (EPE)*, May 2017, pp. 1–6.

[130] Y. Bak, E. Lee, and K.-B. Lee, "Indirect matrix converter for hybrid electric vehicle application with three-phase and single-phase outputs," *Energies*, vol. 8, no. 5, pp. 3849–3866, Apr. 2015.

[131] M. Bou-Rabee, D. Sutanto, F. Barone, and G.-H. Choe, "A new technique for three-phase active power filter," in *Proc. 7th Annu. Appl. Power Electron. Conf. Expo. (APEC)*, 1992, pp. 837–843.

[132] X. Guo, D. Xu, and B. Wu, "Four-leg current-source inverter with a new space vector modulation for common-mode voltage suppression," *IEEE Trans. Ind. Electron.*, vol. 62, no. 10, pp. 6003–6007, Oct. 2015.

[133] J. Liang, T. C. Green, C. Feng, and G. Weiss, "Increasing voltage utilization in split-link, four-wire inverters," *IEEE Trans. Power Electron.*, vol. 24, no. 6, pp. 1562–1569, Jun. 2009.

[134] S.-P. Kim, S.-G. Song, S.-J. Park, and F.-S. Kang, "Output voltage imbalance compensation using DC offset voltage for split DC-link capacitor 3-leg inverter," *Electronics*, vol. 10, no. 9, p. 1029, Apr. 2021.

[135] S.-P. Kim, S.-G. Song, S.-J. Park, and F.-S. Kang, "Imbalance compensation of the grid current using effective and reactive power for split DC-link capacitor 3-leg inverter," *IEEE Access*, vol. 9, pp. 81189–81201, 2021.

[136] Z. Lin, X. Ruan, L. Jia, W. Zhao, H. Liu, and P. Rao, "Optimized design of the neutral inductor and filter inductors in three-phase four-wire inverter with split DC-link capacitors," *IEEE Trans. Power Electron.*, vol. 34, no. 1, pp. 247–262, Jan. 2019.

[137] W. Zhang, M. Dahidah, G. Thompson, V. Pickert, and M. Elgendy, "On investigating EMC filter solutions in soft open points under large unbalanced current," in *Proc. 45th Annu. Conf. IEEE Ind. Electron. Soc. (IECON)*, vol. 1, Oct. 2019, pp. 6152–6157.

[138] Q.-C. Zhong, W.-L. Ming, X. Cao, and M. Krstic, "Control of ripple eliminators to improve the power quality of DC systems and reduce the usage of electrolytic capacitors," *IEEE Access*, vol. 4, pp. 2177–2187, 2016.

[139] A. J. Roscoe, S. J. Finney, and G. M. Butt, "Tradeoffs between AC power quality and DC bus ripple for 3-phase 3-wire inverter-connected devices within microgrids," *IEEE Trans. Power Electron.*, vol. 26, no. 3, pp. 674–688, Mar. 2011.

[140] A. Mohd, E. Ortjohann, N. Hamsic, W. Sinsukthavorn, M. Lingemann, A. Schmelter, and D. Morton, "Control strategy and space vector modulation for three-leg four-wire voltage source inverters under unbalanced load conditions," *IET Power Electron.*, vol. 3, no. 3, pp. 323–333, 2010.

[141] Y. K. Lo and C. L. Chen, "Three-phase four wire voltage controlled AC line conditioner with unity input power factor and minimised output voltage harmonics," *IEE Proc.-Electr. Power Appl.*, vol. 142, no. 1, pp. 43–49, 1995.

[142] M. Dai, M. N. Marwali, J.-W. Jung, and A. Keyhani, "A three-phase four-wire inverter control technique for a single distributed generation unit in island mode," *IEEE Trans. Power Electron.*, vol. 23, no. 1, pp. 322–331, Jan. 2008.

[143] S. Srikanthan and M. K. Mishra, "DC capacitor voltage equalization in neutral clamped inverters for DSTATCOM application," *IEEE Trans. Ind. Electron.*, vol. 57, no. 8, pp. 2768–2775, Aug. 2010.

[144] X.-P. Yang and Y.-X. Zhang, "Three-phase four-wire DSTATCOM based on a three-dimensional PWM algorithm," in *Proc. 3rd Int. Conf. Electr. Utility Deregulation Restructuring Power Technol.*, Apr. 2008, pp. 2061–2066.

[145] O. Vodyakho and C. C. Mi, "Three-level inverter-based shunt active power filter in three-phase three-wire and four-wire systems," *IEEE Trans. Power Electron.*, vol. 24, no. 5, pp. 1350–1363, May 2009.

[146] S. Orts-Grau, F. J. Gimeno-Sales, S. Segui-Chilet, A. Abellán-García, M. Alcaniz, and R. Masot-Peris, "Selective shunt active power compensator applied in four-wire electrical systems based on IEEE Std. 1459," *IEEE Trans. Power Del.*, vol. 23, no. 4, pp. 2563–2574, Oct. 2008.

[147] M. I. Milanes-Montero, E. Romero-Cadaval, and F. Barrero-Gonzalez, "Comparison of control strategies for shunt active power filters in three-phase four-wire systems," *IEEE Trans. Power Electron.*, vol. 22, no. 1, pp. 229–236, Jan. 2007.

[148] D. Shen and P. W. Lehn, "Fixed-frequency space-vector-modulation control for three-phase four-leg active power filters," *IEE Proc.-Electr. Power Appl.*, vol. 149, no. 4, pp. 268–274, Jul. 2002.

[149] M.-C. Wong, Z.-Y. Zhao, Y.-D. Han, and L.-B. Zhao, "Three-dimensional pulse-width modulation technique in three-level power inverters for three-phase four-wired system," *IEEE Trans. Power Electron.*, vol. 16, no. 3, pp. 418–427, May 2001.

[150] M. E. Fraser, C. D. Manning, and B. M. Wells, "Transformerless four-wire PWM rectifier and its application in AC-DC-AC converters," *IEE Proc.-Electr. Power Appl.*, vol. 142, no. 6, pp. 410–416, Nov. 1995.

[151] P. Verdelho, "Space vector based current controller in $\alpha\beta 0$ coordinate system for the PWM voltage converter connected to the AC mains," in *Proc. Rec. 28th Annu. IEEE Power Electron. Spec. Conf. Formerly Power Conditioning Spec. Conf. Power Process. Electron. Spec. Conf. (PESC)*, vol. 2, Jun. 1997, pp. 1115–1120.

[152] M. Aredes, J. Hafner, and K. Heumann, "Three-phase four-wire shunt active filter control strategies," *IEEE Trans. Power Electron.*, vol. 12, no. 2, pp. 311–318, Mar. 1997.

[153] R. S. Herrera, P. Salmerón, and H. Kim, "Instantaneous reactive power theory applied to active power filter compensation: Different approaches, assessment, and experimental results," *IEEE Trans. Ind. Electron.*, vol. 55, no. 1, pp. 184–196, Jan. 2008.

[154] M. Aredes and E. H. Watanabe, "New control algorithms for series and shunt three-phase four-wire active power filters," *IEEE Trans. Power Del.*, vol. 10, no. 3, pp. 1649–1656, Jul. 1995.

[155] R. Faranda and I. Valade, "UPQC compensation strategy and design aimed at reducing losses," in *Proc. IEEE Int. Symp. Ind. Electron. (ISIE)*, vol. 4, Jul. 2002, pp. 1264–1270.

[156] C. Zhan, A. Arulampalam, V. K. Ramachandaramurthy, C. Fitzer, A. Barnes, and N. Jenkins, "Dynamic voltage restorer based on 3-dimensional voltage space vector PWM algorithm," in *Proc. IEEE 32nd Annu. Power Electron. Spec. Conf.*, vol. 2, Jun. 2001, pp. 533–538.

[157] C. Zhan, A. Arulampalam, and N. Jenkins, "Four-wire dynamic voltage restorer based on a three-dimensional voltage space vector PWM algorithm," *IEEE Trans. Power Electron.*, vol. 18, no. 4, pp. 1093–1102, Jul. 2003.

[158] C. Y. Jeong, J. G. Cho, Y. Kang, G. H. Rim, and E. H. Song, "A 100 kVA power conditioner for three-phase four-wire emergency generators," in *Proc. Rec. 29th Annu. IEEE Power Electron. Spec. Conf. (PESC)*, vol. 2, May 1998, pp. 1906–1911.

[159] P. Sanchis, A. Ursua, E. Gubia, J. Lopez, and L. Marroyo, "Control of three-phase stand-alone photovoltaic systems with unbalanced loads," in *Proc. IEEE Int. Symp. Ind. Electron. (ISIE)*, vol. 2, Jun. 2005, pp. 633–638.

[160] M. Yongqing, L. Zheng, S. Yanmin, and Y. Ting, "Study on mathematical model and Lyapunov-based control for three-phase four-wire three-level NPC voltage-source rectifier," in *Proc. IEEE Int. Symp. Ind. Electron. (ISIE)*, vol. 2, Jun. 2005, pp. 669–674.

[161] R. Ghosh and G. Narayanan, "Control of three-phase, four-wire PWM rectifier," *IEEE Trans. Power Electron.*, vol. 23, no. 1, pp. 96–106, Jan. 2008.

[162] M. J. Waite and L. Zhang, "Analysis and comparison of 3D-SVM schemes for flying-capacitor multi-level inverters," in *Proc. 13th Eur. Conf. Power Electron. Appl.*, Sep. 2009, pp. 1–10.

[163] O. Vodyakho and T. Kim, "Shunt active filter based on three-level inverter for three-phase four-wire systems," *IET Power Electron.*, vol. 2, no. 3, pp. 216–226, May 2009.

[164] N.-Y. Dai, M.-C. Wong, and Y.-D. Han, "Application of a three-level NPC inverter as a three-phase four-wire power quality compensator by generalized 3DSVM," *IEEE Trans. Power Electron.*, vol. 21, no. 2, pp. 440–449, Mar. 2006.

[165] X. Yuan, G. Orglmeister, and W. Merk, "Managing the DC link neutral potential of the three-phase-four-wire neutral-point-clamped (NPC) inverter in FACTS application," in *Proc. Conf. 25th Annu. Conf. IEEE Ind. Electron. Soc. (IECON)*, vol. 2, Nov./Dec. 1999, pp. 571–576.

[166] M. C. Wong, J. Tang, and Y. D. Han, "Cylindrical coordinate control of three-dimensional PWM technique in three-phase four-wired trilevel inverter," *IEEE Trans. Power Electron.*, vol. 18, no. 1, pp. 208–220, Jan. 2003.

[167] J. Tang, M.-C. Wong, and Y. Han, "Novel five-level inverter PWM control in 3-phase 4-wire system for power quality," in *Proc. Int. Conf. Power Syst. Technol.*, vol. 1, Oct. 2002, pp. 579–584.

[168] T. Lee, M. Kinoshita, and K. Sanada, "High-efficiency large-capacity uninterruptible power supply for 3-phase 4-wire power system," in *Proc. 7th Int. Power Electron. Motion Control Conf.*, vol. 2, Jun. 2012, pp. 1131–1136.

[169] E. Ortjohann, A. Mohd, N. Hamsic, A. Al-Daib, and M. Lingemann, "Three-dimensional Sace vector modulation algorithm for three-leg four-wire voltage source inverters," in *Proc. Int. Conf. Power Eng., Energy Electr. Drives*, Apr. 2007, pp. 605–610.

[170] M. G. Villalva and F. Ruppert, "3-D space vector PWM for three-leg four-wire voltage source inverters," in *Proc. IEEE 35th Annu. Power Electron. Spec. Conf.*, vol. 5, Jun. 2004, pp. 3946–3951.

[171] N.-Y. Dai, M.-C. Wong, and Y.-D. Han, "Three leg center-split inverter controlled by 3D SVM under DC variation," in *Proc. 4th Int. Power Electron. Motion Control Conf. (IPEMC)*, vol. 3, Aug. 2004, pp. 1362–1367.

[172] N. Y. Dai, M. C. Wong, and Y. D. Han, "Three-dimensional space vector modulation with DC voltage variation control in a three-leg centre-split power quality compensator," *IEE Proc.-Electr. Power Appl.*, vol. 151, no. 2, pp. 198–204, Mar. 2004.

[173] N.-Y. Dai, M.-C. Wong, Y.-D. Han, and C.-S. Lam, "A 3-D generalized direct PWM for 3-phase 4-wire APFs," in *Proc. 14th IAS Annu. Meeting Conf. Rec. Ind. Appl. Conf.*, vol. 2, Oct. 2005, pp. 1261–1266.

[174] M.-C. Wong, N.-Y. Dai, J. Tang, and Y.-D. Han, "Theoretical study of 3 dimensional hysteresis PWM techniques," in *Proc. 4th Int. Power Electron. Motion Control Conf.*, vol. 3, Aug. 2004, pp. 1635–1640.

[175] J. Alahuhtala and H. Tuusa, "Experimental results of a three-level four-wire unidirectional AC-DC-AC converter," in *Proc. Int. Power Electron. Conf. (ECCE ASIA)*, Jun. 2010, pp. 3080–3086.

[176] P. Rodriguez, R. Pindado, and J. Bergas, "Alternative topology for three-phase four-wire PWM converters applied to a shunt active power filter," in *Proc. IEEE 28th Annu. Conf. Ind. Electron. Soc. (IECON)*, vol. 4, Nov. 2002, pp. 2939–2944.

[177] J. De Kooning, B. Meersman, T. Vandoorn, B. Renders, and L. Vandevelde, "Comparison of three-phase four-wire converters for distributed generation," in *Proc. 45th Int. Universities Power Eng. Conf. (UPEC)*, Aug./Sep. 2010, pp. 1–6.

[178] Y. Fu, Y. Huang, X. Lu, K. Zou, C. Chen, and H. Bai, "Imbalanced load regulation based on virtual resistance of a three-phase four-wire inverter for EV vehicle-to-home applications," *IEEE Trans. Transp. Electr.*, vol. 5, no. 1, pp. 162–173, Mar. 2019.

[179] S. Bifaretti, A. Lidozzi, L. Solero, and F. Crescimbini, "Modulation with sinusoidal third-harmonic injection for active split DC-bus four-leg inverters," *IEEE Trans. Power Electron.*, vol. 31, no. 9, pp. 6226–6236, Sep. 2016.

[180] S. Fouzey, S. El-Barbari, W. Hofmann, and C. Unsalver, "A new space vector modulation scheme for three phase four wire inverter for standalone photovoltaic systems," in *Proc. Eur. Conf. Power Electron. Appl.*, 2005, p. 10.

[181] S. Ceballos, J. Pou, J. Zaragoza, J. L. Martin, E. Robles, I. Gabiola, and P. Ibanez, "Efficient modulation technique for a four-leg fault-tolerant neutral-point-clamped inverter," *IEEE Trans. Ind. Electron.*, vol. 55, no. 3, pp. 1067–1074, Mar. 2008.

[182] M. Azizi, M. Mohamadian, A. Yazdian, and A. Fatemi, "Dual-output four-leg inverter," in *Proc. 28th Annu. IEEE Appl. Power Electron. Conf. Expo. (APEC)*, Mar. 2013, pp. 144–149.

[183] T. Kominami and Y. Fujimoto, "A novel nine-switch inverter for independent control of two three-phase loads," in *Proc. IEEE Ind. Appl. Annu. Meeting*, Sep. 2007, pp. 2346–2350.

[184] M. Azizi, S. Aznavi, P. Fajri, and A. Khoshkbar-Sadigh, "Space vector modulation scheme for dual-output four-leg inverter," in *Proc. IEEE Appl. Power Electron. Conf. Expo. (APEC)*, Mar. 2020, pp. 2937–2943.

[185] V. Khadkikar, A. Chandra, and B. Singh, "Digital signal processor implementation and performance evaluation of split capacitor, four-leg and three H-bridge-based three-phase four-wire shunt active filters," *IET Power Electron.*, vol. 4, no. 4, pp. 463–470, 2011.

[186] Z. Li, Y. Li, P. Wang, H. Zhu, C. Liu, and F. Gao, "Single-loop digital control of high-power 400-Hz ground power unit for airplanes," *IEEE Trans. Ind. Electron.*, vol. 57, no. 2, pp. 532–543, Feb. 2010.

[187] J. P. R. A. Mello, C. B. Jacobina, and M. B. R. Correa, "Three-phase four-wire inverters based on cascaded three-phase converters with four and three legs," in *Proc. IEEE Energy Convers. Congr. Expo. (ECCE)*, Sep. 2016, pp. 1–8.

[188] A. C. N. Maia, C. B. Jacobina, N. B. Freitas, A. P. D. Queiroz, and E. R. C. Silva, "Three-phase four-wire AC-DC-AC multilevel topologies obtained from an interconnection of three-leg converters," in *Proc. IEEE Energy Convers. Congr. Expo. (ECCE)*, Sep. 2016, pp. 1–8.

[189] H. P. Mohammadi and M. T. Bina, "A transformerless medium-voltage STATCOM topology based on extended modular multilevel converters," *IEEE Trans. Power Electron.*, vol. 26, no. 5, pp. 1534–1545, May 2011.

[190] A. Viatkin, R. Mandrioli, M. Hammami, M. Ricco, and G. Grandi, "AC current ripple in three-phase four-leg PWM converters with neutral line inductor," *Energies*, vol. 14, no. 5, p. 1430, Mar. 2021.

[191] R. Teodorescu, M. Liserre, and P. Rodriguez, *Grid Converters for Photovoltaic and Wind Power Systems*, vol. 29. Hoboken, NJ, USA: Wiley, 2011.

[192] C. Nardi, C. M. O. Stein, E. G. Carati, J. P. Costa, and R. Cardoso, "A methodology of LCL filter design for grid-tied power converters," in *Proc. IEEE 13th Brazilian Power Electron. Conf. 1st Southern Power Electron. Conf. (COBEP/SPEC)*, Nov. 2015, pp. 1–5.

[193] S. Tolani, V. Gautam, and P. Sensarma, "Improved selective frequency active damping for voltage source inverter with output *LC* filter," *IEEE Trans. Ind. Appl.*, vol. 56, no. 5, pp. 5194–5201, Sep./Oct. 2020.

[194] X. Wang, Y. W. Li, F. Blaabjerg, and P. C. Loh, "Virtual-impedance-based control for voltage-source and current-source converters," *IEEE Trans. Power Electron.*, vol. 30, no. 12, pp. 7019–7037, Dec. 2015.

[195] F. Botteron, R. F. D. Camargo, H. L. Hey, J. R. Pinheiro, H. A. Grundling, and H. Pinheiro, "New limiting algorithms for space vector modulated three-phase four-leg voltage source inverters," *IEE Proc.-Electr. Power Appl.*, vol. 150, no. 6, pp. 733–742, Nov. 2003.

[196] C. L. Fortescue, "Method of symmetrical co-ordinates applied to the solution of polyphase networks," *Trans. Amer. Inst. Electr. Eng.*, vol. XXXVII, no. 2, pp. 1027–1140, Jul. 1918.

[197] B.-G. Cho, S.-K. Sul, H. Yoo, and S.-M. Lee, "LCL filter design and control for grid-connected PWM converter," in *Proc. 8th Int. Conf. Power Electron. (ECCE Asia)*, May 2011, pp. 756–763.

[198] M. H. Mahlooji, H. R. Mohammadi, and M. Rahimi, "A review on modeling and control of grid-connected photovoltaic inverters with LCL filter," *Renew. Sustain. Energy Rev.*, vol. 81, pp. 563–578, Jan. 2018.

[199] R. H. Lasseter, "Smart distribution: Coupled microgrids," *Proc. IEEE*, vol. 99, no. 6, pp. 1074–1082, Jun. 2011.

[200] S. Pettersson, M. Salo, and H. Tuusa, "Four-wire current source active power filter with an open-loop current control," in *Proc. Power Convers. Conf. (Nagoya)*, Apr. 2007, pp. 542–549.

[201] R. Cárdenas, C. Juri, R. Peña, P. Wheeler, and J. Clare, "Resonant controllers for the control of 4-leg matrix converters," in *Proc. 14th Eur. Conf. Power Electron. Appl.*, Aug./Sep. 2011, pp. 1–10.

[202] Y. Zhang, Y. Kang, and J. Chen, "The zero-sequence circulating currents between parallel three-phase inverters with three-pole transformers and reactors," in *Proc. 21st Annu. IEEE Appl. Power Electron. Conf. Expo. (APEC)*, Mar. 2006, p. 7.

[203] Z. Ye, D. Boroyevich, and F. C. Lee, "Modeling and control of zero-sequence current in parallel multi-phase converters," in *Proc. IEEE 31st Annu. Power Electron. Spec. Conf.*, vol. 2, Jun. 2000, pp. 680–685.

[204] O. Ojo and P. M. Kshirsagar, "Concise modulation strategies for four-leg voltage source inverters," *IEEE Trans. Power Electron.*, vol. 19, no. 1, pp. 46–53, Jan. 2004.

[205] B. Wu, *High-Power Converters and AC Drives*. Hoboken, NJ, USA: Wiley, 2007.

[206] G. Holmes, T. Lipo, and T. Lipo, *Pulse Width Modulation for Power Converters: Principles and Practice*. Hoboken, NJ, USA: Wiley, 2003.

[207] V. Jayakumar, B. Chokkalingam, and J. L. Munda, "A comprehensive review on space vector modulation techniques for neutral point clamped multi-level inverters," *IEEE Access*, vol. 9, pp. 112104–112144, 2021.

[208] R. Zhang, D. Boroyevich, V. H. Prasad, H.-C. Mao, F. C. Lee, and S. Dubovsky, "A three-phase inverter with a neutral leg with space vector modulation," in *Proc. IEEE Appl. Power Electron. Conf. (APEC)*, vol. 2, Feb. 1997, pp. 857–863.

[209] V. H. Prasad, D. Borojevic, and R. Zhang, "Analysis and comparison of space vector modulation schemes for a four-leg voltage source inverter," in *Proc. Appl. Power Electron. Conf. (APEC)*, vol. 2, Feb. 1997, pp. 864–871.

[210] R. Zhang, V. H. Prasad, D. Boroyevich, and F. C. Lee, "Three-dimensional space vector modulation for four-leg voltage-source converters," *IEEE Trans. Power Electron.*, vol. 17, no. 3, pp. 314–326, May 2002.

[211] M. A. Perales, M. M. Prats, R. Portillo, J. L. Mora, J. I. Leon, and L. G. Franquelo, "Three-dimensional space vector modulation in ABC coordinates for four-leg voltage source converters," *IEEE Power Electron Lett.*, vol. 1, no. 4, pp. 104–109, Dec. 2003.

[212] P. K. Padhmakumar, M. P. Flower Queen, and P. B. Aurtherson, "Three dimensional space vector modulation for three phase four leg inverters–A review," in *Proc. Int. Conf. Emerg. Trends Innov. Eng. Technological Res. (ICETIETR)*, Jul. 2018, pp. 1–8.

[213] P. Szczepankowski and J. Nieznanski, "Application of barycentric coordinates in space vector PWM computations," *IEEE Access*, vol. 7, pp. 91499–91508, 2019.

[214] I. Ahmed, V. B. Borghate, A. Matsa, P. M. Meshram, H. M. Suryawanshi, and M. A. Chaudhari, "Simplified space vector modulation techniques for multilevel inverters," *IEEE Trans. Power Electron.*, vol. 31, no. 12, pp. 8483–8499, Dec. 2016.

[215] W. Wu, Y. He, T. Tang, and F. Blaabjerg, "A new design method for the passive damped LCL and LLCL filter-based single-phase grid-tied inverter," *IEEE Trans. Ind. Electron.*, vol. 60, no. 10, pp. 4339–4350, Oct. 2013.

[216] P. Szczepankowski, N. Poliakov, D. Vertegel, K. J. Szwarc, and R. Strzelecki, "A new concept of PWM duty cycle computation using the barycentric coordinates in a three–dimensional voltage vectors arrangement," *IEEE Access*, vol. 8, pp. 8019–8031, 2020.

[217] C. Liu, D. Peng, J. Lai, F. C. Lee, D. Boroyevich, and R. Zhang, "Four-legged converter 3-D SVM scheme over-modulation study," in *Proc. 15th Annu. IEEE Appl. Power Electron. Conf. Expo. (APEC)*, vol. 1, Feb. 2000, pp. 562–568.

[218] J.-H. Kim and S.-K. Sul, "Overmodulation strategy for a three-phase four-leg voltage source converter," in *Proc. 38th IAS Annu. Meeting Conf. Rec. Ind. Appl. Conf.*, vol. 1, Oct. 2003, pp. 656–663.

[219] Ó. López, J. Álvarez, J. Doval-Gandoy, and F. D. Freijedo, "Multilevel multiphase space vector PWM algorithm," *IEEE Trans. Ind. Electron.*, vol. 55, no. 5, pp. 1933–1942, May 2008.

[220] O. Lopez, J. Alvarez, J. Doval-Gandoy, F. Freijedo, A. Lago, and C. M. Penalver, "Four-dimensional space vector PWM algorithm for multilevel four-leg converters," in *Proc. 34th Annu. Conf. IEEE Ind. Electron.*, Nov. 2008, pp. 3252–3259.

[221] L. G. Franquelo, M. A. M. Prats, R. C. Portillo, J. I. L. Galvan, and M. A. Perales, "Three-dimensional space-vector modulation algorithm for four-leg multilevel converters using abc coordinates," *IEEE Trans. Ind. Electron.*, vol. 53, no. 2, pp. 458–466, Apr. 2006.

[222] M. J. Ryan, R. W. De Doncker, and R. D. Lorenz, "Decoupled control of a four-leg inverter via a new 4×4 transformation matrix," *IEEE Trans. Power Electron.*, vol. 16, no. 5, pp. 694–701, Sep. 2001.

[223] P. H. I. Hayashi and L. Matakas, "Decoupled stationary ABC frame current control of three-phase four-leg four-wire converters," in *Proc. Brazilian Power Electron. Conf. (COBEP)*, Nov. 2017, pp. 1–6.

[224] E. V. Liberado, J. A. Pomilio, A. M. S. Alonso, E. Tedeschi, F. P. Marafao, and J. F. Guerreiro, "Three/four-leg inverter current control based on generalized symmetrical components," in *Proc. IEEE 19th Workshop Control Modeling Power Electron. (COMPEL)*, Jun. 2018, pp. 1–7.

[225] O. Lopez, J. Alvarez, A. G. Yepes, F. Baneira, D. Perez-Estevez, F. D. Freijedo, and J. Doval-Gandoy, "Carrier-based PWM equivalent to multilevel multiphase space vector PWM techniques," *IEEE Trans. Ind. Electron.*, vol. 67, no. 7, pp. 5220–5231, Jul. 2020.

[226] F. A. da C. Bahia, C. B. Jacobina, I. R. F. M. P. da Silva, N. Rocha, B. E. De O. B. Luna, and P. L. S. Rodrigues, "Hybrid three-phase four-wire inverters based on modular multilevel cascade converter," in *Proc. IEEE Energy Convers. Congr. Expo. (ECCE)*, Sep. 2016, pp. 1–8.

[227] N. Y. Dai, M. C. Wong, F. Ng, and Y. D. Han, "A FPGA-based generalized pulse width modulator for three-leg center-split and four-leg voltage source inverters," *IEEE Trans. Power Electron.*, vol. 23, no. 3, pp. 1472–1484, May 2008.

[228] S. M. Ali and M. P. Kazmierkowski, "PWM voltage and current control of four-leg VSI," in *Proc. IEEE Int. Symp. Ind. Electron. (ISIE)*, vol. 1, Jul. 1998, pp. 196–201.

[229] A. Fereidouni, M. A. S. Masoum, and K. M. Smedley, "Supervisory nearly constant frequency hysteresis current control for active power filter applications in stationary reference frame," *IEEE Power Energy Technol. Syst. J.*, vol. 3, no. 1, pp. 1–12, Mar. 2016.

[230] V. George and M. K. Mishra, "User-defined constant switching frequency current control strategy for a four-leg inverter," *IET Power Electron.*, vol. 2, no. 4, pp. 335–345, Jul. 2009.

[231] L. Kunyu, T. Shun, Z. Lei, Y. Liting, and X. Xiangning, "A balance compensation method based on negative sequence weighted equivalent model of unbalanced load," in *Proc. 18th Int. Conf. Harmon. Quality Power (ICHQP)*, May 2018, pp. 1–6.

[232] Q. Zhao, F. Liang, and W. Li, "A new control scheme for LCL-type grid-connected inverter with a notch filter," in *Proc. 27th Chin. Control Decis. Conf. (CCDC)*, May 2015, pp. 4073–4077.

[233] Z. Ye and H. Mohamadian, "Comparative study of generalized electrical and optical notch filters via classical control theory," in *Proc. 5th Int. Conf. Modern Circuits Syst. Technol. (MOCAST)*, May 2016, pp. 1–4.

[234] Z. Zhihao, L. Yanmin, F. Liang, and M. Liangzhi, "A novel control strategy based on notch filter for four-leg STATCOM," in *Proc. IEEE Int. Conf. Power Syst. Technol. (POWERCON)*, Sep. 2016, pp. 1–6.

[235] P. H. I. Hayashi and L. Matakas, "Decoupled stationary ABC frame current control of three-phase four-leg four-wire converters," in *Proc. Brazilian Power Electron. Conf. (COBEP)*, Nov. 2017, pp. 1–6.

[236] E. Demirkutlu and A. M. Hava, "A scalar resonant-filter-bank-based output-voltage control method and a scalar minimum-switching-loss discontinuous PWM method for the four-leg-inverter-based three-phase four-wire power supply," *IEEE Trans. Ind. Appl.*, vol. 45, no. 3, pp. 982–991, May 2009.

[237] I. Vechiu, O. Curea, and H. Camblong, "Transient operation of a four-leg inverter for autonomous applications with unbalanced load," *IEEE Trans. Power Electron.*, vol. 25, no. 2, pp. 399–407, Feb. 2010.

[238] H. Awad, J. Svensson, and M. Bollen, "Mitigation of unbalanced voltage dips using static series compensator," *IEEE Trans. Power Electron.*, vol. 19, no. 3, pp. 837–846, May 2004.

[239] J. Svensson, M. Bongiorno, and A. Sannino, "Practical implementation of delayed signal cancellation method for phase-sequence separation," *IEEE Trans. Power Del.*, vol. 22, no. 1, pp. 18–26, Jan. 2007.

[240] R. Cárdenas, M. Díaz, F. Rojas, and J. Clare, "Fast convergence delayed signal cancellation method for sequence component separation," *IEEE Trans. Power Del.*, vol. 30, no. 4, pp. 2055–2057, Aug. 2015.

[241] S.-J. Lee, J.-K. Kang, and S.-K. Sul, "A new phase detecting method for power conversion systems considering distorted conditions in power system," in *Proc. Conf. Rec. IEEE Ind. Appl. Conf. 34th IAS Annu. Meeting*, vol. 4, Oct. 1999, pp. 2167–2172.

[242] A. Mora, R. Cardenas, M. Urrutia, M. Espinoza, and M. Diaz, "A vector control strategy to eliminate active power oscillations in four-leg grid-connected converters under unbalanced voltages," *IEEE J. Emerg. Sel. Topics Power Electron.*, vol. 8, no. 2, pp. 1728–1738, Jun. 2020.

[243] B. Kaka and A. Maji, "Performance evaluation of shunt active power filter (SAPF) connected to three phase four wire distribution networks," in *Proc. IEEE Int. Telecommun. Energy Conf. (INTELEC)*, Oct. 2016, pp. 1–9.

[244] V. D. Bacon, S. A. O. da Silva, V. de Souza, and L. B. G. Campanhol, "Impact of the phase-angle detection inaccuracies on the performance of a three-phase grid-tied system," in *Proc. 21st Eur. Conf. Power Electron. Appl. (EPE ECCE Europe)*, Sep. 2019, pp. P.1–P.8.

[245] M. Diaz and R. Cardenas, "Analysis of synchronous and stationary reference frame control strategies to fulfill LVRT requirements in wind energy conversion systems," in *Proc. 9th Int. Conf. Ecol. Vehicles Renew. Energies (EVER)*, Mar. 2014, pp. 1–8.

[246] P. Rodriguez, J. Pou, J. Bergas, J. I. Candela, R. P. Burgos, and D. Boroyevich, "Decoupled double synchronous reference frame PLL for power converters control," *IEEE Trans. Power Electron.*, vol. 22, no. 2, pp. 584–592, Mar. 2007.

[247] S. Jiao, R. R. Krishna, and K. Rajashekara, "A novel phase-locked loop based four-leg converter control for unbalanced load compensation under distorted and unbalanced grid condition," in *Proc. IEEE Energy Convers. Congr. Expo. (ECCE)*, Oct. 2020, pp. 4749–4754.

[248] R. M. Santos Filho, P. F. Seixas, P. C. Cortizo, L. A. B. Torres, and A. F. Souza, "Comparison of three single-phase PLL algorithms for UPS applications," *IEEE Trans. Ind. Electron.*, vol. 55, no. 8, pp. 2923–2932, Aug. 2008.

[249] V. Kaura and V. Blasko, "Operation of a phase locked loop system under distorted utility conditions," *IEEE Trans. Ind. Appl.*, vol. 33, no. 1, pp. 58–63, Jan./Feb. 1997.

[250] M. Li, X. Zhang, and W. Zhao, "A novel stability improvement strategy for a multi-inverter system in a weak grid utilizing dual-mode control," *Energies*, vol. 11, no. 8, p. 2144, Aug. 2018.

[251] D. Dong, B. Wen, D. Boroyevich, P. Mattavelli, and Y. Xue, "Analysis of phase-locked loop low-frequency stability in three-phase grid-connected power converters considering impedance interactions," *IEEE Trans. Ind. Electron.*, vol. 62, no. 1, pp. 310–321, Jan. 2015.

[252] C. Burgos-Mellado, A. Costabeber, M. Sumner, R. Cárdenas-Dobson, and D. Sáez, "Small-signal modelling and stability assessment of phase-locked loops in weak grids," *Energies*, vol. 12, no. 7, p. 1227, Mar. 2019.

[253] H. Akagi, Y. Kanazawa, and A. Nabae, "Instantaneous reactive power compensators comprising switching devices without energy storage components," *IEEE Trans. Ind. Appl.*, vol. IA-20, no. 3, pp. 625–630, May 1984.

[254] F. Z. Peng and J.-S. Lai, "Generalized instantaneous reactive power theory for three-phase power systems," *IEEE Trans. Instrum. Meas.*, vol. 45, no. 1, pp. 293–297, Feb. 1996.

[255] L. S. Czarnecki, "Currents' physical components (CPC) concept: A fundamental of power theory," in *Proc. Int. School Nonsinusoidal Currents Compensation*, Jun. 2008, pp. 1–11.

[256] M. Depenbrock, "The FBD-method, a generally applicable tool for analyzing power relations," *IEEE Trans. Power Syst.*, vol. 8, no. 2, pp. 381–387, May 1993.

[257] J. L. Willems, "A new interpretation of the Akagi-Nabae power components for nonsinusoidal three-phase situations," *IEEE Trans. Instrum. Meas.*, vol. 41, no. 4, pp. 523–527, Aug. 1992.

[258] P. Tenti, H. K. M. Paredes, and P. Mattavelli, "Conservative power theory, a framework to approach control and accountability issues in smart microgrids," *IEEE Trans. Power Electron.*, vol. 26, no. 3, pp. 664–673, Mar. 2011.

[259] N. L. Kusters and W. J. M. Moore, "On the definition of reactive power under non-sinusoidal conditions," *IEEE Trans. Power App. Syst.*, vol. PAS-99, no. 5, pp. 1845–1854, Sep. 1980.

[260] F. Harirchi and M. G. Simões, "Enhanced instantaneous power theory decomposition for power quality smart converter applications," *IEEE Trans. Power Electron.*, vol. 33, no. 11, pp. 9344–9359, Nov. 2018.

[261] R. S. Herrera and P. Salmeron, "Instantaneous reactive power theory: A reference in the nonlinear loads compensation," *IEEE Trans. Ind. Electron.*, vol. 56, no. 6, pp. 2015–2022, Jun. 2009.

[262] A. Ozdemir and Z. Ozdemir, "Digital current control of a three-phase four-leg voltage source inverter by using p–q–r theory," *IET Power Electron.*, vol. 7, no. 3, pp. 527–539, 2014.

[263] M. E. Ortuzar, R. E. Carmi, J. W. Dixon, and L. Moran, "Voltage-source active power filter based on multilevel converter and ultracapacitor DC link," *IEEE Trans. Ind. Electron.*, vol. 53, no. 2, pp. 477–485, Apr. 2006.

[264] E. H. Watanabe, M. Aredes, and H. Akagi, "The p-q theory for active filter control: Some problems and solutions," *Sba: Controle Automação Sociedade Brasileira de Automatica*, vol. 15, no. 1, pp. 78–84, Mar. 2004.

[265] H. Kim, F. Blaabjerg, and B. Bak-Jensen, "Spectral analysis of instantaneous powers in single-phase and three-phase systems with use of p–q–r theory," *IEEE Trans. Power Electron.*, vol. 17, no. 5, pp. 711–720, Sep. 2002.

[266] E. H. Watanabe, R. M. Stephan, and M. Aredes, "New concepts of instantaneous active and reactive powers in electrical systems with generic loads," *IEEE Trans. Power Del.*, vol. 8, no. 2, pp. 697–703, Apr. 1993.

[267] H. Kim, F. Blaabjerg, B. Bak-Jensen, and J. Choi, "Instantaneous power compensation in three-phase systems by using p–q–r theory," *IEEE Trans. Power Electron.*, vol. 17, no. 5, pp. 701–710, Sep. 2002.

[268] C. Burgos-Mellado, C. Hernández-Carimán, and R. Cárdenas, "Experimental evaluation of a CPT-based four-leg active power compensator for distributed generation," *IEEE J. Emerg. Sel. Topics Power Electron.*, vol. 5, no. 2, pp. 747–759, Jun. 2017.

[269] M. Rajeev and S. Divya, "Harmonic compensation by transformer-less grid-tied PV inverter using conservative power theory," in *Proc. IEEE 5th Int. Conf. Converg. Technol. (I2CT)*, Mar. 2019, pp. 1–5.

[270] A. M. S. Alonso, H. K. M. Paredes, J. A. O. Filho, J. P. Bonaldo, D. I. Brandao, and F. P. Marafao, "Selective power conditioning in two-phase three-wire systems based on the conservative power theory," in *Proc. IEEE Ind. Appl. Soc. Annu. Meeting*, Sep. 2019, pp. 1–6.

[271] A. A. Bohari, H. H. Goh, A. K. Tonni, S. S. Lee, S. Y. Sim, K. C. Goh, C. S. Lim, and Y. C. Luo, "Predictive direct power control for dual-active-bridge multilevel inverter based on conservative power theory," *Energies*, vol. 13, no. 11, p. 2951, Jun. 2020.

[272] M. G. Simões, T. D. C. Busarello, A. S. Bubshait, F. Harirchi, J. A. Pomilio, and F. Blaabjerg, "Interactive smart battery storage for a PV and wind hybrid energy management control based on conservative power theory," *Int. J. Control*, vol. 89, no. 4, pp. 850–870, Apr. 2016.

[273] H. K. M. Paredes, F. P. Marafao, P. Mattavelli, and P. Tenti, "Application of conservative power theory to load and line characterization and revenue metering," in *Proc. IEEE Int. Workshop Appl. Meas. Power Syst. (AMPS)*, Sep. 2012, pp. 1–6.

[274] P. Tenti, H. K. M. Paredes, F. P. Marafao, and P. Mattavelli, "Accountability in smart microgrids based on conservative power theory," *IEEE Trans. Instrum. Meas.*, vol. 60, no. 9, pp. 3058–3069, Sep. 2011.

[275] P. Tenti, A. Costabeber, P. Mattavelli, F. P. Marafao, and H. K. M. Paredes, "Load characterization and revenue metering under non-sinusoidal and asymmetrical operation," *IEEE Trans. Instrum. Meas.*, vol. 63, no. 2, pp. 422–431, Feb. 2014.

[276] F. P. Marafão, D. I. Brandão, F. A. S. Gonçalves, and H. K. M. Paredes, "Decoupled reference generator for shunt active filters using the conservative power theory," *J. Control, Automat. Elect. Syst.*, vol. 24, pp. 522–534, Aug. 2013.

[277] C. Burgos-Mellado, J. J. Llanos, R. Cardenas, D. Saez, D. E. Olivares, M. Sumner, and A. Costabeber, "Distributed control strategy based on a consensus algorithm and on the conservative power theory for imbalance and harmonic sharing in 4-wire microgrids," *IEEE Trans. Smart Grid*, vol. 11, no. 2, pp. 1604–1619, Mar. 2020.

[278] D. I. Brandao, H. K. M. Paredes, A. Costabeber, and F. P. Marafão, "Flexible active compensation based on load conformity factors applied to non-sinusoidal and asymmetrical voltage conditions," *IET Power Electron.*, vol. 9, no. 2, pp. 356–364, 2016.

[279] A. Shri, J. Popovic, J. A. Ferreira, and M. B. Gerber, "Design and control of a three-phase four-leg inverter for solid-state transformer applications," in *Proc. 15th Eur. Conf. Power Electron. Appl. (EPE)*, Sep. 2013, pp. 1–9.

[280] W. Zhao and G. Chen, "Comparison of active and passive damping methods for application in high power active power filter with LCL-filter," in *Proc. Int. Conf. Sustain. Power Gener. Supply*, Apr. 2009, pp. 1–6.

[281] A. Aapro, T. Messo, T. Roinila, and T. Suntio, "Effect of active damping on output impedance of three-phase grid-connected converter," *IEEE Trans. Ind. Electron.*, vol. 64, no. 9, pp. 7532–7541, Sep. 2017.

[282] Z. Xin, P. C. Loh, X. Wang, F. Blaabjerg, and Y. Tang, "Highly accurate derivatives for LCL-filtered grid converter with capacitor voltage active damping," *IEEE Trans. Power Electron.*, vol. 31, no. 5, pp. 3612–3625, May 2016.

[283] Z. Li, C. Zang, P. Zeng, H. Yu, and S. Li, "Fully distributed hierarchical control of parallel grid-supporting inverters in islanded AC microgrids," *IEEE Trans. Ind. Electron.*, vol. 14, no. 2, pp. 679–690, Feb. 2018.

[284] T. Kerdphol, F. S. Rahman, Y. Mitani, M. Watanabe, and S. Küfeoğlu, "Robust virtual inertia control of an islanded microgrid considering high penetration of renewable energy," *IEEE Access*, vol. 6, pp. 625–636, 2018.

[285] M. Savaghebi, A. Jalilian, J. C. Vasquez, and J. M. Guerrero, "Autonomous voltage unbalance compensation in an islanded droop-controlled microgrid," *IEEE Trans. Ind. Electron.*, vol. 60, no. 4, pp. 1390–1402, Apr. 2013.

[286] K. Ge, Z. Fan, L. Fang, and J. Chen, "Inverter control based on virtual impedance under unbalanced load," in *Proc. IEEE 29th Int. Symp. Ind. Electron. (ISIE)*, Jun. 2020, pp. 1167–1172.

[287] J. Zhou, S. Kim, H. Zhang, Q. Sun, and R. Han, "Consensus-based distributed control for accurate reactive, harmonic, and imbalance power sharing in microgrids," *IEEE Trans. Smart Grid*, vol. 9, no. 4, pp. 2453–2467, Jul. 2016.

[288] C. J. O'Rourke, M. M. Qasim, M. R. Overlin, and J. L. Kirtley, "A geometric interpretation of reference frames and transformations: Dq0, clarke, and park," *IEEE Trans. Energy Convers.*, vol. 34, no. 4, pp. 2070–2083, Dec. 2019.

[289] R. Teodorescu, F. Blaabjerg, M. Liserre, and P. C. Loh, "Proportional-resonant controllers and filters for grid-connected voltage-source converters," *IEE Proc.-Electr. Power Appl.*, vol. 153, no. 5, pp. 750–762, 2006.

[290] A. G. Yepes, F. D. Freijedo, J. Doval-Gandoy, O. Lopez, J. Malvar, and P. Fernandez-Comesana, "Effects of discretization methods on the performance of resonant controllers," *IEEE Trans. Power Electron.*, vol. 25, no. 7, pp. 1692–1712, Jul. 2010.

[291] R. I. Bojoi, G. Griva, M. Guerriero, F. Farina, and F. Profumo, "Current control strategy for power conditioners using sinusoidal signal integrators in synchronous reference frame," *IEEE Trans. Power Electron.*, vol. 20, no. 6, pp. 1402–1412, Nov. 2005.

[292] A. G. Yepes, F. D. Freijedo, Ó. López, and J. Doval-Gandoy, "Analysis and design of resonant current controllers for voltage-source converters by means of Nyquist diagrams and sensitivity function," *IEEE Trans. Ind. Electron.*, vol. 58, no. 11, pp. 5231–5250, Nov. 2011.

[293] A. Lidozzi, C. Ji, L. Solero, P. Zanchetta, and F. Crescimbini, "Resonant–repetitive combined control for stand-alone power supply units," *IEEE Trans. Ind. Appl.*, vol. 51, no. 6, pp. 4653–4663, Dec. 2015.

[294] E. Kurniawan, Z. Cao, O. Mahendra, and R. Wardoyo, "A survey on robust repetitive control and applications," in *Proc. IEEE Int. Conf. Control Syst., Comput. Eng. (ICCSCE)*, Nov. 2014, pp. 524–529.

[295] C. Hackl, F. Larcher, A. Dötlinger, and R. Kennel, "Is multiple-objective model-predictive control 'optimal?'" in *Proc. IEEE Int. Symp. Sensorless Control Elect. Drives Predictive Control Elect. Drives Power Electron. (SLED/PRECEDE)*, Oct. 2013, pp. 1–8.

[296] J. Rodríguez and M. P. Kazmierkowski, "State of the art of finite control set model predictive control in power electronics," *IEEE Trans. Ind. Informat.*, vol. 9, no. 2, pp. 1003–1016, May 2013.

[297] V. Yaramasu, B. Wu, M. Rivera, J. Rodriguez, and A. Wilson, "Cost-function based predictive voltage control of two-level four-leg inverters using two step prediction horizon for standalone power systems," in *Proc. 27th Annu. IEEE Appl. Power Electron. Conf. Expo. (APEC)*, Feb. 2012, pp. 128–135.

[298] H. A. Young, M. A. Perez, J. Rodriguez, and H. Abu-Rub, "Assessing finite-control-set model predictive control: A comparison with a linear current controller in two-level voltage source inverters," *IEEE Ind. Electron. Mag.*, vol. 8, no. 1, pp. 44–52, Mar. 2014.

[299] V. Yaramasu, M. Rivera, M. Narimani, B. Wu, and J. Rodriguez, "Model predictive approach for a simple and effective load voltage control of four-leg inverter with an output LC filter," *IEEE Trans. Ind. Electron.*, vol. 61, no. 10, pp. 5259–5270, Oct. 2014.

[300] S. K. Gannamraju, D. Valluri, and R. Bhimasingu, "Comparison of fixed switching frequency based optimal switching vector MPC algorithms applied to voltage source inverter for stand-alone applications," in *Proc. Nat. Power Electron. Conf. (NPEC)*, Dec. 2019, pp. 1–6.

[301] K. S. Alam, D. Xiao, M. P. Akter, S. M. Showybul Islam Shakib, and M. F. Rahman, "Predictive load voltage control for four-leg inverter with fixed switching frequency," in *Proc. 9th Int. Conf. Power Energy Syst. (ICPES)*, Dec. 2019, pp. 1–6.

[302] A. P. Kumar, G. Siva Kumar, and D. Sreenivasarao, "Model predictive control with constant switching frequency for four-leg DSTATCOM using three-dimensional space vector modulatio," *IET Gener., Transmiss. Distrib.*, vol. 14, no. 17, pp. 3571–3581, 2020.

[303] F. Donoso, A. Mora, R. Cárdenas, A. Angulo, D. Sáez, and M. Rivera, "Finite-set model-predictive control strategies for a 3L-NPC inverter operating with fixed switching frequency," *IEEE Trans. Ind. Electron.*, vol. 65, no. 5, pp. 3954–3965, May 2018.

[304] R. R. Sawant and M. C. Chandorkar, "A multifunctional four-leg grid-connected compensator," *IEEE Trans. Ind. Appl.*, vol. 45, no. 1, pp. 249–259, Jan./Feb. 2009.

[305] P. Mattavelli, "An improved deadbeat control for UPS using disturbance observers," *IEEE Trans. Ind. Electron.*, vol. 52, no. 1, pp. 206–212, Feb. 2005.

[306] Y. A.-R. I. Mohamed and E. F. El-Saadany, "An improved deadbeat current control scheme with a novel adaptive self-tuning load model for a three-phase PWM voltage-source inverter," *IEEE Trans. Ind. Electron.*, vol. 54, no. 2, pp. 747–759, Apr. 2007.

[307] A. Kaszewski, L. M. Grzesiak, and B. Ufnalski, "Multi-oscillatory LQR for a three-phase four-wire inverter with $L_{3n}C$ output filter," in *Proc. 38th Annu. Conf. IEEE Ind. Electron. Soc. (IECON)*, Oct. 2012, pp. 3449–3455.

[308] H. Nazaripouya, H. Mokhtari, and E. Amiri, "Using optimal controller to parallel three-phase 4-leg inverters with unbalance loads," in *Proc. IEEE 1st Int. Conf. Power Electron., Intell. Control Energy Syst. (ICPEICES)*, Jul. 2016, pp. 1–6.

[309] A. Kaszewski, B. Ufnalski, and L. M. Grzesiak, "An LQ controller with disturbance feedforward for the 3-phase 4-leg true sine wave inverter," in *Proc. IEEE Int. Conf. Ind. Technol. (ICIT)*, Feb. 2013, pp. 1924–1930.

[310] R. M. Cuzner, A. R. Bendre, P. J. Faill, and B. Semenov, "Implementation of a four pole neutral-point clamped three phase inverter with low common mode voltage output," in *Proc. IEEE Ind. Appl. Annu. Meeting*, Sep. 2007, pp. 923–930.

[311] V. Vineeth and S. Bindu, "Closed loop control of a four leg inverter for unbalanced power networks," in *Proc. Int. Conf. Control Commun. Comput. (ICCC)*, Dec. 2013, pp. 500–505.

[312] S. Sedghi, A. Dastfan, A. Ahmadyfard, and A. Akbarzadeh Kalat, "Adaptive control strategy of four-leg active power filter with LCL grid filter," in *Proc. 8th Power Electron., Drive Syst. Technol. Conf. (PEDSTC)*, Feb. 2017, pp. 531–536.

[313] P. Mattavelli, "A closed-loop selective harmonic compensation for active filters," *IEEE Trans. Ind. Appl.*, vol. 37, no. 1, pp. 81–89, Jan./Feb. 2001.

[314] H. Lei, L. Fei, J. Xiong, X. Lin, and Y. Kang, "Research on paralleled three-phase four-leg voltage source inverters based on dual-loop control in $\alpha\beta$o coordinate," in *Proc. 8th Int. Conf. Power Electron. (ECCE Asia)*, May/Jun. 2011, pp. 2912–2919.

[315] M. Liserre, R. Teodorescu, and F. Blaabjerg, "Stability of photovoltaic and wind turbine grid-connected inverters for a large set of grid impedance values," *IEEE Trans. Power Electron.*, vol. 21, no. 1, pp. 263–272, Jan. 2006.

[316] S. Jiao, K. R. R, and K. Rajashekara, "A novel DROGI algorithm for non-linear unbalanced load compensation using four-leg converter," in *Proc. IEEE Appl. Power Electron. Conf. Expo. (APEC)*, Mar. 2020, pp. 3282–3286.
[317] H. Nazifi and A. Radan, "Current control assisted and non-ideal proportional-resonant voltage controller for four-leg three-phase inverters with time-variant loads," in *Proc. 4th Annu. Int. Power Electron., Drive Syst. Technol. Conf.*, Feb. 2013, pp. 355–360.
[318] L. Zhishan and Q. Yinfeng, "Passivity-based control for three-phase four-leg shunt active power filter," in *Proc. IEEE Int. Conf. Control Autom.*, Dec. 2009, pp. 2106–2110.
[319] S. Pettersson, M. Salo, and H. Tuusa, "Applying an LCL-filter to a four-wire active power filter," in *Proc. 37th IEEE Power Electron. Spec. Conf.*, Jun. 2006, pp. 1–7.
[320] S. Bayhan, M. Trabelsi, and H. Abu-Rub, "Model predictive control of Z-source four-leg inverter for standalone photovoltaic system with unbalanced load," in *Proc. IEEE Appl. Power Electron. Conf. Expo. (APEC)*, Mar. 2016, pp. 3663–3668.
[321] L. R. A. Pinto, S. P. Pimentel, E. G. Marra, B. Alvarenga, T. D. M. Cesar, and C. K. D. Lima, "Proposal of model predictive control (MPC) method for a three-phase four-leg inverter applied in a distributed generation system," in *Proc. Brazilian Power Electron. Conf. (COBEP)*, Nov. 2017, pp. 1–6.
[322] S. Colombi, N. Katukuri, Y. Kolhatkar, K. M. Dora, and P. Nerella, "Control of four-leg transformerless uninterruptible power supply," U.S. Patent 8 093 746 B2, Jan. 10, 2012.
[323] S. S. Seyedalipour, M. Shahparasti, A. Hajizadeh, and M. Savaghebi, "Model-based control of four-leg inverter for UPS applications considering the effect of neutral line inductor," *IET Power Electron.*, vol. 14, no. 8, pp. 1468–1479, 2021.
[324] C. Burgos, D. Saez, M. E. Orchard, and R. Cardenas, "Fuzzy modelling for the state-of-charge estimation of lead-acid batteries," *J. Power Sources*, vol. 274, pp. 355–366, Jan. 2015.
[325] S. Bayhan, M. Trabelsi, H. Abu-Rub, and M. Malinowski, "Finite-control-set model-predictive control for a quasi-Z-source four-leg inverter under unbalanced load condition," *IEEE Trans. Ind. Electron.*, vol. 64, no. 4, pp. 2560–2569, Apr. 2017.
[326] M. Shirazi, C. Niebylski, and J. Deplitch, "Integration of a DC transformer, four-leg inverter, and flexible grid input into the consolidated utility base electrical (CUBE) system," NREL, Golden, CO, USA, Tech. Rep. NREL/TP-5D00-66612, Jun. 2016.
[327] T. F. Podlesak, D. C. Katsis, P. W. Wheeler, J. C. Clare, L. Empringham, and M. Bland, "A 150-kVA vector-controlled matrix converter induction motor drive," *IEEE Trans. Ind. Appl.*, vol. 41, no. 3, pp. 841–847, May 2005.
[328] P. W. Wheeler, J. C. Clare, M. Apap, D. Lampard, S. J. Pickering, K. J. Bradley, and L. Empringham, "An integrated 30 kw matrix converter based induction motor drive," in *Proc. IEEE 36th Power Electron. Spec. Conf.*, Jun. 2005, pp. 2390–2395.
[329] F. Yue, P. W. Wheeler, N. Mason, L. Empringham, and J. C. Clare, "Indirect space vector modulation for a 4-leg matrix converter," in *Proc. IEEE Power Electron. Spec. Conf.*, Jun. 2007, pp. 639–645.
[330] C. Garcia, M. Rivera, J. Rodriguez, and P. Wheeler, "Experimental evaluation of predictive voltage control for a four-leg two-stage matrix converter," *IET Power Electron.*, vol. 12, no. 12, pp. 3077–3084, 2019.
[331] V. Vasquez, R. Ortega, L. M. Ortega, V. H. Garcia, and O. Carranza, "Three phase four-wire inverter for grid-disconnected operation," *IEEE Access*, vol. 8, pp. 118324–118339, 2020.
[332] A. Kaszewski, B. Ufnalski, and L. M. Grzesiak, "The LQ controller for the 3-phase 4-leg inverter with an LC output filter—Choosing the right reference frame," in *Proc. 15th Eur. Conf. Power Electron. Appl. (EPE)*, Sep. 2013, pp. 1–9.
[333] M. Rivera, V. Yaramasu, J. Rodriguez, and B. Wu, "Model predictive current control of two-level four-leg inverters—Part II: Experimental implementation and validation," *IEEE Trans. Power Electron.*, vol. 28, no. 7, pp. 3469–3478, Jul. 2013.
[334] V. Yaramasu, M. Rivera, B. Wu, and J. Rodriguez, "Model predictive current control of two-level four-leg inverters—Part I: Concept, algorithm, and simulation analysis," *IEEE Trans. Power Electron.*, vol. 28, no. 7, pp. 3459–3468, Jul. 2013.
[335] J. Rodriguez, B. Wu, M. Rivera, A. Wilson, V. Yaramasu, and C. Rojas, "Model predictive control of three-phase four-leg neutral-point-clamped inverters," in *Proc. Int. Power Electron. Conf. (ECCE ASIA)*, Jun. 2010, pp. 3112–3116.
[336] D. Ali, A. Houari, A. Saim, M. Ait-Ahmed, S. Pierfederici, M. F. Benkhoris, M. Machmoum, and M. Ghanes, "Flatness-based grey wolf control for load voltage unbalance mitigation in three-phase four-leg voltage source inverters," *IEEE Trans. Ind. Appl.*, vol. 56, no. 2, pp. 1869–1881, Mar./Apr. 2020.
[337] M. Soheil-Hamedani, M. Zandi, R. Gavagsaz-Ghoachani, B. Nahid-Mobarakeh, and S. Pierfederici, "Flatness-based control method: A review of its applications to power systems," in *Proc. 7th Power Electron. Drive Syst. Technol. Conf. (PEDSTC)*, Feb. 2016, pp. 547–552.
[338] A. Djerioui, A. Houari, M. Ait-Ahmed, M.-F. Benkhoris, A. Chouder, and M. Machmoum, "Grey wolf based control for speed ripple reduction at low speed operation of PMSM drives," *ISA Trans.*, vol. 74, pp. 111–119, Mar. 2018.
[339] Z. Zhao, B. Horn, and R. Leidhold, "Investigation of common-mode current elimination in four-wire inverter-fed motor," in *Proc. IEEE Int. Power Electron. Appl. Conf. Expo. (PEAC)*, Nov. 2018, pp. 1–5.
[340] SAE_Int, *Ways of Dealing With Power Regeneration Onto an Aircraft Electrical Power System Bus*, Standard AIR6139, Warrandale PA, USA, 2014, pp. 1–15.
[341] G. Escobar, A. A. Valdez, J. Leyva-Ramos, and P. Mattavelli, "Repetitive-based controller for a UPS inverter to compensate unbalance and harmonic distortion," *IEEE Trans. Ind. Electron.*, vol. 54, no. 1, pp. 504–510, Feb. 2007.
[342] P. Cortes, G. Ortiz, J. I. Yuz, J. Rodriguez, S. Vazquez, and L. G. Franquelo, "Model predictive control of an inverter with output LC filter for UPS applications," *IEEE Trans. Ind. Electron.*, vol. 56, no. 6, pp. 1875–1883, Jun. 2009.
[343] S. L. Arevalo, P. Zanchetta, P. W. Wheeler, A. Trentin, and L. Empringham, "Control and implementation of a matrix-converter-based AC ground power-supply unit for aircraft servicing," *IEEE Trans. Ind. Electron.*, vol. 57, no. 6, pp. 2076–2084, Jun. 2010.
[344] A. S. Vijay, S. Doolla, and M. C. Chandorkar, "Control approaches for enhanced sharing of unbalanced powers amongst inverter based DGs in islanded AC microgrids," in *Proc. IEEE Int. Conf. Power Electron., Drives Energy Syst. (PEDES)*, Dec. 2020, pp. 1–5.
[345] C. Ahumada, R. Cárdenas, D. Sáez, and J. M. Guerrero, "Secondary control strategies for frequency restoration in islanded microgrids with consideration of communication delays," *IEEE Trans. Smart Grid*, vol. 7, no. 3, pp. 1430–1441, May 2016.
[346] S. Alepuz, S. Busquets-Monge, J. Bordonau, and J. A. Martinez-Velasco, "Control strategies based on symmetrical components for grid-connected converters under voltage dips," *IEEE Trans. Ind. Electron.*, vol. 56, no. 6, pp. 2162–2173, Jun. 2009.
[347] I. Sadeghkhani, M. E. H. Golshan, A. Mehrizi-Sani, and J. M. Guerrero, "Low-voltage ride-through of a droop-based three-phase four-wire grid-connected microgrid," *IET Gener., Transm. Distrib.*, vol. 12, no. 8, pp. 1906–1914, Apr. 2018.
[348] A. Vijay, S. Doolla, and M. C. Chandorkar, "Unbalance mitigation strategies in microgrids," *IET Power Electron.*, vol. 13, no. 9, pp. 1687–1710, 2020.
[349] A. Mortezaei, M. G. Simões, M. Savaghebi, J. M. Guerrero, and A. Al-Durra, "Cooperative control of multi-master–slave islanded microgrid with power quality enhancement based on conservative power theory," *IEEE Trans. Smart Grid*, vol. 9, no. 4, pp. 2964–2975, Jul. 2018.
[350] A. Mortezaei, M. G. Simoes, A. A. Durra, F. P. Marafao, and T. D. Curi Busarello, "Coordinated operation in a multi-inverter based microgrid for both grid-connected and islanded modes using conservative power theory," in *Proc. IEEE Energy Convers. Congr. Expo. (ECCE)*, Sep. 2015, pp. 4602–4609.
[351] F. Tang, X. Zhou, L. Meng, J. M. Guerrero, and J. C. Vasquez, "Secondary voltage unbalance compensation for three-phase four-wire islanded microgrids," in *Proc. IEEE 11th Int. Multi-Conf. Syst., Signals Devices (SSD)*, Feb. 2014, pp. 1–5.
[352] J. M. Guerrero, J. C. Vasquez, J. Matas, L. G. de Vicuna, and M. Castilla, "Hierarchical control of droop-controlled AC and DC microgrids-a general approach toward standardization," *IEEE Trans. Ind. Electron.*, vol. 58, no. 1, pp. 158–172, Jan. 2011.
[353] Y. Sun, X. Hou, J. Yang, H. Han, M. Su, and J. M. Guerrero, "New perspectives on droop control in AC microgrid," *IEEE Trans. Ind. Electron.*, vol. 64, no. 7, pp. 5741–5745, Jul. 2017.
[354] P. Piagi and R. H. Lasseter, "Autonomous control of microgrids," in *Proc. IEEE Power Eng. Soc. Gen. Meeting*, Jun. 2006, p. 8.

[355] S. P. Oe, E. Christopher, M. Sumner, S. Pholboon, M. Johnson, and S. A. Norman, "Microgrid unbalance compensator–mitigating the negative effects of unbalanced microgrid operation," in *Proc. IEEE PES ISGT Eur.*, Oct. 2013, pp. 1–5.

[356] M. Abdel-Akher, M. M. Aly, Z. Ziadi, H. El-kishky, and M. A. Abdel-Warth, "Voltage stability modeling and analysis of unbalanced distribution systems with wind turbine energy systems," in *Proc. IEEE Int. Conf. Ind. Technol. (ICIT)*, Feb. 2014, pp. 565–570.

[357] E. Nasr-Azadani, C. A. Cañizares, D. E. Olivares, and K. Bhattacharya, "Stability analysis of unbalanced distribution systems with synchronous machine and DFIG based distributed generators," *IEEE Trans. Smart Grid*, vol. 5, no. 5, pp. 2326–2338, Sep. 2014.

[358] *American National Standard For Electric Power Systems and Equipment-Voltage Ratings (60 Hertz)*, Standard ANSI C84.1, 2006.

[359] L. Meng, F. Tang, M. Savaghebi, J. C. Vasquez, and J. M. Guerrero, "Tertiary control of voltage unbalance compensation for optimal power quality in islanded microgrids," *IEEE Trans. Energy Convers.*, vol. 29, no. 4, pp. 802–815, Dec. 2014.

[360] C. Burgos-Mellado, J. Gutierrez, C. Pineda, F. Donoso, A. Watson, M. Sumner, R. Cardenas, and A. Mora, "Distributed control strategy based on a consensus algorithm for the inter-cell and inter-cluster voltage balancing of a cascaded H-bridge based STATCOM," in *Proc. IEEE 21st Workshop Control Modeling Power Electron. (COMPEL)*, Nov. 2020, pp. 1–8.

[361] F. Guo, C. Wen, and Y.-D. Song, *Distributed Control and Optimization Technologies in Smart Grid Systems*. Boca Raton, FL, USA: CRC Press, Nov. 2017.

[362] G. Chen and E. Feng, "Distributed secondary control and optimal power sharing in microgrids," *IEEE/CAA J. Automatica Sinica*, vol. 2, no. 3, pp. 304–312, Jul. 2015.

[363] F. Guo, C. Wen, J. Mao, and Y.-D. Song, "Distributed economic dispatch for smart grids with random wind power," *IEEE Trans. Smart Grid*, vol. 7, no. 3, pp. 1572–1583, May 2016.

[364] M. A. Rustam, B. Khan, S. M. Ali, M. B. Qureshi, C. A. Mehmood, M. U. S. Khan, and R. Nawaz, "An adaptive distributed averaging integral control scheme for micro-grids with renewable intermittency and varying operating cost," *IEEE Access*, vol. 8, pp. 455–464, 2020.

[365] S. Halpin, "Revisions to IEEE standard 519–1992," in *Proc. IEEE/PES Transmiss. Distrib. Conf. Exhib.*, May 2006, pp. 1149–1151.

[366] *American National Standard for Electric Power Systems and Equipment-Voltage Ratings (60 Hertz)*. National Electrical Manufacturers Association, Rosslyn, VA, USA, 1996.

[367] M. J. Hossain, F. H. M. Rafi, G. Town, and J. Lu, "Multifunctional three-phase four-leg PV-SVSI with dynamic capacity distribution method," *IEEE Trans. Ind. Informat.*, vol. 14, no. 6, pp. 2507–2520, Jun. 2018.

[368] F. H. Md Rafi, M. J. Hossain, G. Town, and J. Lu, "Smart voltage-source inverters with a novel approach to enhance neutral-current compensation," *IEEE Trans. Ind. Electron.*, vol. 66, no. 5, pp. 3518–3529, May 2019.

[369] M. Moghimi, J. Liu, P. Jamborsalamati, F. Rafi, S. Rahman, J. Hossain, S. Stegen, and J. Lu, "Internet of Things platform for energy management in multi-microgrid system to improve neutral current compensation," *Energies*, vol. 11, no. 11, p. 3102, Nov. 2018.

[370] M. Moghimi, F. HasanMd Rafi, P. Jamborsalamati, J. Liu, M. J. Hossain, and J. Lu, "Improved unbalance compensation for energy management in multi-microgrid system with Internet of Things platform," in *Proc. IEEE Int. Conf. Environ. Electr. Eng. IEEE Ind. Commercial Power Syst. Eur. (EEEIC/I&CPS Europe)*, Jun. 2018, pp. 1–6.

[371] Y. Karimi, H. Oraee, and J. M. Guerrero, "Decentralized method for load sharing and power management in a hybrid single/three-phase-islanded microgrid consisting of hybrid source PV/battery units," *IEEE Trans. Power Electron.*, vol. 32, no. 8, pp. 6135–6144, Aug. 2017.

[372] J. Zhou, Y. Xu, H. Sun, Y. Li, and M.-Y. Chow, "Distributed power management for networked AC–DC microgrids with unbalanced microgrids," *IEEE Trans. Ind. Informat.*, vol. 16, no. 3, pp. 1655–1667, Mar. 2020.

[373] J. Zhou, H. Sun, Y. Xu, R. Han, Z. Yi, L. Wang, and J. M. Guerrero, "Distributed power sharing control for islanded single-/three-phase microgrids with admissible voltage and energy storage constraints," *IEEE Trans. Smart Grid*, vol. 12, no. 4, pp. 2760–2775, Jul. 2021.

[374] D. I. Brandao, T. Caldognetto, F. P. Marafão, M. G. Simões, J. A. Pomilio, and P. Tenti, "Centralized control of distributed single-phase inverters arbitrarily connected to three-phase four-wire microgrids," *IEEE Trans. Smart Grid*, vol. 8, no. 1, pp. 437–446, Jan. 2017.

[375] F. Nejabatkhah and Y. W. Li, "Flexible unbalanced compensation of three-phase distribution system using single-phase distributed generation inverters," *IEEE Trans. Smart Grid*, vol. 10, no. 2, pp. 1845–1857, Mar. 2019.

[376] Y. Li, D. M. Vilathgamuwa, and P. C. Loh, "Microgrid power quality enhancement using a three-phase four-wire grid-interfacing compensator," *IEEE Trans. Ind. Appl.*, vol. 41, no. 6, pp. 1707–1719, Nov./Dec. 2005.

[377] P. L. S. Rodrigues, C. B. Jacobina, M. B. R. Correa, and I. R. F. M. P. da Silva, "Single-phase universal active power filter based on four-leg AC/DC/AC converters," in *Proc. IEEE Energy Convers. Congr. Expo. (ECCE)*, Oct. 2017, pp. 2954–2961.

[378] Y. Yang, K. Zhou, and F. Blaabjerg, "Current harmonics from single-phase grid-connected inverters—Examination and suppression," *IEEE Trans. Emerg. Sel. Topics Power Electron.*, vol. 4, no. 1, pp. 221–233, Mar. 2016.

[379] N. Chitra, P. Sivakumar, A. Devisree, and S. Priyanka, "Shunt active power filter for harmonic reduction in microgrid exploiting distinctive compensation theory: A technical and eminence review," in *Proc. Int. Conf. Power, Energy, Control Transmiss. Syst. (ICPECTS)*, Feb. 2018, pp. 147–153.

[380] D. Schwanz, A. Bagheri, M. Bollen, and A. Larsson, "Active harmonic filters: Control techniques review," in *Proc. 17th Int. Conf. Harmon. Quality Power (ICHQP)*, Oct. 2016, pp. 36–41.

[381] M. El-Habrouk, M. Darwish, and P. Mehta, "Active power filters: A review," *IEE Proc.-Electr. Power Appl.*, vol. 147, no. 5, pp. 403–413, 2000.

[382] R. Rajagopal, K. Palanisamy, and S. Paramasivam, "A technical review on control strategies for active power filters," in *Proc. Int. Conf. Emerg. Trends Innov. Eng. Technol. Res. (ICETIETR)*, Jul. 2018, pp. 1–6.

[383] A. M. Massoud, S. J. Finney, and B. W. Williams, "Review of harmonic current extraction techniques for an active power filter," in *Proc. 11th Int. Conf. Harmon. Quality Power*, Sep. 2004, pp. 154–159.

[384] M. Depenbrock and V. Staudt, "The FBD-method as tool for compensating total nonactive currents," in *Proc. 8th Int. Conf. Harmon. Quality Power*, vol. 1, Oct. 1998, pp. 320–324.

[385] F. P. Marafao, S. M. Deckmann, J. A. Pomilio, and R. Q. Machado, "Selective disturbance compensation and comparisons of active filtering strategies," in *Proc. 10th Int. Conf. Harmon. Quality Power*, vol. 2, Oct. 2002, pp. 484–489.

[386] B. Singh, S. R. Arya, C. Jain, and S. Goel, "Implementation of four-leg distribution static compensator," *IET Gener., Transmiss. Distrib.*, vol. 8, no. 6, pp. 1127–1139, Jun. 2014.

[387] B. Singh, V. Verma, and J. Solanki, "Neural network-based selective compensation of current quality problems in distribution system," *IEEE Trans. Ind. Electron.*, vol. 54, no. 1, pp. 53–60, Feb. 2007.

[388] G. D. Marques, "A comparison of active power filter control methods in unbalanced and non-sinusoidal conditions," in *Proc. 24th Annu. Conf. IEEE Ind. Electron. Soc. (IECON)*, vol. 1, Aug./Sep. 1998, pp. 444–449.

[389] S. Bhattacharya, D. Divan, and B. Banerjee, "Synchronous frame harmonic isolator using active series filter," in *Proc. Eur. Conf. Power Electron. Appl.*, vol. 3, 1992, p. 30.

[390] H. K. Paredes, F. P. Marafão, and L. C. Da Silva, "A comparative analysis of FBD, PQ and CPT current decompositions—Part I: Three-phase, three-wire systems," in *Proc. IEEE Bucharest PowerTech*, Jun./Jul. 2009, pp. 1–8.

[391] F. Z. Peng, G. W. Ott, Jr., and D. J. Adams, "Harmonic and reactive power compensation based on the generalized instantaneous reactive power theory for three-phase four-wire systems," *IEEE Trans. Power Del.*, vol. 13, no. 6, pp. 1174–1181, Nov. 1998.

[392] C.-C. Chen and Y.-Y. Hsu, "A novel approach to the design of a shunt active filter for an unbalanced three-phase four-wire system under nonsinusoidal conditions," *IEEE Trans. Power Del.*, vol. 15, no. 4, pp. 1258–1264, Oct. 2000.

[393] C. A. Quinn and N. Mohan, "Active filtering of harmonic currents in three-phase, four-wire systems with three-phase and single-phase nonlinear loads," in *Proc. 7th Annu. Appl. Power Electron. Conf. Expo. (APEC)*, Feb. 1992, pp. 829–836.

[394] C. A. Quinn, N. Mohan, and H. Mehta, "A four-wire, current-controlled converter provides harmonic neutralization in three-phase, four-wire systems," in *Proc. 8th Annu. Appl. Power Electron. Conf. Expo.*, Mar. 1993, pp. 841–846.
[395] A. Cavini, F. Ronchi, and A. Tilli, "Four-wires shunt active filters: Optimized design methodology," in *Proc. 29th Annu. Conf. IEEE Ind. Electron. Soc. (IECON)*, vol. 3, Nov. 2003, pp. 2288–2293.
[396] K. Antoniewicz, M. Jasinski, and M. P. Kazmierkowski, "Model predictive control of three-level four-leg flying capacitor converter operating as shunt active power filter," in *Proc. IEEE Int. Conf. Ind. Technol. (ICIT)*, Mar. 2015, pp. 2288–2294.
[397] D. A. Fernandes and S. R. Naidu, "A novel PWM scheme for the 4-leg voltage source converter and its use in dynamic voltage restoration," in *Proc. IEEE Power Eng. Soc. Gen. Meeting*, Jun. 2007, pp. 1–5.
[398] S. R. Naidu and D. A. Fernandes, "Generation of unbalanced 3-phase voltages for dynamic voltage restoration using the 4-leg voltage source converter," in *Proc. IEEE Power Electron. Spec. Conf.*, Jun. 2007, pp. 1195–1200.
[399] S. R. Naidu and D. A. Fernandes, "The 4-leg voltage source converter and its application to dynamic voltage restoration," in *Proc. IEEE Int. Symp. Ind. Electron.*, Jun. 2007, pp. 781–786.
[400] Y. Xu, L. M. Tolbert, J. N. Chiasson, J. B. Campbell, and F. Z. Peng, "A generalised instantaneous non-active power theory for STATCOM," *IET Electric Power Appl.*, vol. 1, no. 6, pp. 853–861, Nov. 2007.
[401] A. Navas-Fonseca, C. Burgos-Mellado, J. S. Gomez, F. Donoso, L. Tarisciotti, D. Saez, R. Cardenas, and M. Sumner, "Distributed predictive secondary control for imbalance sharing in AC microgrids," *IEEE Trans. Smart Grid*, vol. 13, no. 1, pp. 20–37, Jan. 2022.
[402] M. Urrutia, R. Cardenas, J. C. Clare, and A. Watson, "Circulating current control for the modular multilevel matrix converter based on model predictive control," *IEEE J. Emerg. Sel. Topics Power Electron.*, vol. 9, no. 5, pp. 6069–6085, Oct. 2021.
[403] A. Mora, R. Cardenas, R. P. Aguilera, A. Angulo, P. Lezana, and D. D.-C. Lu, "Predictive optimal switching sequence direct power control for grid-tied 3L-NPC converters," *IEEE Trans. Ind. Electron.*, vol. 68, no. 9, pp. 8561–8571, Sep. 2021.

FÉLIX ROJAS (Member, IEEE) was born in Santiago, Chile. He received the B.Eng. and M.Sc. degrees (Hons.) in electrical engineering from the Universidad de Santiago de Chile, Santiago, in 2009, and the doctoral degree in electrical engineering from the Technical University of Munich, Munich, Germany, in 2016. From 2016 to 2021, he was an Associate Professor with the Electrical Engineering, Universidad de Santiago de Chile; and the Head of the Electrical Energy Technologies Research Center (E2TECH), USACH. Currently, he is an Associate Professor with the Electrical Department, Pontificia Universidad Católica de Chile; and the Principal Investigator of the Electric Vehicle Laboratory and the Power and Energy Conversion Laboratory (PEClab). He is also an Associate Research with the Solar Energy Research Center (SERC Chile) and the UC Energy Research Center. His research interests include control of modular multilevel converters, solid state transformers, renewable energy conversion, electric vehicles chargers, and machine drives.

ROBERTO CÁRDENAS (Senior Member, IEEE) was born in Punta Arenas, Chile. He received the B.Sc. degree in electrical engineering from the University of Magallanes, Punta Arenas, in 1988, and the M.Sc. degree in electronic engineering and the Ph.D. degree in electrical and electronic engineering from the University of Nottingham, Nottingham, U.K., in 1992 and 1996, respectively.

From 1989 to 1991 and 1996 to 2008, he was a Lecturer with the University of Magallanes. From 1991 to 1996, he was with the Power Electronics Machines and Control Group, University of Nottingham. From 2009 to 2011, he was with the Electrical Engineering Department, University of Santiago, Santiago, Chile. He is currently a Professor of power electronics and drives with the Electrical Engineering Department, University of Chile. He was a recipient of the 2019 Third Prize Paper Award from the IAS Industrial Power Converter Committee. He was also the recipient of the IEEE TRANSACTIONS ON INDUSTRIAL ELECTRONICS Best Paper Award, in 2005 and 2019. From 2014 to 2021, he was an Associate Editor of the IEEE TRANSACTIONS ON INDUSTRIAL ELECTRONICS.

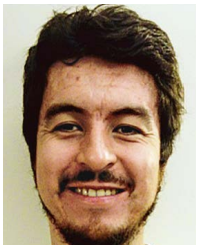

CLAUDIO BURGOS-MELLADO (Member, IEEE) was born in Cunco, Chile. He received the B.Sc. and M.Sc. degrees in electrical engineering from the University of Chile, Santiago, Chile, in 2012 and 2013, respectively, and the dual Ph.D. degree in electrical and electronic engineering from the University of Nottingham, U.K., and in electrical engineering from the University of Chile, in 2019. From 2019 to 2021, he was a Research Fellow with the Power Electronics, Machines and Control Group (PEMC Group), University of Nottingham, U.K. Currently, he is an Assistant Professor with the Institute of Engineering Sciences, Universidad de O'Higgins, Rancagua, Chile. His current interests include battery energy storage systems, electrical vehicle technologies, power electronics, microgrids, power quality issues, and modular multilevel converters. In 2021, he received the Best Ph.D. Thesis Award in the category of exact science from the Chilean Academy of Sciences.

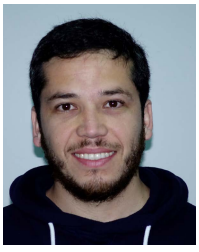

ENRIQUE ESPINA (Student Member, IEEE) was born in Santiago, Chile. He received the B.Sc. degree in electrical engineering from the University of Santiago, Santiago, in 2013, the M.Sc. degree in electrical engineering from the University of Chile, Santiago, in 2017, and the dual Ph.D. degree in electrical and computer engineering from the University of Waterloo, ON, Canada, and in electrical engineering from the University of Chile, in 2021. Currently, he is an Assistant Professor with the Department of Electrical Engineering, University of Santiago. His main research interests include the control of hybrid ac/dc microgrids, energy storage systems, electrical vehicle technologies, renewable energies, and power electronic converters.

JAVIER PEREDA (Member, IEEE) received the B.Sc. (Eng.) degree (Hons.) in electrical engineering and the M.Sc. and Ph.D. degrees in electrical engineering from the Pontifical Catholic University of Chile (PUC), Santiago, Chile, in 2009 and 2013, respectively. In 2013, he joined the Electrical Department, Pontificia Universidad Católica de Chile, where he is currently an Associate Professor. From 2014 to 2016, he was an Associate Research of the Control and Power Group, Department of Electrical and Electronic Engineering, Imperial College London. He is an Associate Research of the Solar Energy Research Center, Chile; and the UC Energy Research Center, Chile. He is a Principal Investigator of the Electric Vehicle Laboratory and the Power and Energy Conversion Laboratory (PEClab), Pontificia Universidad Católica de Chile. His research interests include power electronics and control applied to electric vehicles, energy storage, AC and DC electric networks and microgrids, renewable energy, multilevel converters, industrial applications, and motor drives.

CRISTIAN PINEDA (Student Member, IEEE) received the B.Sc. degree (Hons.) in electrical engineering from the Universidad de Chile, Santiago, in 2010. He is currently pursuing the joint Ph.D. degree with the Pontificia Universidad Católica de Chile and the University of Nottingham. Since 2017, he has been a part-time Lecturer with the Universidad de Santiago de Chile. His current research interests include power electronics and control applied to DC-DC power conversion, renewable energy, and industrial applications.

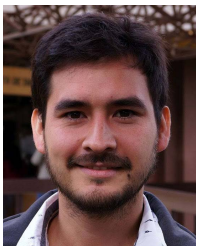

DAVID ARANCIBIA was born in La Serena, Chile, in 1988. He received the bachelor's and master's degrees in electronic engineering from Universidad Técnica Federico Santa María, Valparaíso, Chile, in 2013. He has been working as a Develop Engineer in innovation projects related to mining, solar farms, and water treatment, where his tasks were PCB prototyping, control systems, and power electronics converters. His current research interests include power electronics, multilevel converters, and embedded systems programming.

MATÍAS DÍAZ (Member, IEEE) was born in Santiago, Chile. He received the B.Sc. and M.Sc. degrees in electrical engineering from the University of Santiago, Chile, in 2011, and the dual Ph.D. degree from the University of Nottingham, U.K., and the University of Chile, Chile, in 2017. Currently, he is an Associate Professor and the Head of the Electrical Technologies Research Group, University of Santiago. His main research interests include power electronics, renewable energy technologies, and electromobility.